THE EFFECT OF COLLECTIVE EXCITATIONS

ON THE OPTICAL MODEL

by

Virginia R. Brown, B. Sc.

A thesis submitted to the Faculty of Graduate Studies and Research in partial fulfilment of the requirements for the degree of Doctor of Philosophy.

Department of Physics,
McGill University,
Montreal.

October, 1963.

ACKNOWLEDGEMENTS

The author is extremely grateful to her thesis advisor, Professor Bernard Margolis, for indicating the present thesis topic as well as for the many important suggestions and discussions during the course of this investigation. Sincere thanks also goes to Professor T. Morris for many interesting and fruitful discussions regarding interpretation.

The author is most appreciative for the essential use of the IBM computing machines at The McGill University Computing Centre. Members of the computing staff, in particular, Mrs. Manley were extremely cooperative and helpful during the many hours of calculating.

In regard to the preparation of the manuscript, a special thanks goes to Marilyn D. Tavares for freely donating her time to typing the first draft and to Mary Armey for typing the final copy. Gil Greenberg generously helped the author in preparing the curves for reproduction. The author also wishes to thank Arthur B. Cicero and American Science and Engineering, Inc. of Cambridge for the gratuitous use of photographic reproduction equipment.

TABLE OF CONTENTS

Table of Contents (Continued) Page

Ph. D. PHYSICS

Virginia R. Brown

THE EFFECT OF COLLECTIVE EXCITATIONS ON THE OPTICAL MODEL

A simple model is proposed for the description of the scattering of neutrons by a vibrational even-even nucleus employing a complex spheroidal well surface interaction. This model is particularly convenient since it allows an exact analytic solution, which can be written in the form of correction terms to the spherical optical model.

The application of this model to the s wave strength function results in a splitting of the single peak at A = 55. The inclusion of the effect of octupole excitation introduces desirable but minor modifications.

Determination of the total neutron cross sections with this model substantiates the view that the flattening of giant resonances away from closed shell regions can be attributed to the effect of quadrupole excitation. There is also some evidence from this model that the effect of collective excitations could account for the characteristic shift of the maxima associated with these resonances. The scattering and reaction cross sections as well as the differential shape elastic scattering are also calculated.

LIST OF ILLUSTRATIONS

LIST OF TABLES

CHAPTER 1

INTRODUCTION AND SUMMARY

This thesis is a study of the effect of collective excitations on the optical model. The Introduction will be devoted to a sketch of the historical developments which are pertinent to this investigation. The spherical optical model or the optical model before the effects of collective excitation are imposed is discussed at some length. Various gross properties of the neutron - nucleus scattering problem which are particularly suitable for prediction by the optical model are reviewed; the gross properties to which we refer are the cross sections and the strength function appropriately averaged over resonances. The success of the spherical optical model in predicting these properties is qualitatively considered. Consideration of the corrections for collective effects on the spherical optical model and the resulting improvement in the prediction of the aforementioned gross properties is discussed. The particular contribution made by the present thesis to this area of nuclear physics is also described.

For many years the principal nuclear reaction mechanism for the interaction of nuclear particles with complex nuclei was the idea of the compound nucleus introduced by Niels Bohr[1] in 1936. Under the assumptions of this model a particle, which has entered the nucleus, quickly shares its energy with the other nucleons and can be thought of as absorbed, thereby forming a compound nucleus in an excited state. This state is one in which the motions of all particles are so intimately

coupled that a statistical equilibrium is reached, and the incident neutron is no longer distinguishable from the target nucleons. The state of the compound nucleus and its manner of decay are independent of the way in which it was formed except for the correlations and restrictions connected with the over-all conservation laws.

In 1949, with assumptions akin to the Bohr hypothesis, Feshbach and Weisskopf[2] calculated the energy dependence of neutron - nuclear cross sections. The results represented average values over individual fluctuations and resonances, and the cross sections were smooth functions of energy which decreased monotonically with increasing energy. However, the decisive experiments of Barschall[3] and his co-workers have clearly demonstrated that this is not the case. Instead, the experimental curves appropriately averaged over resonances have pronounced maxima and minima reminiscent of wave interference. Furthermore, these maxima and minima demonstrate not a random, but a gradual change when examined as a function of mass number and energy, that is, there is a significant change over the full range of the mass number, A, but the cross sections of neighboring nuclei have a similar energy dependence.

This type of behavior is indicative of a general flaw in the theory since it shows up systematically in all nuclides. The characteristic shapes that appear in the total averaged neutron cross sections, $\bar{\sigma}_T$, depend on general properties that vary slowly with A rather than on the detailed features of nuclear reactions. The widely spaced shallow maxima and minima are what might be expected in scattering from a potential well, where resonances occur whenever a whole number of

wavelengths can be fitted into the well, but this type of interaction is just what was needed for the nuclear shell model. It was also evident that the damping which would be necessary to produce the observed widths of these resonances was smaller than that expected from compound nucleus arguments. In fact, the results obtained by Feshbach and Weisskopf[2] had no resonance character because of their assumption of total damping based on the Bohr hypothesis.

It seemed clear, then, that compound nucleus ideas had to be modified to encompass the shell model point of view. The basis of the Bohr assumption was that every nucleon incident on the nucleus is absorbed, that is, captured immediately into the compound nucleus. This is, of course, in direct conflict with the shell model which necessitates long nucleon mean-free-paths in nuclear matter. One might interpret the success of the shell model as evidence that a neutron could move about in the nucleus without interacting with the other particles present. However, the shell model evidence comes from ground states and low excitation levels where the exclusion principle is most effective. Since nucleons of incident energies of a few Mev form, with the targets, excited states of the order 8 Mev, one does not expect the long mean-free-paths associated with the shell model ground states to be valid.

The optical model was devised to combine the virtues of the shell model and the compound nucleus assumptions. The use of the optical model implies the use of a complex potential to represent the target nucleus. If the Schrodinger equation is adjusted to include a complex potential, it can be shown that the imaginary part of this potential has

the effect of adding a term to the continuity equation which corresponds to the removal of particles. The magnitude of the imaginary part of the potential bears a direct relation to the probability per second that the neutron will form a compound state. In the optical model the strong coupling or total absorption suggested by the compound nucleus theory is replaced by a weak absorption where the capture into the compound nucleus takes place with a probability less than unity. The probability that is required for compound nucleus formation is expected to be consistent with nucleon mean-free-paths in nuclear matter that lie somewhere between the short mean- free-paths of the compound nucleus theory and the longer paths associated with the shell model. Thus, in the optical model the incident neutron is considered to enter the nucleus and move inside the nuclear boundaries making many internal motions before subsequently being either emitted or absorbed. When the incident nucleon is not absorbed, the target nucleus acts as a potential well.

The representation of the nucleus by a potential well is analogous to the representation of an optical medium by a refractive index. To account for the absorption of light in the optical case, an imaginary part of the refractive index is introduced. In nuclear reactions the elastically scattered beam has an intensity which is diminished relative to the incident beam because some particles initiate reactions and are lost to the incident beam. This absorption is represented by an imaginary part of the potential, again in analogy with the optical case. These analogies constitute the basis for the name optical model or clouded crystal ball model.

Referring back to the experimental work of Barschall and others we had stated that the damping necessary to produce the resonances must be smaller than previously expected from Bohr assumptions. Another way of stating this in terms of a clouded crystal ball model is that the imaginary part of the well must be of the right order of magnitude to give the constructive interference necessary to produce the observed broad maxima and minima. These giant resonances of the order of 1 Mev wide and located in the energy region of about 0.1 Mev to 10 Mev will be important in our considerations in this thesis and will be discussed in more detail in future contexts.

The optical model in this form was first presented in 1954 by Feshbach, Porter, and Weisskopf[4] to which we will hereafter refer as FPW. In particular, the FPW optical model was devised to explain the results of the Barschall experiments which were mentioned earlier. The FPW optical model gave surprisingly good results in reproducing the giant resonance structure of the total neutron cross sections averaged over resonances and plotted versus mass number and energy. The natural explanation of these resonances is that they represent the effect of the independent particle levels superimposed on the actual width and spacing of the numerous resonances of the many-body system hidden beneath the averaging.

In connection with the actual many-body system, it might be mentioned here that by replacing the target nucleus by a complex potential well we have disregarded the complicated structure of the nucleus, and at best we can only see the gross-structure associated with the scattering.

Also we have lumped all reactions, inelastic scattering, and even compound elastic scattering together as an absorption. By disregarding the intricate quantum mechanical nature of the problem we have failed to account for the sharp resonances or the competition between nuclear reactions. The point is that by using a shell model potential we have determined the average interaction between the nucleus and the neutron. It is the fluctuation away from the average that gives rise to the compound nuclear resonances. Nevertheless, the clouded crystal ball model gives a good description of the average cross sections, and one might say that it accounts for nuclear reactions in a global fashion.

It should be noted that the position of the optical model has moved amazingly since the time of FPW both from the point of view of its phenomenology and also from the point of view of its underlying foundations. Phenomenologically the optical potential for spherical nuclei which has in general been employed is a combination of central and spin-orbit potentials. For energies that are not too high it should be much like the single-particle potential for bound nucleons in which,for example, non-local effects should be included. The main improvement on the original square well model is the effect of diffusing the well. The reflectivity of the square well is too large, consequently, the reaction cross section which is sensitive to the nature of the surface is too small.

The other aspect of the optical model deals with the relationship of the optical model to more basic theory. This involves the proof of existence of the optical model from a many-body Hamiltonian and then, in turn, the derivation of the parameters of the optical model from the two-body interaction. In this thesis we will be concerned with the phenomenological optical model only.

One of the more outstanding successes of the optical model has been the determination of the strength function, $\overline{\Gamma_m^0}/D$, which is the ratio of the neutron level width to the neutron level spacing averaged over resonances and normalized to 1 ev. In the low-energy regions of well spaced levels the strength function is simply related to the average absorption cross section. The strength function is of particular interest to recent nuclear models and is not a property of the nuclear energy level system, but rather it is a property of the nuclear surface itself. To see this consider the following definitions:

$\Gamma_m/\hbar$ = probability per second for disintegration of a nuclear level by neutron emission.

$\hbar/D$ = time between collisions with the nuclear surface, or to put it another way, it is the time for all the excitation energy to be reconcentrated on one neutron so that it could escape.

Clearly the strength function which is the product of these quantities within a factor of 2π is just the penetrability of the nuclear surface. Because the strength function has this property of being essentially independent of the method of excitation or equivalently because it is external in nature, it is particularly useful in determining the parameters of the optical model potential.

The strength function plotted against mass number for the spherical optical model shows peaks in the vicinity of A = 55 and A = 155. The overall agreement with experiment is quite good and can be qualitatively understood on the basis of the spherically symmetric potential well used

by FPW. The maxima in the strength function correspond to the resonances that occur when the energy of the incident neutron, which is essentailly zero, is near an s-level of the potential employed in the optical model. If one examines the level structure of the spherical nuclei of a shell model potential designed to predict the magic numbers, it is seen that the resonance at A = 55 corresponds to a 3s resonance, that is, the 2 s level is filled, bu the 3s state is more than a major shell away and, therefore, just positive. Likewise the resonance associated with A = 155 can be identified as a 4s resonance.

The approximate condition for an s-resonance can be determined analytically for a square well and is given when the inside wave number times the radius is an odd multiple of $\pi/2$. This is just the condition for which new energy levels with l = 0 appear in the bound state problem. From the point of view of a real well, the physical interpretation is that the incident particle has nearly the right energy to be bound, and, therefore, it has a tendency to concentrate in this region. Consequently, there is a large distortion produced in the wave function and, in turn, a large amount of scattering. The use of a complex well, however, reveals these resonances as absorption peaks; therefore, the interpretation is different although the condition which locates the position of the peaks is still approximately determined by the real part of the well. The imaginary component of the well has the effect of broadening the resonances. These resonances are often called size resonances; the reason for this is that since $R = R_o A^{1/3}$, an increase in mass number has the effect of increasing the extent of the well.

The strength function peak which falls in the region of A = 155 is in the vicinity of strong deformations and rotational nuclei. The interpretation of this region of nuclei is that the number of particles outside closed shells is so numerous that the nuclear equilibrium shape is permanently deformed, thus, giving rise to rotational excitations. Although the representation of the target nucleus by a spherical well gave good qualitative agreement with experimental results in this region, it did not account for the irregularities that existed there.

By using a spheroidal well to represent the deformation of these nuclei, Margolis and Troubetzkoy[5] have been able to present a simple argument to explain the observed splitting of this 4s resonance in terms of the deformation of the nuclei in this region. These authors considered the problem of s-wave scattering from a complex spheroidal potential in the limit of no recoil of the rotator. This has been called the adiabatic approximation where the use of a fixed spheroidal well is justified in that the rotation of the target nucleus is slow compared to the nucleon transit time. The solution was effected by joining the inside and out side wave functions and their derivatives at the surface of the well as a function of eccentricity.

In the case of a non-spherical potential well, angular momentum is not a good quantum number, and as a result there is mixing of d-states and higher states into the particle wave function inside the well. These states resonate at different values of A;consequently, there is a mixing in the final result which produces a double peak in the strength function. Increasing the eccentricity has the effect of further deforming the well which mixes in higher l-states with a resulting additional increase in splitting.

An extensive study of neutron scattering from non-spherical, even-even nuclei in the rotational region of nuclear spectra has been considered by Chase, Wilets, and Edmonds[6] (CWE). These authors have used a diffuse-surfaced potential well which was chosen to be complex in order to allow for inelastic scattering and reactions. In this study a target Hamiltonian has been included so as to account for the excitation of the low-lying rotational states which, because of the deformed shape of the nucleus, are directly coupled to the particle motion. Since angular momentum is not conserved for a deformed well, there is an energy exchange between the incident neutron and the target; the neglect of this is just what was meant by the adiabatic approximation in the discussion of the work presented in Reference 5.

The paper presented by CWE was in part a study of the importance of direct interactions compared with compound-nucleus interactions. A plentitude of experimental data on U^{238} provided a propitious case for investigation. According to CWE the cross section for the direct process compared to that for compound nucleus formation is relatively small at low energies ($\leq$1 Mev). It becomes important, of course, as the incident neutron energy is increased. It is suggested, however, that the contribution of the direct interaction to the differential cross section at low energies is significant because of the large anisotropy which is associated with this process. Other cross sections and effects are also presented. In particular, the strength function is determined as a function of mass number with a variable deformation parameter based on measured quadrupole moments. This is the physically

reasonable thing to do, and there is a corresponding improvement in the fitting of the experimental curve. It might be mentioned here that the validity of the adiabatic approximation used by Margolis and Troubetzkoy for s-wave scattering was confirmed by CWE.

The peak in the strength function located in the vicinity of A = 55 is in the region of vibrational nuclei, that is, near closed shells where the equilibrium shape of the nucleus is still spherical, and there is the possibility of vibrational excited states but not rotational. The interpretation of vibrational nuclei is that there exist particles outside closed shells, but there are not enough to permanently deform the nuclear equilibrium shape. The experimental strength function in the vicinity of A = 55 shows asymmetry when compared to the spherical well predictions. It is well known that many even-even nuclei demonstrate a strong excitation of 2^+ states by inelastic scattering. It is, therefore, conjectured that this dynamical quadrupole distortion may be responsible for the asymmetry in the strength function in much the same way as was evidenced for the permanently distorted nuclei at A = 155.

This effect has been considered by Professor Bernard Margolis and the author of this thesis and independently by B. Buck and F. Perey[7]. The particular advantage of the model used by the former is that it yields to a particularly nice analytic solution which can be compared directly with the work of FPW in the form of correction terms, and it is primarily for this reason that it is presented in a later chapter. The work of Buck and Perey is more extensive in that it includes the p-wave strength functions. In addition they have used a diffuse interaction

potential, and, in general, the method of attack is different from ours.

We have been discussing the giant resonances in the strength function; we shall now consider the giant resonances that appear in the total neutron cross section. The consideration of the effect of collective excitations on these giant resonances and on the associated cross sections constitute the main contribution of the present thesis. The calculation of the total cross section presents a much more difficult problem than the one which we have been considering because the strength function involves only s-wave calculations, but the giant resonances in the total cross section occur at energies up to 10 Mev and higher, and, therefore, consideration of the effect of distortion on these giant resonances involves the inclusion of many partial waves.

Upon examination of the experimental total cross sections versus mass number there can be observed a gradual tendency for these giant resonances to flatten out in the regions tending away from closed shells. There is also a characteristic shift in the energy at which the maximum in the cross section occurs. It was inferred that these effects could be understood in the region of vibrational nuclei, that is, just away from closed shells by taking into account the effect of collective excitations. The particular regions under investigation in this study are the regions near $_{20}Ca^{40}_{20}$ and $_{82}Pb^{208}_{126}$ which are doubly magic closed shell nuclei. To our knowledge an investigation of this sort has never previously been attempted.

In Chapter 2 we summarize some essential features of the nuclear models that will be important in the subsequent developments of the theory.

In particular this involves the optical model and the collective model of the nucleus. In Chapter 3 we shall formulate the model for the inclusion of the effect of collective excitations for vibrational nuclei. In Chapter 4 we present some numerical results in graphic form, and a discussion of these results will be presented in Chapter 5. The exact solution of the coupled radial equations is outlined in Appendix I, and certain important recursive relations are given in Appendix II.

CHAPTER 2

BASIC NUCLEAR MODELS

2.1 Optical Model Cross Sections

We have stated that in the optical model, compound nucleus formation is considered as an absorption of the incident beam as represented by the imaginary part of the potential. The real part of the potential predicts the shape-elastic scattering, that is, no compound nucleus is formed. Now, the compound elastic scattering is considered as an absorption process in this model even though it involves the subsequent emission of the incident particle by the entrance channel. As a result the optical model predicts only the shape-elastic scattering and the compound nucleus formation. In order to relate the optical model to experiment it is necessary to define a set of cross sections which are averaged over resonances. Of course, at higher energy when the level width becomes comparable in size to the distance between levels the averaging is done automatically.

According to usual scattering theory when a target nucleus is bombarded with neutrons, the differential cross section for scattering neglecting spin effects is given as follows:[8]

$$\frac{d\sigma_{el}}{d\Omega} = \frac{\pi}{k_0^2}\left|\sum_l \sqrt{2l+1}\,(1-\eta_l)\,Y_{l,0}\right|^2 \qquad (2.1)$$

Where η_l is the measure of the amplitude and phase of the coherent outgoing l^{th} partial wave relative to the unit amplitude and zero phase

angle of the incoming wave. The $Y_{\ell,0}$'s are the spherical harmonics as given by Reference 8, and k_0 is the outside wave number. The total elastic cross section is obtained by integrating the differential elastic cross section over all angles, and because of the orthonormality of the spherical harmonics, σ_{el} becomes:

$$\sigma_{el} = \frac{\pi}{k_0^2} \sum_{\ell} (2\ell+1) \left| 1 - \eta_\ell \right|^2 . \tag{2.2}$$

The reaction cross section represents all incoherent processes, that is, all processes where the incident neutron interacts with the target nucleus in such a way that it does not leave through the entrance channel.. The reaction cross section can be obtained by subtracting the intensity of the outgoing coherent wave from the incident wave and is, therefore,

$$\sigma_R = \frac{\pi}{k_0^2} \sum_{\ell} (2\ell+1) \left\{ 1 - |\eta_\ell|^2 \right\} . \tag{2.3}$$

The total cross section is just the sum of σ_{el} and σ_R and in terms of partial waves

$$\sigma_T = \sum_{\ell} \sigma_T^{(\ell)} = \sum_{\ell} \left(\sigma_{el}^{(\ell)} + \sigma_R^{(\ell)} \right) . \tag{2.4}$$

η_ℓ exhibits rapid fluctuations as a function of energy in the regions of closely spaced resonances of the compound nucleus. The theory of average cross sections as represented by FPW replaces η_ℓ with an average value of η_ℓ where the averaging is defined by

$$\overline{\eta}_\ell(\epsilon) = \frac{1}{I} \int_{\epsilon - I/2}^{\epsilon + I/2} \eta_\ell(\epsilon') \, d\epsilon' . \tag{2.5}$$

I is an energy interval containing many closely spaced resonances yet chosen much smaller than the energy, ϵ, such that slowly varying functions of ϵ like k_0^2 need not be averaged. The average cross sections are defined in the same way, and without going into detail it is easily shown[4] that

$$\bar{\sigma}_T = \sum_{\ell=0}^{\infty} \bar{\sigma}_T^{(\ell)} = \sum_{\ell=0}^{\infty} (\sigma_c^{(\ell)} + \sigma_{se}^{(\ell)}) \quad , \tag{2.6}$$

where $\sigma_c^{(\ell)}$ is the cross section for the formation of the compound nucleus, and $\sigma_{se}^{(\ell)}$ is the shape elastic cross section. These cross sections are given by

$$\begin{aligned} \sigma_{se} &= \sum_{\ell=0}^{\infty} \sigma_{se}^{(\ell)} = \frac{\pi}{k_0^2} \sum_{\ell=0}^{\infty} (2\ell+1) \left| 1 - \bar{\eta}_\ell \right|^2 \\ \sigma_c &= \sum_{\ell=0}^{\infty} \sigma_c^{(\ell)} = \frac{\pi}{k_0^2} \sum_{\ell=0}^{\infty} (2\ell+1) \left\{ 1 - |\bar{\eta}_\ell|^2 \right\} \end{aligned} \tag{2.7}$$

The angular distribution for the shape elastic scattering is given by

$$\frac{d\sigma_{se}}{d\omega} = \frac{\pi}{k_0^2} \left| \sum_{\ell=0}^{\infty} \sqrt{2\ell+1} \, (1 - \bar{\eta}_\ell) \, Y_{\ell,0} \right|^2 \tag{2.8}$$

These newly defined quantities are, if you like, the scattering and reaction cross sections of a new problem which is defined by the slowly varying function $\bar{\eta}_\ell$. The optical model potential is that potential for which $\bar{\eta}_\ell$ is the amplitude and phase of the outgoing coherent wave, and it is for this reason that the optical potential is said to predict the gross properties of neutron-nucleus scattering.

2.2 Square Well Optical Model

The simplest type of well that one can assume for the optical model is a square well as was first utilized by FPW. As has been mentioned, we shall cast our theory for the effect of collective excitations on the optical model in a form in which the results appear as correction terms for the square well optical model. In the light of this, we shall present here the features of the square well model which are essential for our purposes. The square well optical potential is defined by

$$\begin{aligned} \overline{V}(r) &= -V_0(1+i\xi) \quad ; \quad r<R \\ \overline{V}(r) &= 0 \qquad\qquad\quad ; \quad r>R \,, \end{aligned} \tag{2.9}$$

where V_0 is the real well depth and is taken here as a constant. ξ is the absorption parameter and represents the percentage of V_0 that corresponds to absorption; ξV_0 is the imaginary part of the potential and has the same radial dependence as the real part in this model. The nuclear radius, R, is a function of mass number, A, according to the relation,

$$R = R_0 A^{1/3} \tag{2.10}$$

We had written down expressions for the various cross section in terms of the quantity $\overline{\eta}_\ell$. For our purposes it is convenient to write the cross sections in terms of the logarithmic derivative, f_ℓ , which is defined by

$$f_\ell \equiv R \frac{1}{u_\ell} \left.\frac{du_\ell}{dr}\right|_R \tag{2.11}$$

where $u_\ell(r)$ is the radial part of the wave function of the scattering problem and satisfies the Schrodinger equations.

$$\frac{d^2u_\ell(r)}{dr^2} + \left[k_0^2 - \frac{\ell(\ell+1)}{r^2}\right]u_\ell(r) = 0 \quad ; \quad r > R \tag{2.12}$$

and

$$\frac{d^2u_\ell(r)}{dr^2} + \left[K_0^2 - \frac{\ell(\ell+1)}{r^2}\right]u_\ell(r) = 0 \quad ; \quad r < R \tag{2.13}$$

where

$$k_0^2 = \frac{2m}{\hbar^2}E \quad \text{and,} \quad K_0^2 = \frac{2m}{\hbar^2}\left[E + V_0(1+i\xi)\right]. \tag{2.14}$$

$\bar{\eta}_\ell$ can be written in terms of f_ℓ as follows:

$$\bar{\eta}_\ell = e^{2i\delta_\ell}\ \frac{f_\ell - \Delta_\ell + iS_\ell}{f_\ell - \Delta_\ell - iS_\ell}\ , \tag{2.15}$$

where for the complex square well

$$\delta_\ell(x) = \tan^{-1}\left[j_\ell(x)/n_\ell(x)\right], \tag{2.16}$$

$$\Delta_\ell(x) + iS_\ell(x) = 1 + x\ \frac{h_\ell^{(1)\prime}(x)}{h_\ell^{(1)}(x)}\ , \tag{2.17}$$

and

$$f_\ell(X) = 1 + X\, j_\ell'(X)/j_\ell(X) \qquad (2.18)$$

In these equations, j_ℓ, n_ℓ and $h_\ell^{(1)}$ are, respectively the spherical Bessel, Neumann, and Hankel functions. The Hankel function is of the first kind, that is, it corresponds to outgoing waves only. In fact, $\Delta_\ell + i S_\ell$ is the logarithmic derivative of the outgoing portion of $u_\ell(r)$, where Δ_ℓ and S_ℓ are both real. In the notation of (2.16), (2.17) and (2,18),

$$x = k_0 R \,, \qquad (2.19)$$

$$X = K_0 R \,, \qquad (2.20)$$

and the prime denotes differentiation with respect to the argument; this notation will be used consistently throughout. The ratio of the outgoing part of the radial wave function to the incoming part is a pure phase, and the identification of $e^{2i\delta_\ell}$ with this ratio leads to the expression for δ_ℓ given by (2.16).

$\bar{\eta}_\ell$ has been expressed in terms of functions evaluated at the nuclear surface by (2.15); we can now rewrite the cross sections defined in (2.1), (2.2), (2.3), and (2.4) in terms of these functions.

$$\sigma_{se}^{(\ell)} = \frac{\pi}{k_0^2}(2\ell+1)\left| e^{-2i\delta_\ell} - 1 - \frac{2iS_\ell}{(f_\ell - \Delta_\ell) - iS_\ell} \right|^2 , \qquad (2.21)$$

$$\sigma_c^{(\ell)} = \frac{\pi}{k_0^2}(2\ell+1) \frac{-4 s_\ell \, \mathrm{Im} f_\ell}{(\mathrm{Re} f_\ell - \Delta_\ell)^2 + (\mathrm{Im} f_\ell - s_\ell)^2} \quad ; \tag{2.22}$$

$$\bar{\sigma}_T^{(\ell)} = \frac{\pi}{k_0^2}(2\ell+1) \left\{ \sin^2 \delta_\ell - s_\ell \frac{\cos 2\delta_\ell (\mathrm{Im} f_\ell - s_\ell) - \sin 2\delta_\ell (\mathrm{Re} f_\ell - \Delta_\ell)}{(\mathrm{Re} f_\ell - \Delta_\ell)^2 + (\mathrm{Im} f_\ell - s_\ell)^2} \right\} . \tag{2.23}$$

The differential shape elastic cross section (2.8) can be written in terms of $\overline{\sigma_T}$ and the Legendre polynomials, $P_\ell(\cos\theta)$, with the aid of (2.15) and (2.23)

$$\frac{d\sigma_{se}}{d\Omega} = \frac{k_0^2}{(4\pi)^2} \left\{ \sum_\ell \bar{\sigma}_T^{(\ell)} P_\ell(\cos\theta) \right\}^2 + \frac{1}{4k_0^2} \left\{ \sum_\ell (2\ell+1) \left\langle \sin 2\delta_\ell \left[1 + \frac{2 s_\ell (\mathrm{Im} f_\ell - s_\ell)}{(\mathrm{Re} f_\ell - \Delta_\ell)^2 + (\mathrm{Im} f_\ell - s_\ell)^2} \right] \right. \right.$$

$$\left. \left. + \cos 2\delta_\ell \frac{2 s_\ell (\mathrm{Re} f_\ell - \Delta_\ell)}{(\mathrm{Re} f_\ell - \Delta_\ell)^2 + (\mathrm{Im} f_\ell - s_\ell)^2} \right\rangle \right\} . \tag{2.24}$$

2.3 Vibrational Nuclei

There is ample evidence[2] that nuclei exhibit collective effects which are necessarily due to the cooperative behavior of large numbers of individual nucleons. This collective effect is due to correlations in individual particle motion and can be identified with the degrees of freedom which describe the shape and orientation of the nuclear field. The nuclear field to a first approximation can be represented by introducing a spherically symmetric potential which describes the average effect of the interaction between the nucleons. The success of the shell model has shown that this is a rather good approximation for closed shell nuclei.

According to the collective model, nuclei away from this closed shell region consist of a relatively stable core made up of particles in closed shells, and the remaining particles are considered to move in the potential of the core. The core is capable of deformation by the nucleons, which are effectively outside the core, and, in turn, once the core is deformed it modifies the field in which the nucleons move. The collective model, is, then, a compromise between the extreme individual particle model and the liquid drop model.

For closed shells the individual orbits of the nucleons are uniformly distributed and the equilibrium shape remains spherical. Particles in unfilled shells, have an anisotropic effect, however, and tend to deform the nucleus according to their own density distribution. The distortion from spherical equilibrium can be thought of as a competition between the tendency for deformation by the individual nucleons in unfilled shells and the residual forces which tend to put equivalent nucleons in a spherically symmetric state.

The distinction between rotational nuclei and vibrational nuclei as mentioned in the Introduction is based upon the stable equilibrium shape. For closed shell nuclei the binding energy is largely due to the special stability of these nuclei. The potential energy curve is stable for the spherical shape and rises steeply for a change in shape. This, of course, implies that nuclear excitations would involve high frequencies. Just away from closed shells where only a few particles have been added, the potential energy minimum still corresponds to a spherical shape,

but now the potential rises less steeply, and excitations involve somewhat lower frequencies than in the case of closed shells.

The addition of particles has the effect of reducing the slope of the potential energy which means that the nucleus is more easily distorted. With only a few particles outside closed shells the equilibrium shape is still spherical and as such exhibits only vibrational excitation. When enough nucleons have been added to make the spherical shape unstable, then the potential energy has a minimum at a nonspherical shape, and we have effectively come into the region of rotational nuclei. These nuclei exhibit rotational as well as vibrational excitation modes. The rotational modes are low frequency collective excitations associated with the rotation of the nonspherical equilibrium shape with the intrinsic structure intact. The individual nucleon correlations necessary to give this effect are long-range correlations such that the over-all space pattern is nearly constant. This may be viewed as a surface effect.

The discussion presented here is dependent upon the separability of the intrinsic and the collective degrees of freedom. The coupling of particle and collective motions can be neglected when the frequencies of collective excitation are small compared to the excitation frequency of a shell model state. We are concerned in this thesis with the regions near closed shells, and due to the high stability of these regions the coupling can be neglected.

Experimentally, vibrational spectra are observed for all even-even nuclei except at closed shells and in the region defined by $A \sim 25$,

$150 < A < 190$, and $A > 220$ where rotational spectra are found. These vibrational excitations can be described in terms of the quantized surface vibrations of a liquid drop. The addition of particles outside closed shells is manifest in the decreased restoring force and the corresponding decrease in the observed frequency of the collective oscillation.

We shall recapitulate the theory of the modes of excitation for a continuous liquid drop using the notation of A. Bohr and B. Mottleson.[10,11] A nuclear surface of general shape can be written as

$$R(\theta,\phi) = R\left[1 + \sum_{\lambda=0}^{\infty}\sum_{\mu=-\lambda}^{\lambda} \alpha_{\lambda\mu} Y_{\lambda\mu}(\theta,\phi)\right] \qquad (2.23)$$

R is the radius of the undeformed liquid drop. The $Y_{\lambda\mu}$'s are, as before[8], the normalized spherical harmonics. Since the radius is a real quantity, the $\alpha_{\lambda\mu}$ satisfy

$$\alpha^{*}_{\lambda\mu} = (-1)^{\mu}\alpha_{\lambda,-\mu} \qquad (2.24)$$

The expansion parameters, $\alpha_{\lambda\mu}$, are the collective coordinates, and they describe the deformation of the nuclear surface. The assumption of incompressibility implies that $\alpha_{0,0} = 0$. The contribution of $\lambda = 1$ gives rise to a rigid translation of the drop. As a result $\lambda = 0$ and $\lambda = 1$ can be dropped from the sum in (2.23).

With the above assumption of incompressibility and the additional assumption of irrotational flow, the Hamiltonian for the system can be

developed. For small oscillations about the equilibrium shape the motion can be described in terms of normal modes, and the resulting Hamiltonian is

$$H = \frac{1}{2} \sum_{\lambda\mu} \left\{ \frac{|\pi_{\lambda\mu}|^2}{B_\lambda} + C_\lambda |\alpha_{\lambda\mu}|^2 \right\} . \tag{2.25}$$

$\pi_{\lambda\mu}$ is the momemtum canonically conjugate to $\alpha_{\lambda\mu}$ and is given by the following relationship:

$$\pi_{\lambda\mu} = \frac{\partial H}{\partial \dot{\alpha}_{\lambda\mu}} = B_\lambda \dot{\alpha}^*_{\lambda\mu} \tag{2.26}$$

B_λ is the inertia parameter, and C_λ is the effective surface tension. The form of the Hamiltonian indicates that the surface oscillations may be considered as a system of harmonic oscillators with frequencies,

$$\omega_\lambda = \sqrt{\frac{C_\lambda}{B_\lambda}} \tag{2.27}$$

The quantization of this system is done in the usual way by reinterpreting the $\pi_{\lambda\mu}$ and $\alpha_{\lambda\mu}$ as quantum mechanical operators satisfying the proper canonical commutation rules. The Hamiltonian can be rewritten by setting

$$\alpha_{\lambda\mu} = \sqrt{\frac{\hbar\omega_\lambda}{2C_\lambda}} \left\{ b_{\lambda\mu} + (-1)^\mu b^*_{\lambda,-\mu} \right\} , \tag{2.28}$$

and

$$\pi_{\lambda\mu} = \lambda \hbar \sqrt{\frac{2C_\lambda}{\hbar\omega_\lambda}} \left\{ b^*_{\lambda\mu} - (-1)^\mu b_{\lambda,-\mu} \right\} , \tag{2.29}$$

where now

$$\left[b_{\lambda\mu}, b^{*}_{\lambda'\mu'}\right] = \delta_{\lambda\lambda'}\delta_{\mu\mu'}\,, \tag{2.30}$$

$$b^{*}_{\lambda\mu} b_{\lambda\mu} = m_{\lambda\mu}\,, \tag{2.31}$$

and

$$b_{\lambda\mu} b^{*}_{\lambda\mu} = m_{\lambda\mu} + 1 \tag{2.32}$$

where $m_{\lambda\mu}$ is the number of quanta in the mode $(\lambda\mu)$. In the usual interpretation $b^{*}_{\lambda\mu}$ and $b_{\lambda\mu}$ are creation and annihilation operators. The Hamiltonian and the z component of angular momentum are diagonal in the $m_{\lambda\mu}$ representation, and the eigenvalues for the deformation of order λ are

$$E_{N,\lambda} = \tfrac{1}{2}\hbar\omega_{\lambda}(2N + 2\lambda + 1) \tag{2.33}$$

and

$$\mathcal{M}_{z} = \hbar \sum_{\mu=-\lambda}^{\lambda} \mu\, m_{\lambda\mu}\,, \tag{2.34}$$

where

$$N = \sum_{\mu=-\lambda}^{\lambda} m_{\lambda\mu} = 0, 1, 2, \cdots \tag{2.35}$$

Each energy level is as many times degenerate as the number of ways the N excitation quanta can be distributed on the $2\lambda + 1$ individual modes of oscillation. The excitation quanta are equivalent to Bose-Einstein phonons of spin λ. The $n_{\lambda\mu}$ in (2.34) is then the number of phonons which has a z component of angular momentum equal to $\mu\hbar$. The energy levels for a particular λ are equally spaced and the separation is $\hbar\omega_\lambda$. The ground state is a zero phonon state with spin zero, and the excited states for deformation of the order λ correspond to increasing the number of phonons of spin λ by one.

The wave functions, $\chi^{(N)}_{\lambda\mu}$, of these vibrational states are the usual harmonic oscillator wave functions with coordinates $\alpha_{\lambda\mu}$. The ground state is

$$\chi^{(0)}_{00} \propto \exp\left[-\sum_{\lambda\mu} \frac{B_\lambda \omega_\lambda \alpha^2_{\lambda\mu}}{2\hbar}\right], \tag{2.36}$$

and the one phonon state of spin λ is given by

$$\chi^{(1)}_{\lambda\mu} \propto b^*_{\lambda\mu} \chi^{(0)}_{00} . \tag{2.37}$$

In this thesis we will be concerned with the 2^+ and 3^- first excited one phonon states. The 2^+ and 3^- states correspond respectively to quadrupole and octupole vibrations. Since we are interested in the ground state and one phonon excited states, then N will take on only the values of zero or one. N = 0 corresponds to the no phonon ground state, and N = 1 designates the first excited one phonon state.

λ = 2 and 3 correspond respectively to the quadrupole and octupole excitations.

We shall have occasion to use the matrix element of $\alpha_{\lambda\mu}$ between different phonon states. The quantity of interest is

$$\int \chi^{*(N)}_{\lambda\mu}\, \alpha_{\lambda\mu}\, \chi^{(M)}_{\lambda\mu}\, d\tau_{\alpha_{\lambda\mu}} \equiv \left\langle \chi^{(N)}_{\lambda\mu} \middle| \alpha_{\lambda\mu} \middle| \chi^{(M)}_{\lambda\mu} \right\rangle \quad . \tag{2.38}$$

Recalling that $\alpha_{\lambda\mu}$ is a combination of raising and lowering operators we obtain the following:

$$\left\langle \chi^{(M)}_{\lambda\mu} \middle| \alpha_{\lambda\mu} \middle| \chi^{(N)}_{\lambda\mu} \right\rangle = \begin{cases} \sqrt{\frac{\hbar\omega_\lambda}{2C_\lambda}}\sqrt{N} & ;\ N = M+1 \\ 0 & ;\ N \neq M \pm 1 \end{cases}$$

$$\left\langle \chi^{(M)}_{\lambda\mu} \middle| \alpha_{\lambda,-\mu} \middle| \chi^{(N)}_{\lambda\mu} \right\rangle = (-1)^{\mu}\sqrt{\frac{\hbar\omega_\lambda}{2C_\lambda}}\sqrt{N+1} \qquad ;\ N = M-1 \tag{2.39}$$

It is seen that the quantity $\alpha_{\lambda\mu}$ has non zero matrix elements only between states which differ by one phonon with quantum numbers λ and μ.

Since we are only considering the no phonon ground state and the one phonon λ = 2 and λ = 3 excited states, we can write the Schrodinger equation unambiguously as

$$H\chi_{\lambda\mu} = \hbar\omega_\lambda \chi_{\lambda\mu} \tag{2.40}$$

where we have taken the ground state to have zero energy.

CHAPTER 3

INCLUSION OF COLLECTIVE EFFECTS

3.1 Formulation of the Model

In this chapter we develop the formalism for the inclusion of the effects of collective vibrations of spherical nuclei on the optical model. The Hamiltonian for the bombarding of a spherical nucleus by a beam of neutrons neglecting neutron spin can be written:

$$H = -\frac{\hbar^2}{2m}\nabla^2 + H_T(\alpha_{\lambda\mu}) + V_{int}(\alpha_{\lambda\mu}, \vec{r}) \qquad (3.1)$$

where the Hamiltonian for the entire system has been written as the sum of the neutron kinetic energy, the target Hamiltonian, and the interaction potential. The $\alpha_{\lambda\mu}$'s are the collective coordinates of the target nucleus and $\vec{r}$ represents the coordinates of the incident neutron.

Since the interaction potential is not spherically symmetric, the angular momentum of the incident neutrons is not conserved, and the change is taken up by the target nucleus via the target Hamiltonian. The target Hamiltonian which will be utilized is the pure vibrational, even-even Hamiltonian as presented in Section 2.3. In writing down the Hamiltonian in (3.1) we have made use of the fact that collective motions are slow compared with nucleon transit times. The collective parameter, $\alpha_{\lambda\mu}$, can, therefore, be considered fixed for the duration of the interaction. The interpretation is that the neutron excites a

collective degree of freedom by interacting with the nucleus as a whole and may leave the target in an excited state.

The interaction potential can be written:

$$V_{int} = V\left[R\left(1+\sum_{\lambda\mu}\alpha_{\lambda\mu}Y_{\lambda\mu}(\theta,\phi)\right)\right] \;, \tag{3.2}$$

where we have assumed that the potential takes the form of the distorted nuclear shape. We have expanded the nuclear surface, $R(\theta,\phi)$, in a series of spherical harmonics as was previously done for the development of the collective model. Now if we assume a complex well and take the first two terms of a Taylor series expanded around r = R, we obtain the following equation:

$$V_{int}(\alpha_{\lambda\mu},\vec{r}) = \overline{V}(r) - RV_0(1+i\xi)\,\delta(r-R)\sum_{\lambda\mu}\alpha_{\lambda\mu}Y_{\lambda\mu}(\theta,\phi) \;, \tag{3.3}$$

where $\overline{V}(r)$ is given by Equation (2.9). In (3.3) we have neglected powers of $\alpha_{\lambda\mu}$ higher than the first since we are considering only small deformations of the surface. The first term in (3.3) contains only neutron coordinates while the second term contains both neutron and collective coordinates. It is worth while, then, to rewrite the Hamiltonian as follows:

$$H = H_N(r) + H_T(\alpha_{\lambda\mu}) + H_{int}(\alpha_{\lambda\mu},\vec{r}) \;, \tag{3.4}$$

where

$$H_N(r) = -\frac{\hbar^2}{2m}\nabla^2 + \bar{V}(r) \quad , \tag{3.5}$$

and

$$H_{int}(\alpha_{\lambda\mu}, \vec{r}) = -RV_0(1+\lambda\xi)\delta(r-R)\sum_{\lambda\mu}\alpha_{\lambda\mu}Y_{\lambda\mu}(\theta,\phi) \tag{3.6}$$

H_N is now the Hamiltonian of the incident neutron and has been written so as to include the interaction of the neutron with the undeformed nucleus. This is exactly the Hamiltonian used in the FPW calculations, and we shall see the analytical advantages of writing the Hamiltonian in this way. H_{int} is the neutron-nucleus interaction potential, and because of the square well potential, the delta function gives rise to a surface interaction.

For the present discussion we will consider quadrupole oscillations only. Therefore, the sum over λ and μ in (3.6) is restricted to $\lambda = 2$, and $|\mu| \leq 2$ corresponding to the five degrees of freedom associated with this degeneracy. Subsequently, in the development of the strength function we will examine the octupole as well as the quadrupole effect, and in that case we will expand the formalism so as to include $\lambda = 3$.

It is clear from (3.6) that only the total angular momentum is a good quantum number. In the present work we shall restrict ourselves to even-even targets, that is to targets with initial target spin $I = 0$. We now construct states of good total angular momentum, J. For the incoming partial wave the orbital angular momentum is equal to J because

the target spin, I, is initially zero. The z component of the total angular momentum will be denoted by M which we take equal to zero from azimuthal symmetry. The wave function, ψ^J , is given by

$$\psi^J = \sum_{\substack{l' \\ I'=0,2}} \frac{1}{r} u^J_{l'I'}(r)\, \mathcal{Y}^0_{Jl'I'}(\theta, \phi, \alpha_{\lambda\mu}) \;, \tag{3.7}$$

where we have considered for the time being only the coupling to the one phonon collective state of spin 2^+.

The $\mathcal{Y}^0_{Jl'I'}$'s contain the entire angular dependence as well as the dependence on collective coordinates. Explicitly,

$$\mathcal{Y}^0_{Jl'I'}(\theta,\phi,\alpha_{\lambda\mu}) = \sum_m C_{l'I'}(m,-m|J0)\, Y_{l'm}(\theta,\phi)\, \chi_{I',-m}(\alpha_{\lambda\mu}) \tag{3.8}$$

where $\chi_{I',-m}(\alpha_{\lambda\mu})$ are the target wave functions. The Schrodinger equation satisfied by these target wave functions is given by Equation (2.40). Adjusted to the present notation we have

$$H_T \chi_{I',-m}(\alpha_{\lambda\mu}) = \hbar\omega_{I'}\, \chi_{I'-m}(\alpha_{\lambda\mu}) \tag{3.9}$$

where we take the ground state $(I'=0)$ to have zero energy. The quantities $C_{l'I'}(m,-m|J0)$ are the usual Clebsch-Gordon coefficients for the composition of angular momentum where $\vec{J} = \vec{l'} + \vec{I'}$ and M = 0.

3.2 The Schrodinger Equation

Substitution of (3.4) and (3.7) into the Schrodinger equation, $H\psi^J = E\psi^J$,

yields the following set of differential equations:

$$\left(-\frac{\hbar^2}{2m}\nabla^2+\bar{V}(r)-E\right)\sum_{l'I'}\frac{1}{r}u^J_{l'I'}\mathcal{Y}^0_{Jl'I'}+\sum_{l'}\frac{\hbar\omega_2}{r}u^J_{l'2}\mathcal{Y}^0_{Jl'2}=$$

$$\sum_{\mu l'I'}\frac{1}{r}u^J_{l'I'}RV_0(1+\lambda\xi)\delta(r-R)\mathcal{Y}_{2\mu}\alpha_{2\mu}\mathcal{Y}^0_{Jl'I'}\,, \tag{3.10}$$

where we have made use of (3.9).

The solution of Equation (3.10) was carried out in the following manner. If we multiply (3.10) by χ^*_{00} and integrate over the target coordinates, we obtain:

$$\left(-\frac{\hbar^2}{2m}\nabla^2+\bar{V}(r)-E\right)\frac{1}{r}u^J_{J0}C_{J0}(0,0|J0)\mathcal{Y}_{J0}=$$

$$\sum_{\mu l'I'}\frac{1}{r}u^J_{l'I'}RV_0(1+\lambda\xi)\delta(r-R)\mathcal{Y}_{2\mu}\sum_m C_{l'I'}(m,-m|J0)\langle 00|\alpha_{2\mu}|I'-m\rangle\mathcal{Y}_{l'm}\,. \tag{3.11}$$

The interaction term on the right side of the equality gives rise to coupled equations since the $\alpha_{2\mu}$ as given by Equation (2.28) is a combination of creation and annihilation operators for one phonon. Because of the restriction on the matrix element to values of I' = 2, we can rewrite (3.11) as follows:

$$\left(-\frac{\hbar^2}{2m}\nabla^2+\bar{V}(r)-E\right)\frac{1}{r}u^J_{J0}C_{J0}(00|J0)\mathcal{Y}_{J0}=$$

$$\sum_{ml'}\frac{1}{r}u^J_{l'2}RV_0(1+\lambda\xi)\delta(r-R)\mathcal{Y}_{2,-m}C_{l'2}(m,-m|J0)\langle 00|\alpha_{2-m}|2-m\rangle\mathcal{Y}_{l'm}\,. \tag{3.12}$$

The equation akin to (3.12) can be obtained in an analogous manner by multiplying (3.10) by χ^{*}_{2-m} and integrating over the target coordinates. The resultant equation is

$$\left(-\frac{\hbar^2}{2m}\nabla^2+\bar{V}(r)-E-\hbar\omega_2\right)\sum_{l'}\frac{1}{r}u^J_{l'2}C_{l'2}(m'_1,-m'|J0)Y_{l'm'} =$$

$$\sum_{\substack{\mu l' \\ I'm}}\frac{1}{r}u^J_{l'I'}R\beta_0(1+\alpha\xi)\delta(r-R)Y_{2\mu}\langle 2_1,-m'|\alpha_{2\mu}|I'_1,-m\rangle C_{l'I'}(m_1,m)J0)Y_{l'm}\,. \tag{3.13}$$

We are now restricted on the right hand side of (3.13) to the values I' = 0 amd m = 0. Further since I' = 0, it follows that $J = l'$, and, in turn, $\mu = m'$ from the target matrix element. We can therefore, rewrite (3.13) as

$$\left(-\frac{\hbar^2}{2m}\nabla^2+\bar{V}(r)-E-\hbar\omega_2\right)\sum_{l'}\frac{1}{r}u^J_{l'2}C_{l'2}(m'_1,-m'|J0)Y_{l'm'} =$$

$$\frac{1}{r}u^J_{J0}R\beta_0(1+\alpha\xi)\delta(r-R)Y_{2m'}Y_{J0}C_{J0}(00|J0)\langle 2_1,m'|\alpha_{2m'}|00\rangle\,. \tag{3.14}$$

Equations (3.12) and (3.14) can be further reduced by multiplying by the appropriate complex conjugate spherical harmonic and integrating over the angular dependence. For each value of J there is a set of coupled differential equations between $u^J_{J0}(r)$ and $u^J_{l'2}(r)$. These equations are developed in Appendix I. It was found that values of $J \leq 8$ were needed in consideration of the cross sections up to 10 Mev.

3.3 Cross Sections with Collective Effects

Before proceeding further it will be useful to write down the cross sections that we will be using in this work. For the purposes of this

thesis we will not be concerned with the explicit contributions to the cross sections of the direct scattering, the mechanism for which having been introduced via the possibility for collective excitation. We wish only to compare the effect of collective excitations on the cross sections that were calculated with the FPW model. For this purpose we need the, yet to be defined, total reaction cross section, the shape elastic cross section, and the differential shape elastic cross section.

Because of our model the total reaction cross section now takes into account the direct inelastic scattering of the I' = 2 collective state as well as the formation of the compound nucleus of the optical model. The cross section for compound nucleus formation is

$$\sigma_c = \frac{\pi}{k_0^2}\sum_{J=0}^{\infty}(2J+1)\left(1-\sum_{l'I'}|\eta_{l'I'}^{J}|^2\right) \quad . \tag{3.15}$$

The cross section for shape elastic scattering (I' = 0) and direct inelastic scattering (I' = 2) is

$$\sigma_{I'} = \frac{\pi}{k_0^2}\sum_{J=0}^{\infty}\sum_{l'=0}^{\infty}(2J+1)\left|\delta_{I'0}\delta_{lJ}-\eta_{l'I'}^{J}\right|^2 \quad . \tag{3.16}$$

The total reaction cross section is, therefore,

$$\sigma_R = \sigma_2+\sigma_c = \frac{\pi}{k_0^2}\sum_{J}(2J+1)\left(1-|\eta_{J0}^{J}|^2\right) \quad . \tag{3.17}$$

The total cross section is the sum of the total reaction cross section of (3.17) and the shape elastic cross section (I' = 0) of (3.16). In comparing

with the FPW cross sections of Section 2.2 we see that $\eta^{J}_{J_0}$ replaces η_ℓ, but otherwise the cross sections which we have specified as being of interest are identical.

3.4 Logarithmic Derivative (J = 0)

For J = 0 there are just two coupled equation which are

$$\left[\frac{d^2}{dr^2} - \frac{6}{r^2} - \frac{2m}{\hbar^2}\bar{V}(r) + \frac{2m}{\hbar^2}(E-\hbar\omega_2)\right] u^0_{22}(r) = - \frac{2m}{\hbar^2}\sqrt{\frac{5}{4\pi}}\sqrt{\frac{\hbar\omega_2}{2C_2}}\, R V_0 (1+\alpha\xi)\,\delta(r-R)\, u^0_{00}(r)\,, \tag{3.18}$$

and

$$\left[\frac{d^2}{dr^2} - \frac{2m}{\hbar^2}\bar{V}(r) + \frac{2m}{\hbar^2}E\right] u^0_{00}(r) = - \frac{2m}{\hbar^2}\sqrt{\frac{5}{4\pi}}\sqrt{\frac{\hbar\omega_2}{2C_2}}\, R V_0 (1+\alpha\xi)\,\delta(r-R)\, u^0_{22}(r) \tag{3.19}$$

from Equations (I.7) and (I.8) of Appendix I. We can integrate (3.18) and (3.19) from R - Δ to R + Δ, and then let $\Delta \to 0$. Because of the δ function surface interaction the results are simply

$$R\left.\frac{du^0_{22}}{dr}\right|_{R^+} - R\left.\frac{du^0_{22}}{dr}\right|_{R^-} = - \frac{2m}{\hbar^2}\sqrt{\frac{5}{4\pi}}\sqrt{\frac{\hbar\omega_2}{2C_2}}\, R V_0 (1+\alpha\xi)\, R\, u^0_{00}(R) \tag{3.20}$$

and

$$R\left.\frac{du^0_{00}}{dr}\right|_{R^+} - R\left.\frac{du^0_{00}}{dr}\right|_{R^-} = - \frac{2m}{\hbar^2}\sqrt{\frac{5}{4\pi}}\sqrt{\frac{\hbar\omega_2}{2C_2}}\, R V_0 (1+\alpha\xi)\, R\, u^0_{22}(R)\,, \tag{3.21}$$

where R_+ and R_- are the limits of the values when approached from outside

and inside the nucleus, respectively. If we divide (3.20) by $u^0_{22}(R)$ and (3.21) by $u^0_{00}(R)$, we obtain expressions for the discontinuities in the logarithmic derivatives, that is,

$$\Delta f^0_{22} = \frac{R}{u^0_{22}(R)}\left[\left.\frac{du^0_{22}}{dr}\right|_{R+} - \left.\frac{du^0_{22}}{dr}\right|_{R-}\right] = -\frac{2m}{\hbar^2}\sqrt{\frac{5}{4\pi}}\sqrt{\frac{\hbar\omega_2}{2C_2}}\, R^2 V_0(1+\lambda\xi)\frac{u^0_{00}(R)}{u^0_{22}(R)} \qquad (3.22)$$

and

$$\Delta f^0_{00} = \frac{R}{u^0_{00}(R)}\left[\left.\frac{du^0_{00}}{dr}\right|_{R+} - \left.\frac{du^0_{00}}{dr}\right|_{R-}\right] = -\frac{2m}{\hbar^2}\sqrt{\frac{5}{4\pi}}\sqrt{\frac{\hbar\omega_2}{2C_2}}\, R^2 V_0(1+\lambda\xi)\frac{u^0_{22}(R)}{u^0_{00}(R)} \,. \qquad (3.23)$$

These equations are easily solved, and we have

$$\Delta f^0_{00} = \left(\frac{2m}{\hbar^2}\right)^2 R^4 V_0^2 (1+\lambda\xi)^2 \frac{\hbar\omega_2}{8\pi C_2}\frac{5}{\Delta f^0_{22}} \,. \qquad (3.24)$$

Now, Δf^0_{22} is particularly easy to write down since there are only outgoing waves for I' = 2. For r greater than the maximum extent of the potential, the radial wave functions have the form

$$r > R: \quad \frac{1}{r}u^J_{l'2} = \sqrt{\frac{k_0}{k_2}}\,\gamma^J_{l'2}\, h^{(1)}_{l'}(k_2 r) \quad ; \; I' = 2 \,, \qquad (3.25)$$

and

$$r > R: \quad \frac{1}{r}u^J_{J0} = \gamma^J_{J0}\, h^{(1)}_J(k_0 r) + h^{(2)}_J(k_0 r) \quad ; \; I' = 0 \,, \qquad (3.26)$$

where $h^{(1)}_l$ and $h^{(2)}_l$ are the usual outgoing and incoming spherical Hankel Functions. The wave numbers k_0 and k_2 are given by

$$k_0^2 = \frac{2m}{\hbar^2} E \tag{3.27}$$

and

$$k_2^2 = \frac{2m}{\hbar^2}(E - \hbar\omega_2) . \tag{3.28}$$

The radial wave functions inside r can be written

$$r < R : \quad \frac{1}{r} u^J_{l'2}(K_2 r) = A^J_{l'2}\, j_{l'}(K_2 r) \quad ; \; I' = 2 \quad , \tag{3.29}$$

and

$$r > R : \quad \frac{1}{r} u^J_{J0}(K_0 r) = B^J_{J0}\, j_J(K_0 r) \quad ; \; I' = 0 \quad , \tag{3.30}$$

where j_l is the usual spherical Bessel function,

$$K_0^2 = \frac{2m}{\hbar^2}\left[E + V_0(1+\lambda\xi)\right] \quad , \tag{3.31}$$

and

$$K_2^2 = \frac{2m}{\hbar^2}\left[E - \hbar\omega_2 + V_0(1+\lambda\xi)\right] . \tag{3.32}$$

Utilizing expressions (3.25) and (3.29), we obtain

$$\Delta f^0_{J22} = y \frac{h_2^{(1)}(y)}{h_2^{(1)}(y)} - \gamma \frac{j_2'(\gamma)}{j_2(\gamma)} \tag{3.33}$$

where

$$y = k_2 R \tag{3.34}$$

and

$$Y = K_2 R \tag{3.35}$$

The prime denotes differentiation with respect to the arguments y and Y, respectively. We can rewrite (3.33) using the expressions for $\Delta_\ell + i S_\ell$ and f_ℓ as presented in Chapter 2 but expanded so as to include the present notation and the appropriate arguments. We have, therefore, that

$$\Delta f^0_{22}(y,Y) = \Delta_2(y) + i S_2(y) - f_2(Y) \tag{3.36}$$

Using (2.18), (3.24), and (3.36) we can write the expression for the logarithmic derivative, f^0_{00}, of our problem:

$$f^0_{00}(X,y,Y) = f_0(X) + \left(\frac{2m}{\hbar^2}\right)^2 R^4 V_0^2 (1+i\xi)^2 \frac{\hbar\omega_2}{8\pi C_2} \frac{5}{\Delta_2(y) + i S_2(y) - f_2(Y)} \tag{3.37}$$

where $f_0(X)$ is the ($\ell = 0$) logarithmic derivative of the square well optical model of the FPW problem, that is, with no collective effects considered. $f^0_{00}(X,y,Y)$ is the ($J = 0$) logarithmic derivative corresponding to leaving the target in an unexcited state and is, therefore, exactly comparable to $f_0(X)$. The correction term due to collective effects is, therefore, simply related to the d-wave discontinuity in the

logarithmic derivative and is due to the δ function surface interaction.

3.5 Logarithmic Derivatives ($0 < J \leq 8$)

The other logarithmic derivatives of interest for this problem are f^1_{10}, f^2_{20}, f^3_{30}, f^4_{40}, f^5_{50}, f^6_{60}, f^7_{70}, and f^8_{80}, and evaluation is similar to that of f^0_{00} as calculated in Section 3.4.

For $J = 1$ there are three coupled equations given by (I.12), (I.13), and (I.14). The integration across the surface is carried out as was done in (3.20) and (3.21) for $J = 0$, and then the equations can be solved to give

$$\Delta f^1_{10} = \left(\frac{2m}{\hbar^2}\right)^2 R^4 V_0^2 (1+\lambda\xi)^2 \frac{\hbar\omega_2}{8\pi C_2}\left[\frac{2}{\Delta f^1_{12}} + \frac{3}{\Delta f^1_{32}}\right] \tag{3.38}$$

Here, again, the discontinuities in f^1_{12} and f^1_{32} are easily obtained because there are only outgoing waves for $I' = 2$. We have then that

$$f^1_{10}(X,y,Y) = f_1(X) + X_0^4 \frac{\hbar\omega_2}{8\pi C_2}\left[\frac{2}{\Delta_1(y)+\lambda S_1(y) - f_1(Y)} + \frac{3}{\Delta_3(y)+\lambda S_3(y) - f_2(Y)}\right], \tag{3.39}$$

where we have introduced the simplified notation that

$$X_0^2 = \frac{2m}{\hbar^2} R^2 V_0 (1+\lambda\xi) \tag{3.40}$$

For each $J \geq 2$ there are four coupled equations given in Appendix I. Proceeding as before we obtain

$$f^2_{20}(X,y,Y) = f_2(X) + X_0^4 \frac{\hbar\omega_2}{8\pi C_2}\left[\frac{1}{\Delta f^2_{02}(y,Y)} + \frac{10/7}{\Delta f^2_{22}(y,Y)} + \frac{18/7}{\Delta f^2_{42}(y,Y)}\right] \tag{3.41}$$

$$f^3_{30}(X,y,Y)=f_3(X)+X_0^4\frac{\hbar\omega_2}{8\pi C_2}\left[\frac{9/7}{\Delta f^3_{12}(y,Y)}+\frac{4/3}{\Delta f^3_{32}(y,Y)}+\frac{50/21}{\Delta f^3_{52}(y,Y)}\right], \quad (3.42)$$

$$f^4_{40}(X,y,Y)=f_4(X)+X_0^4\frac{\hbar\omega_2}{8\pi C_2}\left[\frac{10/7}{\Delta f^4_{22}(y,Y)}+\frac{100/77}{\Delta f^4_{42}(y,Y)}+\frac{25/11}{\Delta f^4_{62}(y,Y)}\right], \quad (3.43)$$

$$f^5_{50}(X,y,Y)=f_5(X)+X_0^4\frac{\hbar\omega_2}{8\pi C_2}\left[\frac{50/33}{\Delta f^5_{32}(y,Y)}+\frac{50/39}{\Delta f^5_{52}(y,Y)}+\frac{315/143}{\Delta f^5_{72}(y,Y)}\right], \quad (3.44)$$

$$f^6_{60}(X,y,Y)=f_6(X)+X_0^4\frac{\hbar\omega_2}{8\pi C_2}\left[\frac{225/143}{\Delta f^6_{42}(y,Y)}+\frac{14/11}{\Delta f^6_{62}(y,Y)}+\frac{28/13}{\Delta f^6_{82}(y,Y)}\right], \quad (3.45)$$

$$f^7_{70}(X,y,Y)=f_7(X)+X_0^4\frac{\hbar\omega_2}{8\pi C_2}\left[\frac{21/13}{\Delta f^7_{52}(y,Y)}+\frac{280/221}{\Delta f^7_{72}(y,Y)}+\frac{36/17}{\Delta f^7_{92}(y,Y)}\right], \quad (3.46)$$

and

$$f^8_{80}(X,y,Y)=f_8(X)+X_0^4\frac{\hbar\omega_2}{8\pi C_2}\left[\frac{28/17}{\Delta f^8_{62}(y,Y)}+\frac{24/19}{\Delta f^8_{82}(y,Y)}+\frac{675/323}{\Delta f^8_{10,2}(y,Y)}\right]. \quad (3.47)$$

The discontinuities of the logarithmic derivatives in the denominators of these equations all correspond to leaving the target in an excited state (I' = 2). There are, therefore, only outgoing waves and we can say in general that

$$\Delta f^J_{l'2}(y,Y)=y\frac{h^{(1)\prime}_{l'}(y)}{h^{(1)}_{l'}(y)}-Y\frac{f'_{l'}(Y)}{f_{l'}(Y)}, \quad (3.48)$$

which can be written

$$\Delta f^J_{l'2}(y,Y)=\Delta_{l'}(y)+\lambda S_{l'}(y)-f_{l'}(Y). \quad (3.49)$$

CHAPTER 4

RESULTS

4.1 Strength Function

The strength function was introduced and discussed at some length in Chapter 1. In this section we shall examine the effect on the strength function when collective quadrupole and octupole vibrations are considered.

In the low-energy region of well-spaced levels, the strength function is simply related to the cross section for the formation of the compound nucleus[4]:

$$\frac{\overline{\Gamma_n^0}}{D} = \frac{k_0^2}{2\pi^2}\,\sigma_c^{(0)} = \frac{2}{\pi}\,\frac{-\,\mathrm{Im}\,f_0(E)\,S_0(x)}{[\mathrm{Re}\,f_0(E)-\Delta S(x)]^2+[\mathrm{Im}\,f_0(E)-S_0(x)]^2} \qquad (4.1)$$

As we have seen, in order to take into account the effect of collective vibrations, we simply replace $f_0(E)$ by $f^0_{00}(E,y,\nu)$, but now we wish to modify f^0_{00} to account for the octupole as well as the quadrupole excitation.

The Hamiltonian given in Equation (3.4) must now be adjusted to include the contribution from $\lambda=3$, and the wave function, ψ^J, of Equation (3.7) becomes

$$\psi^J = \sum_{l'=0}^{\infty}\sum_{I'=0,2,3}\frac{1}{\pi}u^J_{l'I'}(R)\,\mathcal{Y}^0_{l'I'J}(\theta,\phi,\alpha_{\lambda\mu}) \quad . \qquad (4.2)$$

This sum now includes the ground state and the first excited state or the one phonon state for both the quadrupole and the octupole excitations. The target wave functions still satisfy

$$H_T \chi_{I',-m} = \hbar\omega_{I'} \chi_{I',-m} \tag{4.3}$$

where now I' can be equal to 3 as well as 2, and the ground state (I' = 0) has zero energy as before.

The Schrodinger equation is solved in the same manner as previously and the resultant equation for f^0_{00} is

$$f^0_{00}(X, z_m, Z_m) = f_0(X) + \sum_{m=2,3} X_0^4 \frac{\hbar\omega_m}{8\pi C_m} \frac{2m+1}{\Delta_m(z_m) + iS_m(z_m) - f_m(Z_m)} , \tag{4.4}$$

where

$$z_m = k_m R = \sqrt{\frac{2m}{\hbar^2}(E - \hbar\omega_m)}\, R , \tag{4.5}$$

and

$$Z_m = K_m R = \sqrt{\frac{2m}{\hbar^2}\left[E - \hbar\omega_m + V_0(1+i\xi)\right]}\, R \tag{4.6}$$

C_n is the surface tension for the n^{th} multipole vibration; $m=2$ is the quadrupole and $m = 3$ is the octupole contribution. The denominator in (4.4) is the discontinuity in the logarithmic derivative for the d-wave and the f wave, respectively.

$\mathrm{Re}\, f^{0}_{00}(K, z_m, Z_m)$ and $\mathrm{Im}\, f^{0}_{00}(K, z_m, Z_m)$ were determined analytically and programmed on the IBM 1410 employing the recursion relations as indicated in Appendix II. The strength function with and without the collective effect was also calculated and a sampling of the results obtained is plotted in Figures 1 through 12. A discussion of these curves is presented in Chapter 5.

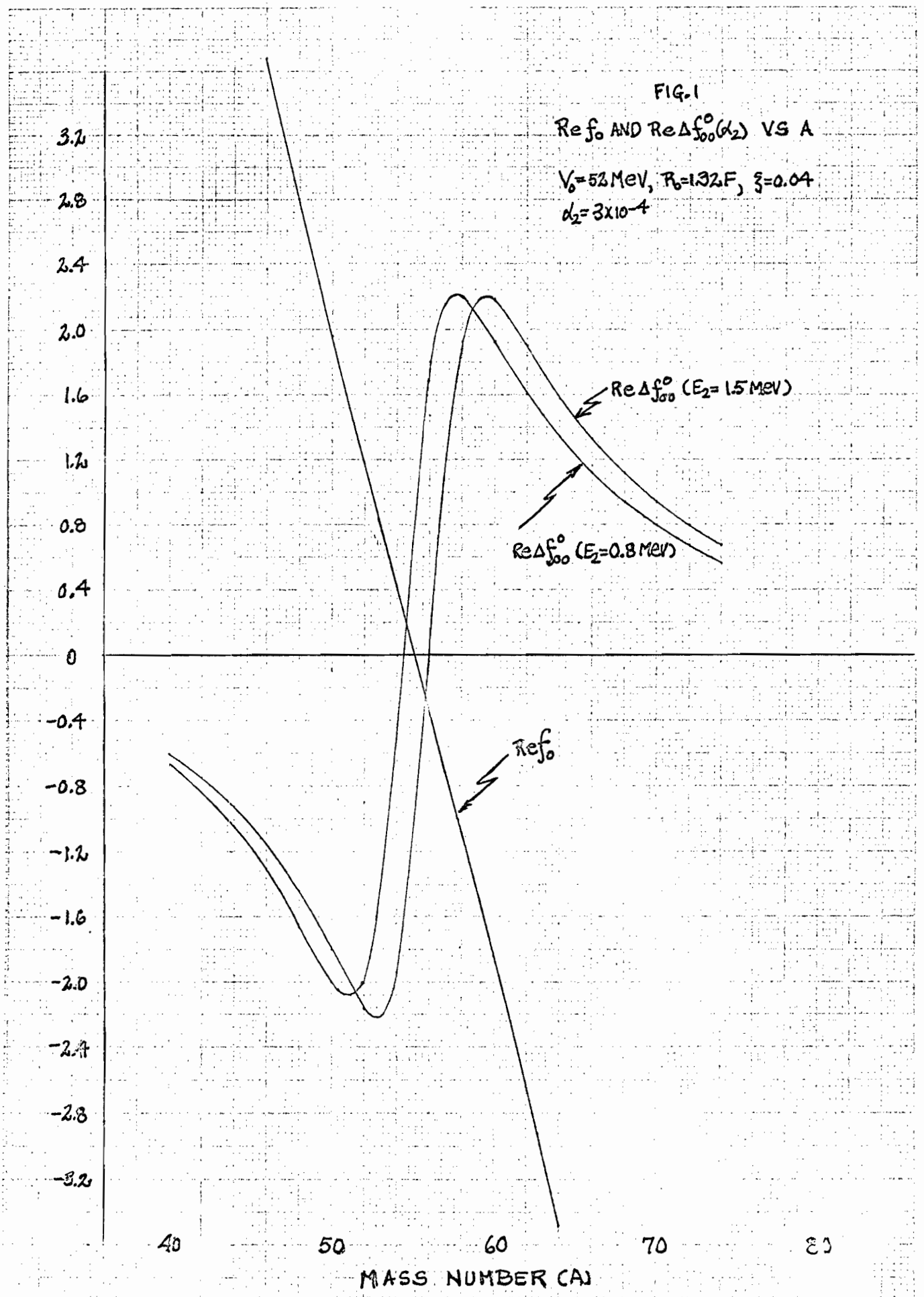
FIG. 1
Re f_0 AND Re $\Delta f^0_{00}(\alpha_2)$ VS A
V_0=52 MeV, R_0=1.32F, ξ=0.04
α_2=3X10-4
3.2
2.8
2.4
2.0
1.6
1.2
0.8
0.4
0
-0.4
-0.8
-1.2
-1.6
-2.0
-2.4
-2.8
-3.2
Re Δf^0_{00} (E_2= 1.5 MeV)
Re Δf^0_{00} (E_2=0.8 MeV)
Re f_0
40
50
60
70
MASS NUMBER (A)

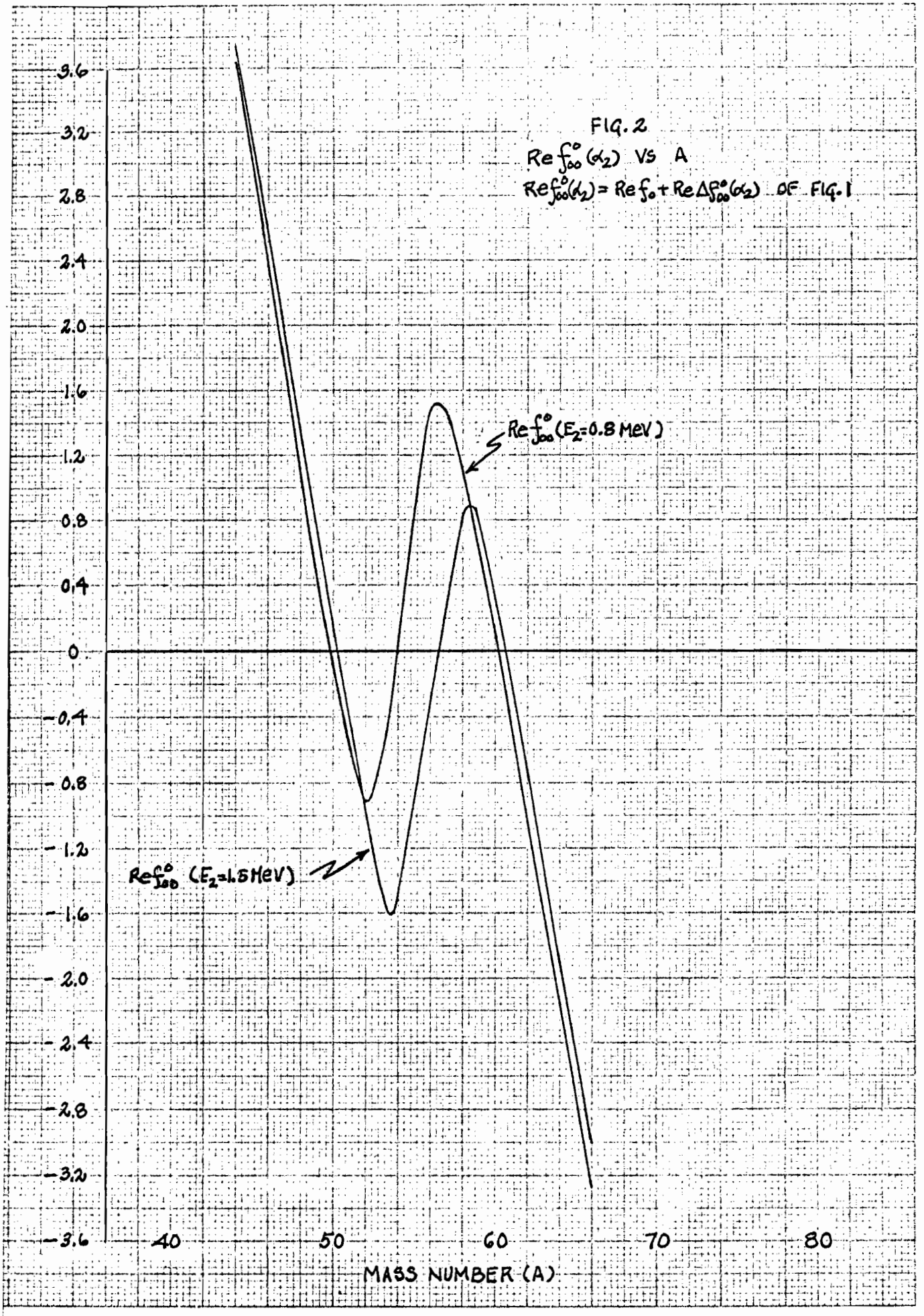
FIG. 2
$Re f^{0}_{00}(\alpha_2)$ VS A
$Re f^{0}_{00}(\alpha_2) = Re f_0 + Re \Delta f^{0}_{00}(\alpha_2)$ OF FIG. 1
$Re f^{0}_{00}$ (E_2=0.8 MeV)
$Re f^{0}_{00}$ (E_2=1.5 MeV)
3.6
3.2
2.8
2.4
2.0
1.6
1.2
0.8
0.4
0
-0.4
-0.8
-1.2
-1.6
-2.0
-2.4
-2.8
-3.2
-3.6
40
50
60
70
80
MASS NUMBER (A)

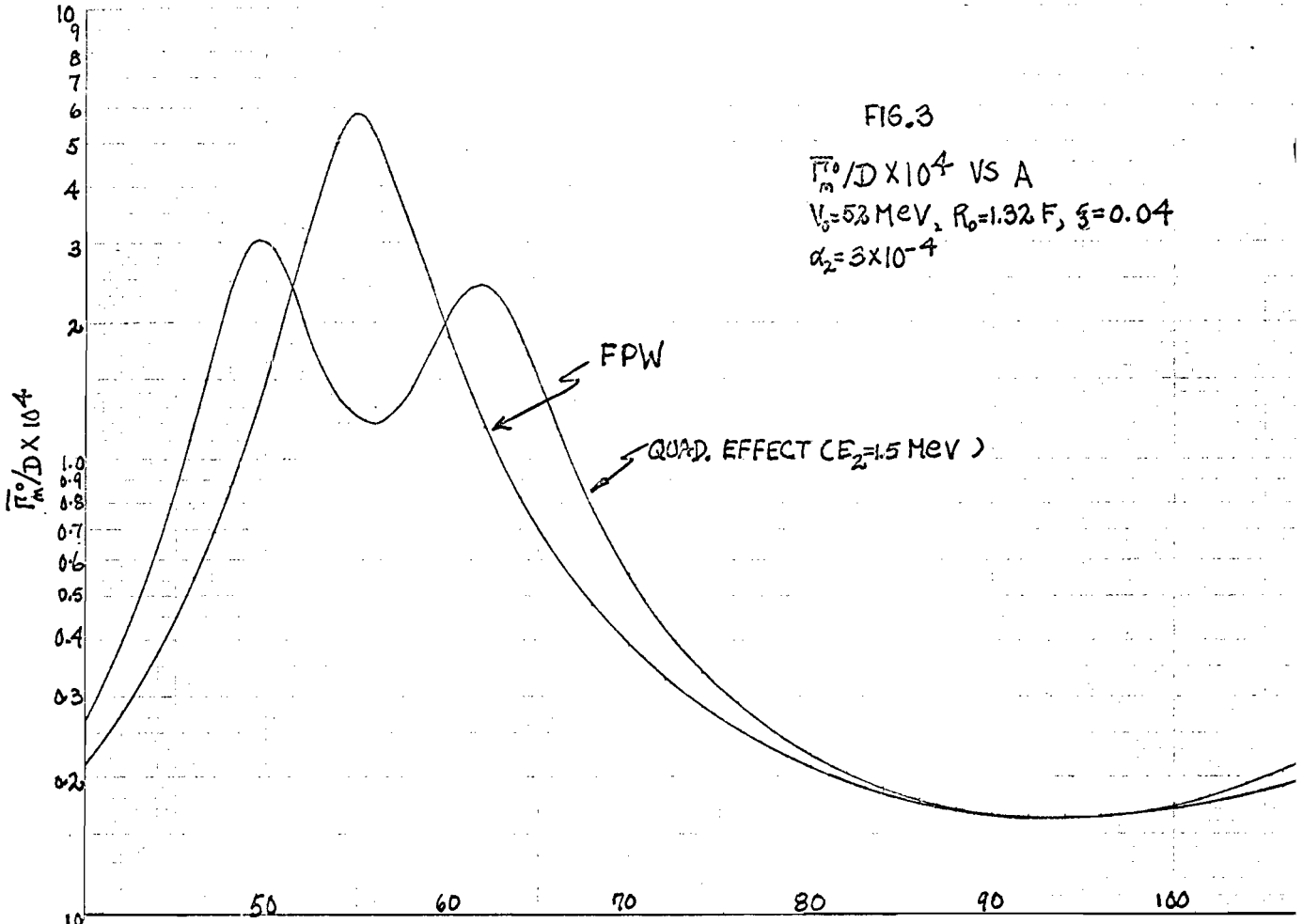
FIG.3
$\bar{\Gamma}_m^0/D \times 10^4$ VS A
V_0=52 MeV, R_0=1.32 F, ξ=0.04
$\alpha_2 = 3 \times 10^{-4}$
FPW
QUAD. EFFECT (E_2=1.5 MeV)
$\bar{\Gamma}_m^0/D \times 10^4$
A →

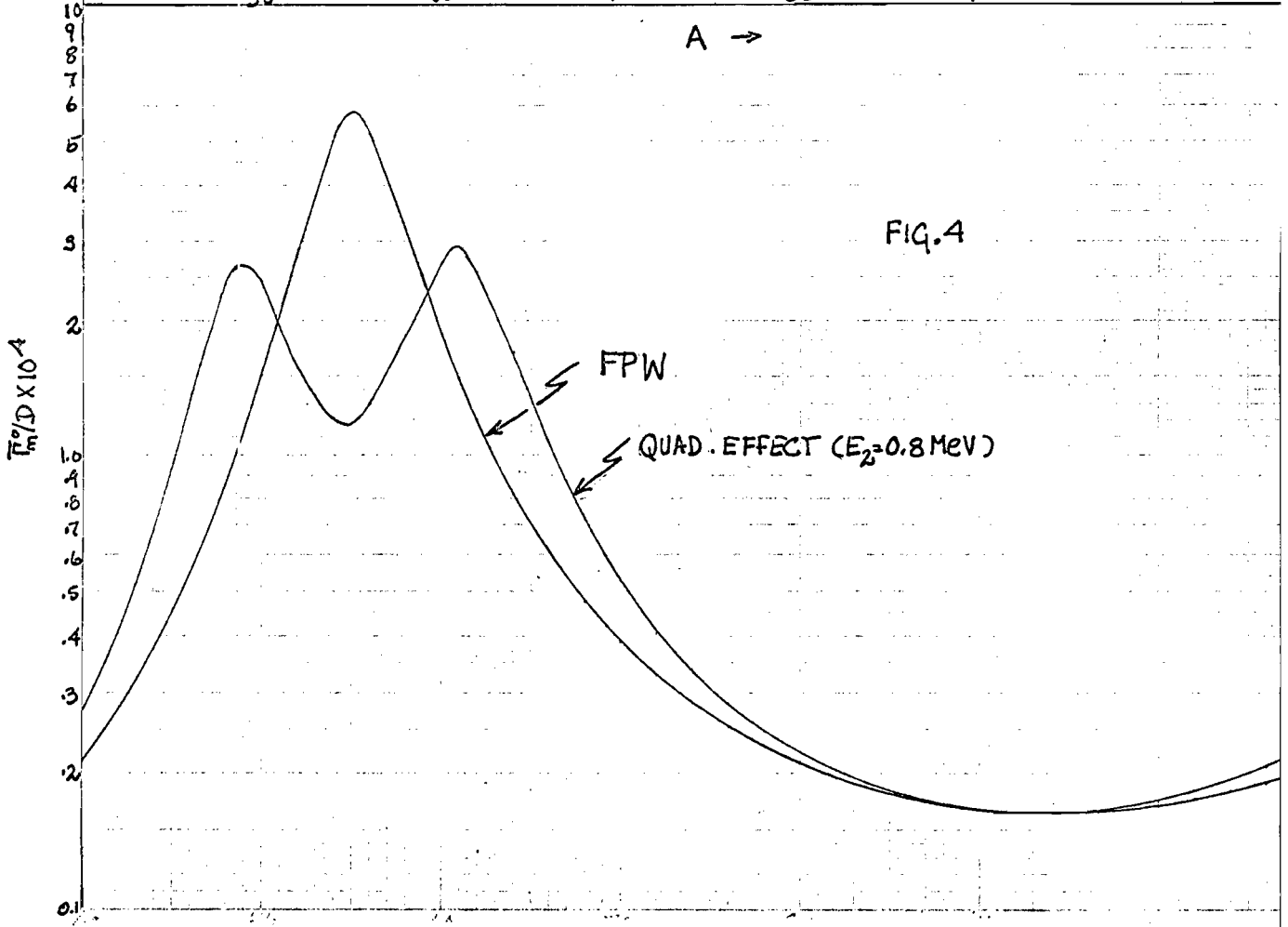
FIG.4
FPW
QUAD. EFFECT (E_2=0.8 MeV)
$\bar{\Gamma}_m^0/D \times 10^4$

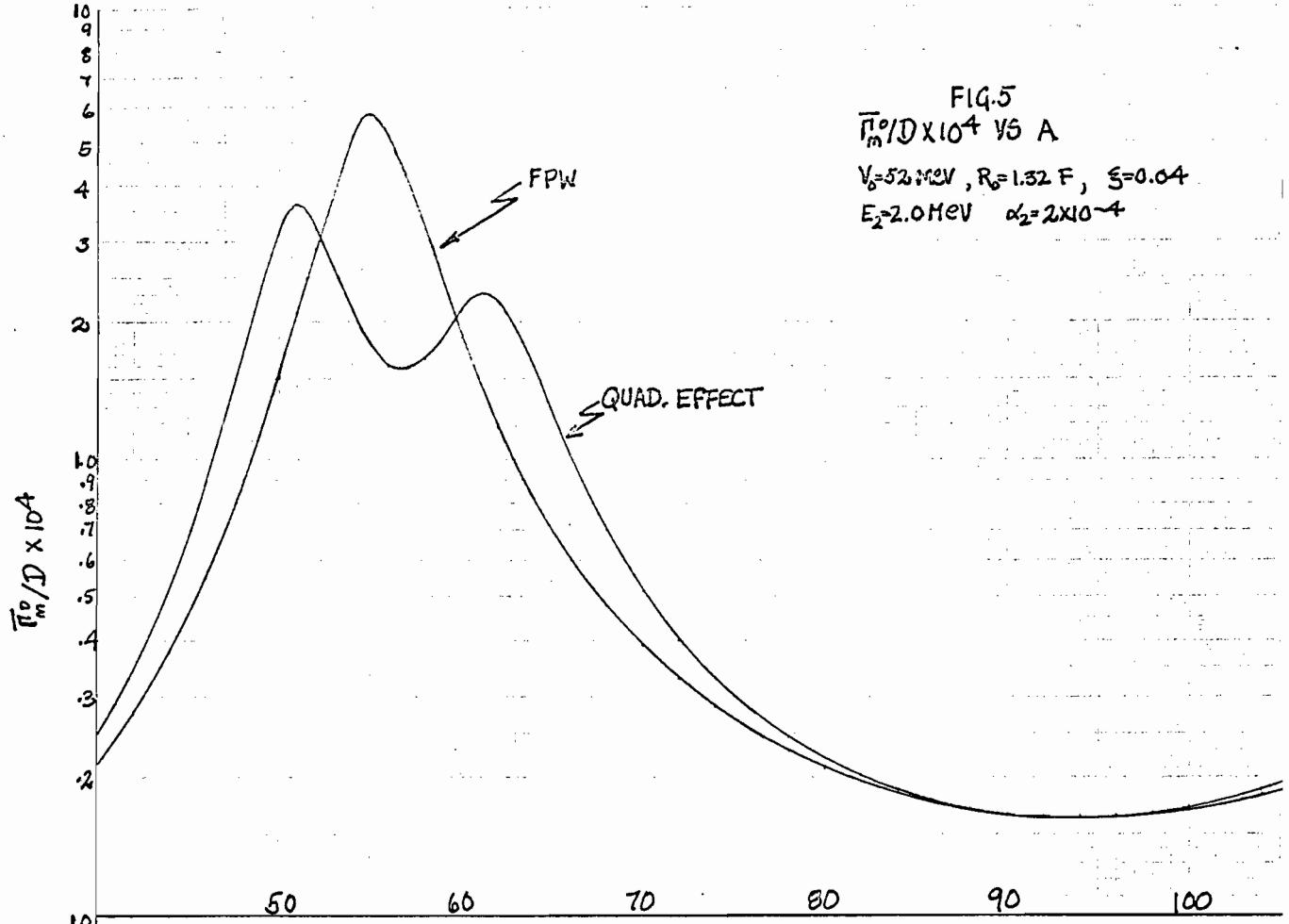

FIG.5
$\bar{\Gamma}^0_m/D \times 10^4$ VS A
V_0=52 MeV, R_0=1.32 F, ξ=0.04
E_2=2.0 MeV $\alpha_2 = 2 \times 10^{-4}$

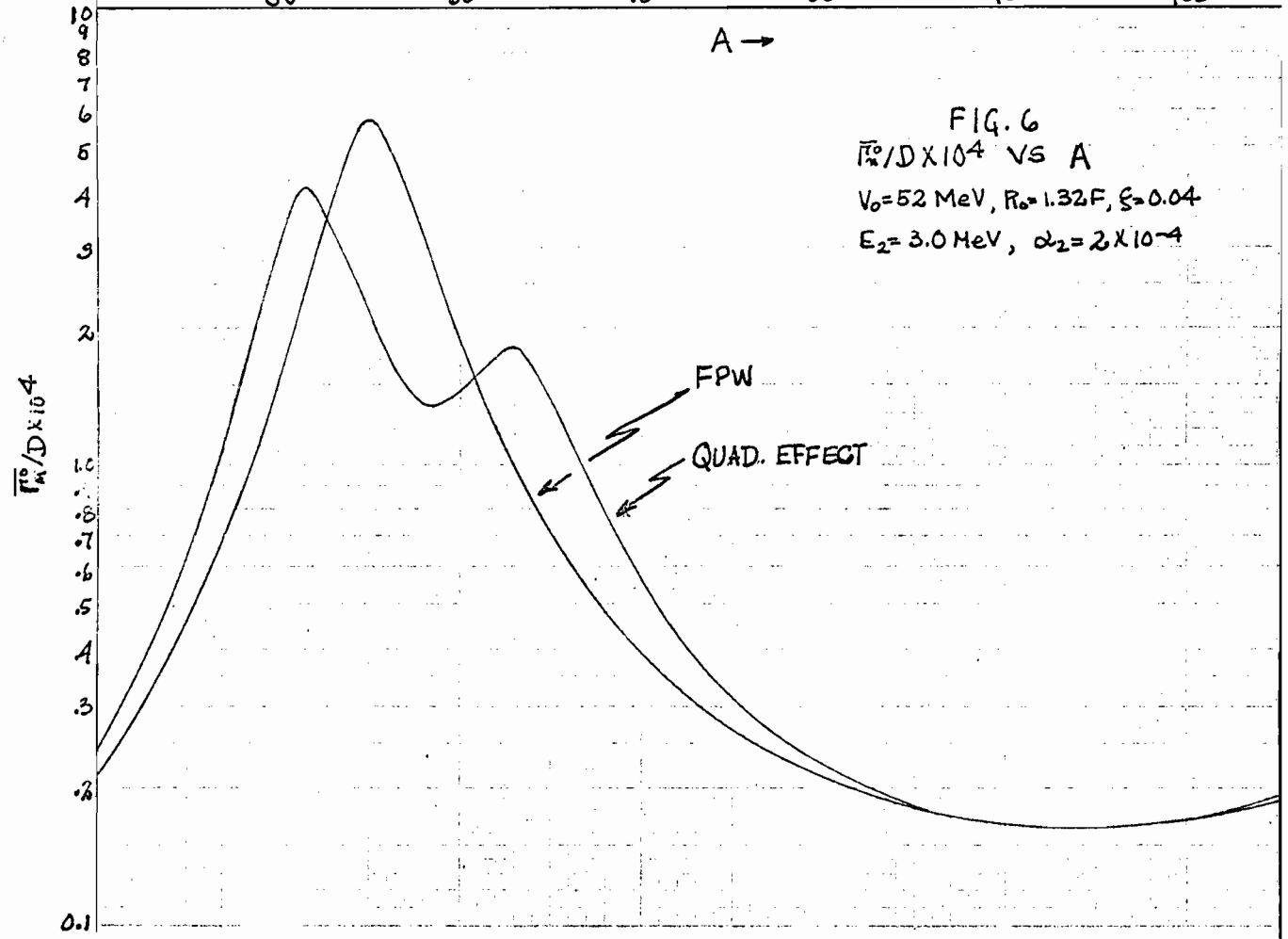

FIG. 6
$\bar{\Gamma}^0_m/D \times 10^4$ VS A
V_0=52 MeV, R_0=1.32F, ξ=0.04
E_2= 3.0 MeV, $\alpha_2 = 2 \times 10^{-4}$

FIG. 7

$Re f_0$, $Re \Delta f^0_{00}(\alpha_2)$, AND $Re \Delta f^0_{00}(\alpha_3)$ VS A

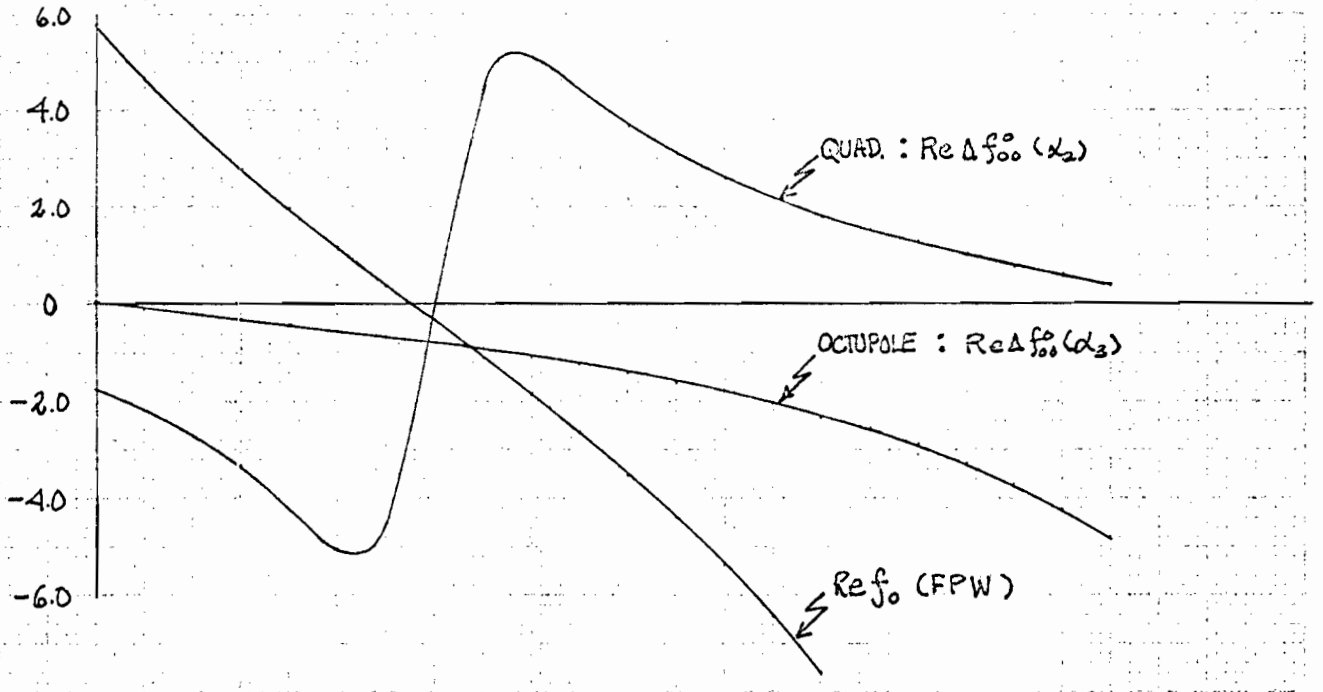

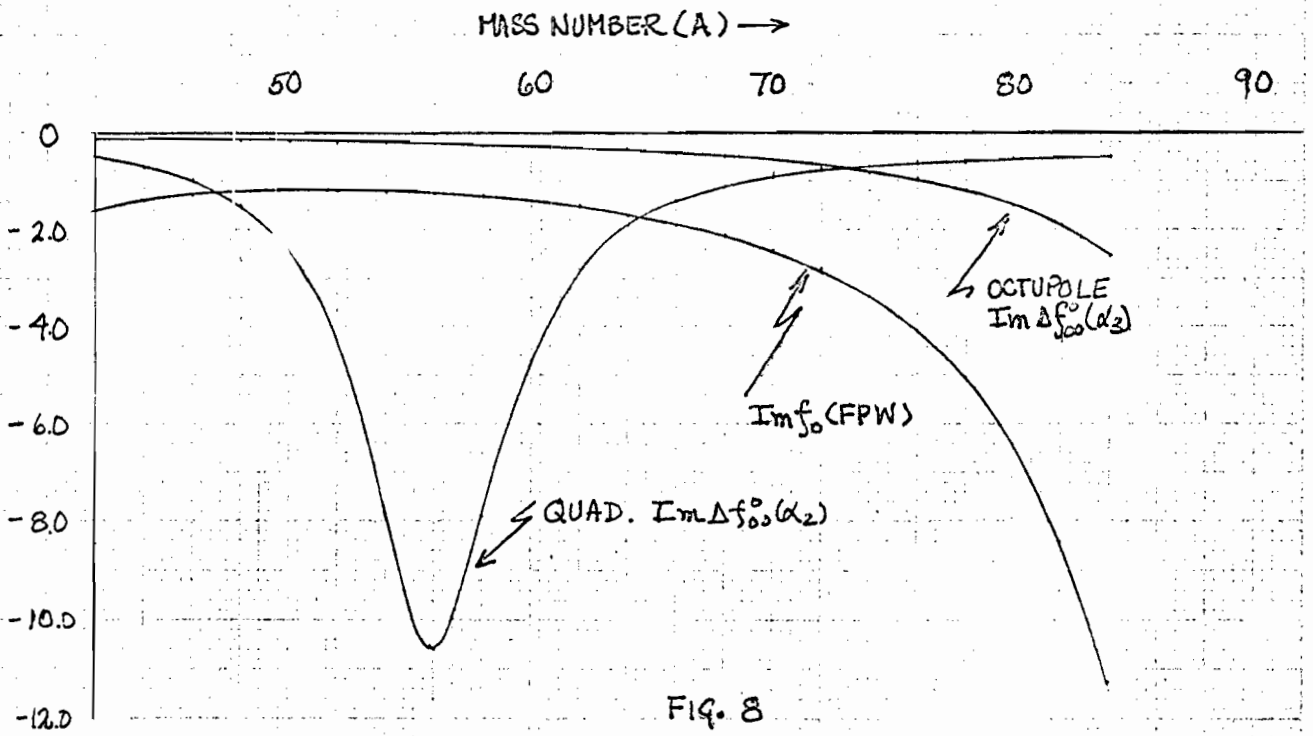

FIG. 8

$Im f_0$, $Im \Delta f^0_{00}(\alpha_2)$, AND $Im \Delta f^0_{00}(\alpha_3)$ VS A

FIG. 9

Re f°_{00} VS A

$\mathrm{Re}\, f^{\circ}_{00} = \mathrm{Re}\, f_0 + \sum_{m=2,3} \mathrm{Re}\, \Delta f^{\circ}_{00}(\alpha_m)$ of Fig. 7

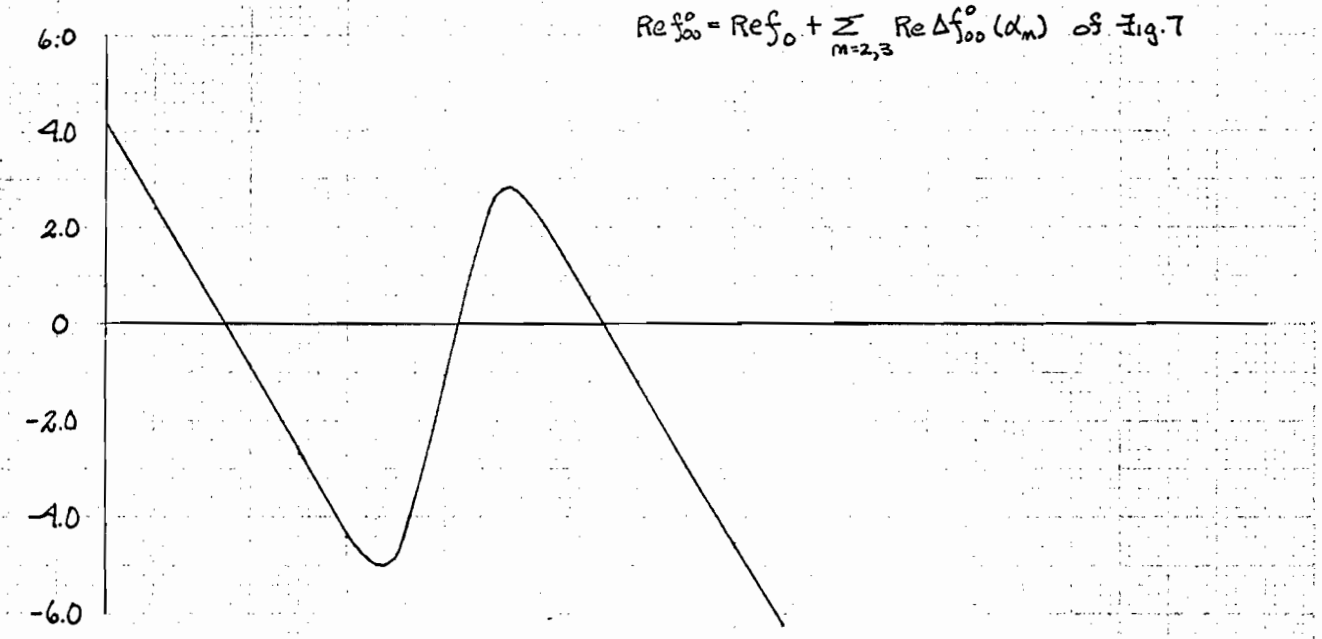

MASS NUMBER (A) →

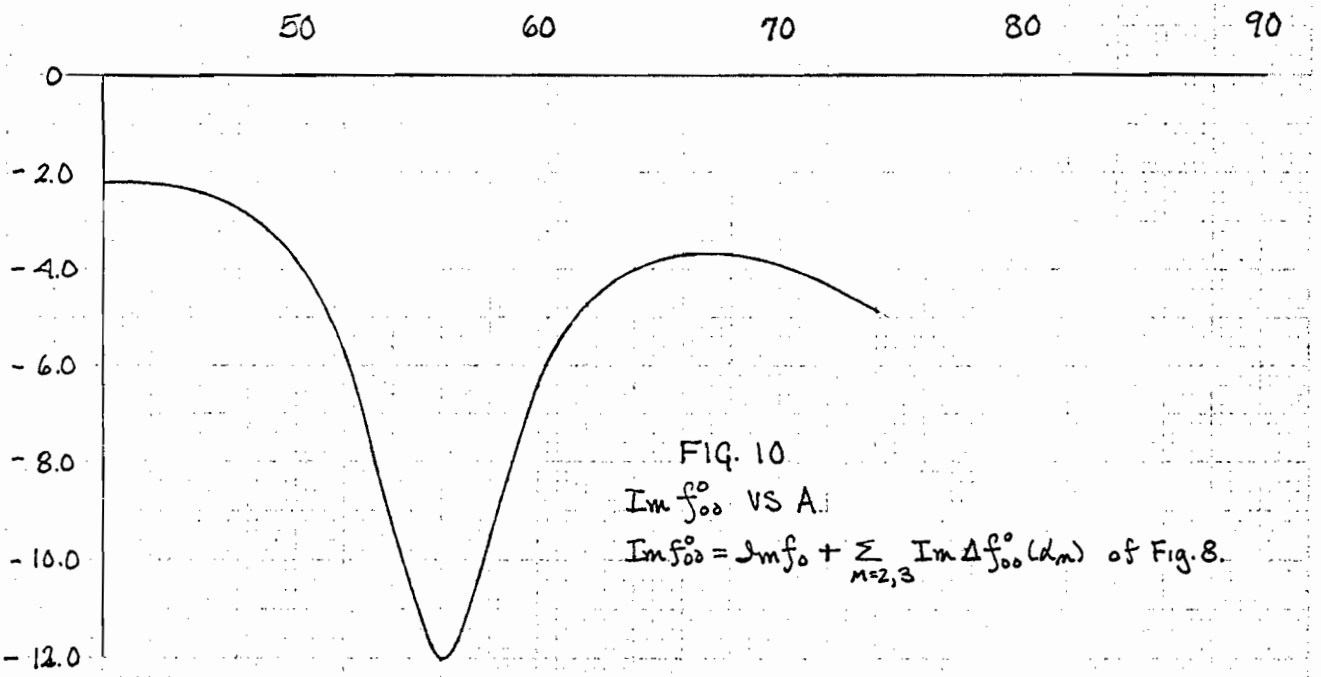

FIG. 10

Im f°_{00} VS A.

$\mathrm{Im}\, f^{\circ}_{00} = \mathrm{Im}\, f_0 + \sum_{m=2,3} \mathrm{Im}\, \Delta f^{\circ}_{00}(\alpha_m)$ of Fig. 8.

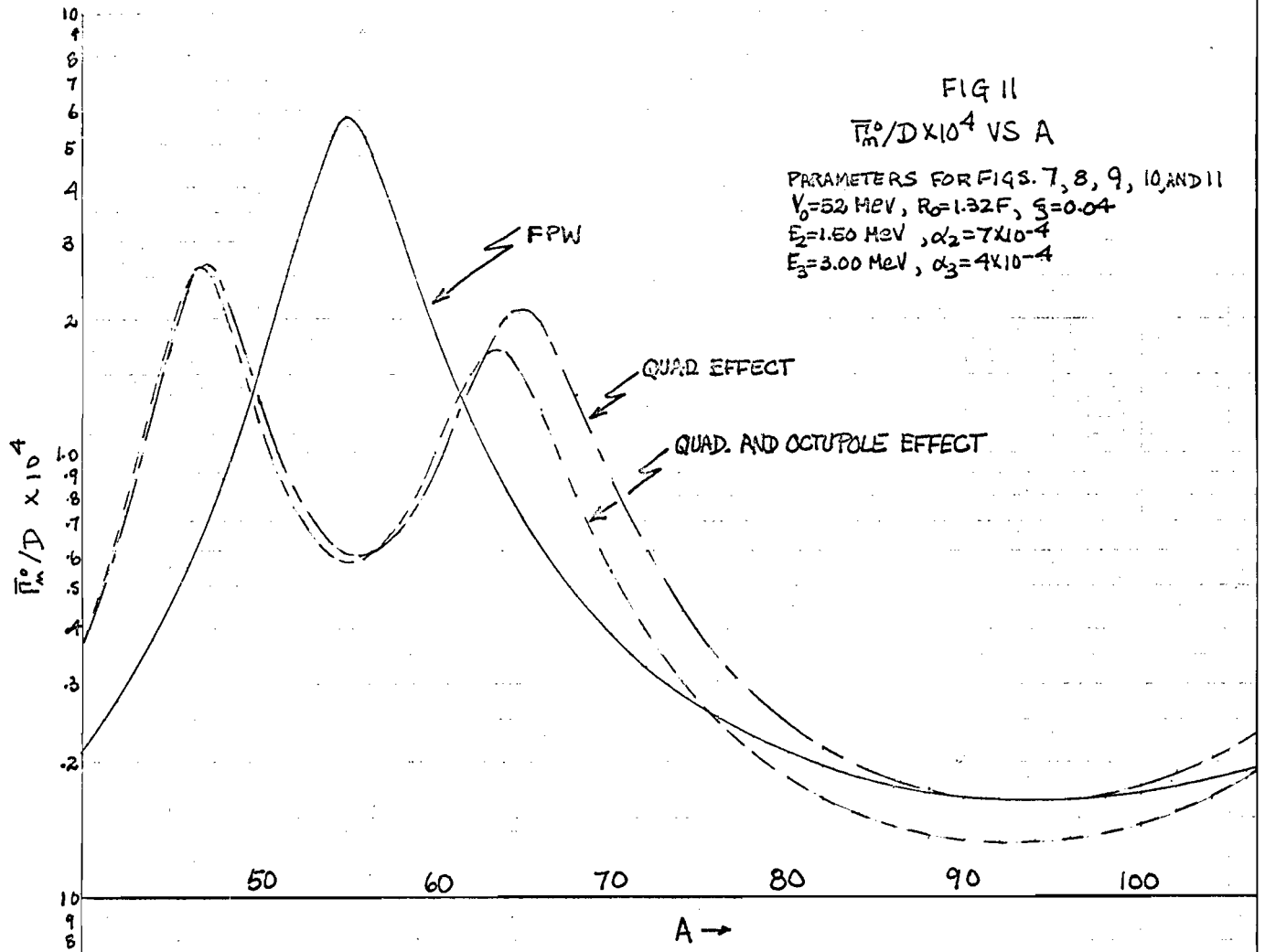

FIG 11

$\overline{\Gamma_m^0}/D \times 10^4$ VS A

PARAMETERS FOR FIGS. 7, 8, 9, 10, AND 11
V_0=52 MeV, R_0=1.32F, ξ=0.04
E_2=1.60 MeV, $\alpha_2 = 7 \times 10^{-4}$
E_3=3.00 MeV, $\alpha_3 = 4 \times 10^{-4}$

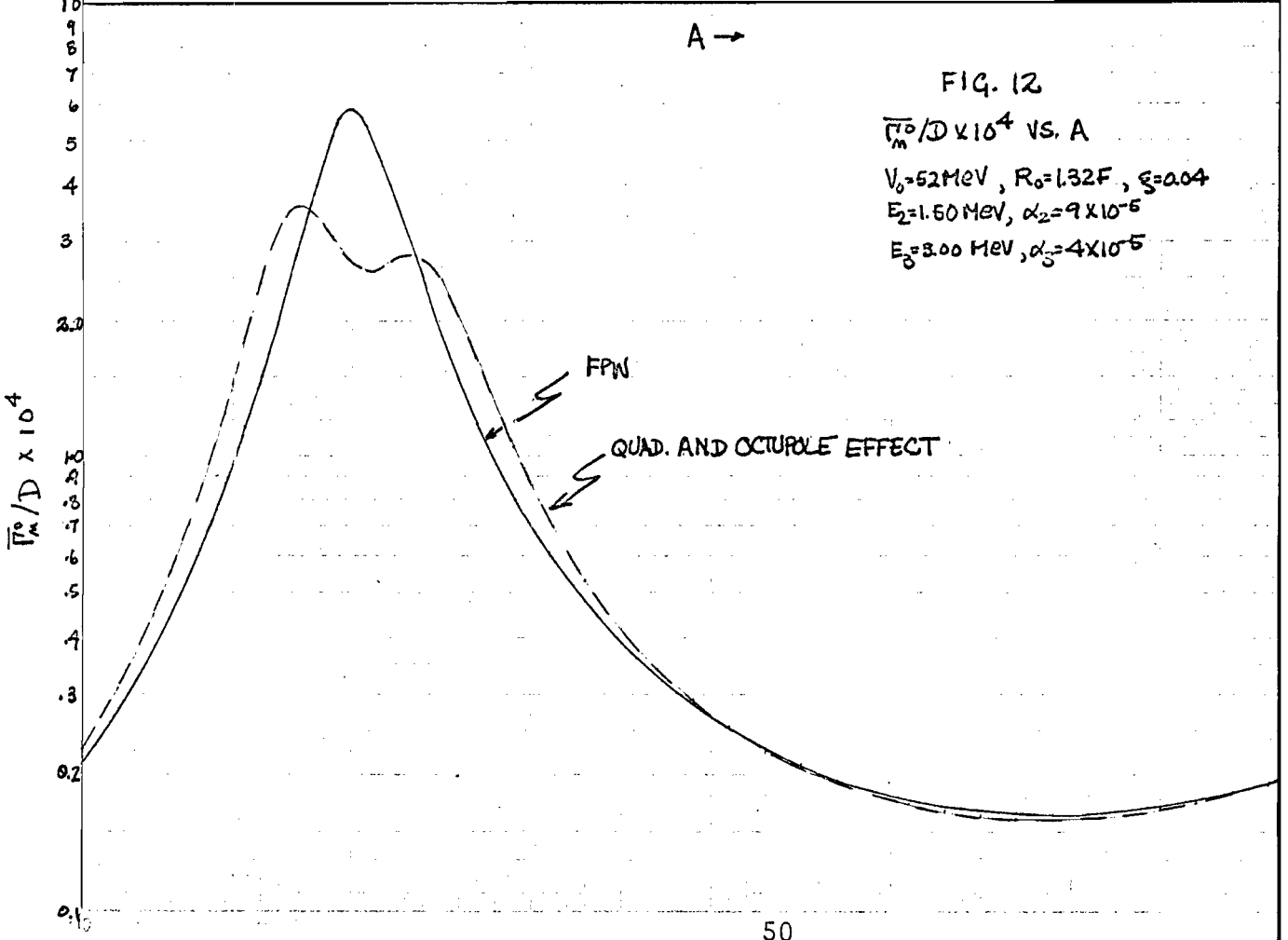

FIG. 12

$\overline{\Gamma_m^0}/D \times 10^4$ VS. A

V_0=52MeV, R_0=1.32F, ξ=0.04
E_2=1.60 MeV, $\alpha_2 = 9 \times 10^{-5}$
E_3=3.00 MeV, $\alpha_3 = 4 \times 10^{-5}$

4.2 Total Cross Section

The total cross section for the FPW model is written in Equation (2.23). We have seen that the total cross section for our model is obtained by replacing $f_\ell(K)$ by $f^J_{\ell' I'}(K,y,V)$ where ℓ corresponds to J. The total cross section with the appropriate arguments is, therefore,

$$\bar{\sigma}_T^{(J)} = \frac{\pi}{k_0^2}(2J+1)\left\{\sin^2\delta_\ell(K) + S_\ell(K)\,\frac{\cos 2\delta_\ell(K)\left[\mathrm{Im}\,f^J_{J0}(K,y,V) - S_\ell(K)\right] - \sin 2\delta_\ell(K)\left[\mathrm{Re}\,f^J_{J0}(K,y,V) - \Delta_\ell(K)\right]}{\left[\mathrm{Re}\,f^J_{J0}(K,y,V) - \Delta_\ell(K)\right]^2 + \left[\mathrm{Im}\,f^J_{J0}(K,y,V) - S_\ell(K)\right]^2}\right\} \qquad (4.7)$$

The total cross sections of (2.23) and (4.7) were programmed and some of the results are plotted in Figures 13 through 22.

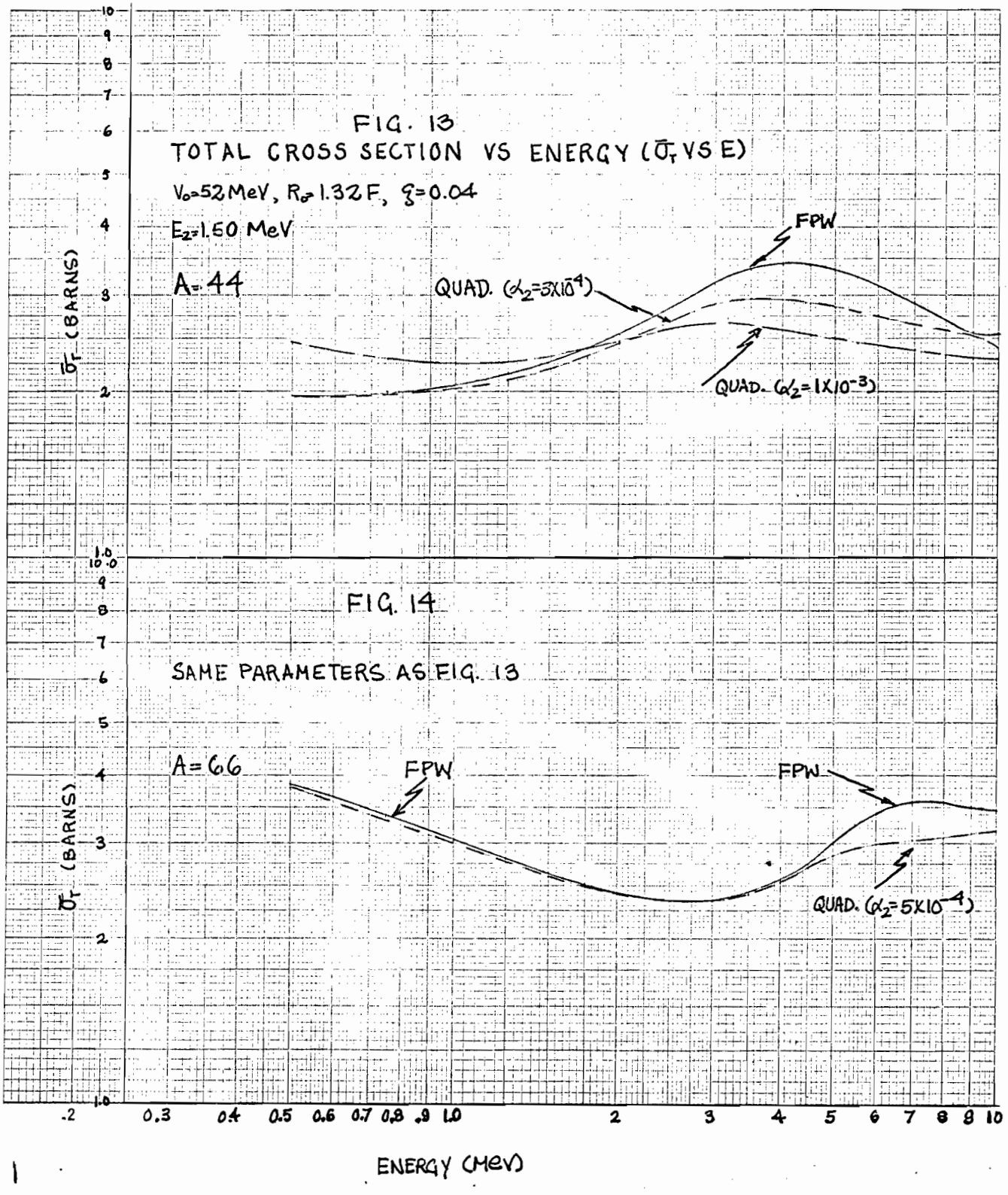
FIG. 13
TOTAL CROSS SECTION VS ENERGY ($\bar{\sigma}_T$ VS E)
V_0=52 MeV, R_0=1.32 F, ξ=0.04
E_2=1.50 MeV
A=44
FPW
QUAD. ($\alpha_2=3\times10^{-4}$)
QUAD. ($\alpha_2=1\times10^{-3}$)
$\bar{\sigma}_T$ (BARNS)
FIG. 14
SAME PARAMETERS AS FIG. 13
A=66
FPW
FPW
QUAD. ($\alpha_2=5\times10^{-4}$)
$\bar{\sigma}_T$ (BARNS)
ENERGY (MeV)

rcles

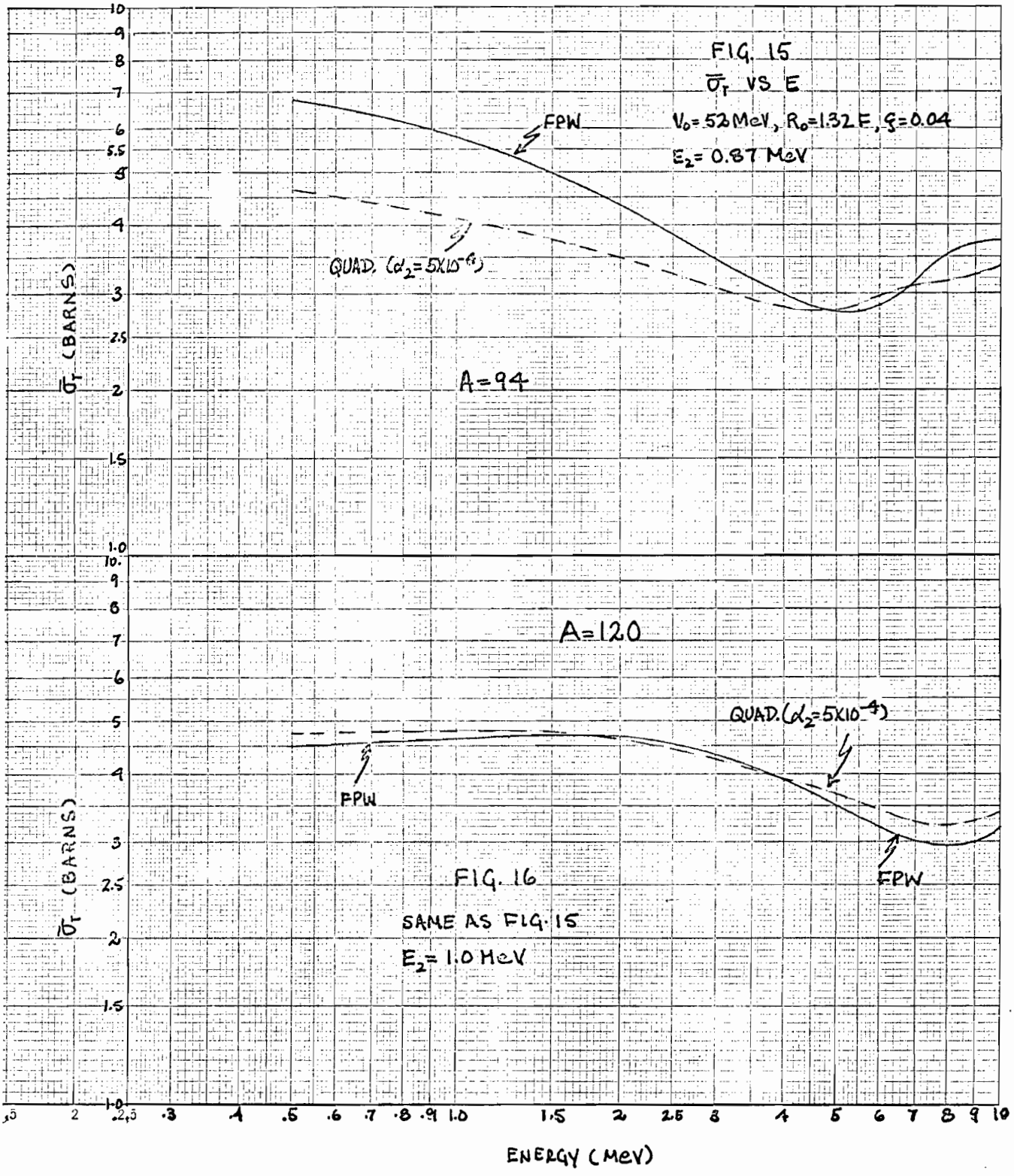
FIG. 15
$\bar{\sigma}_T$ VS E
FPW
V_0= 52 MeV, R_0=1.32 F, ξ=0.04
E_2= 0.87 MeV
QUAD. (α_2=5X10^{-4})
$\bar{\sigma}_T$ (BARNS)
A=94
A=120
QUAD.(α_2=5X10^{-4})
FPW
FPW
FIG. 16
SAME AS FIG. 15
E_2= 1.0 MeV
ENERGY (MeV)

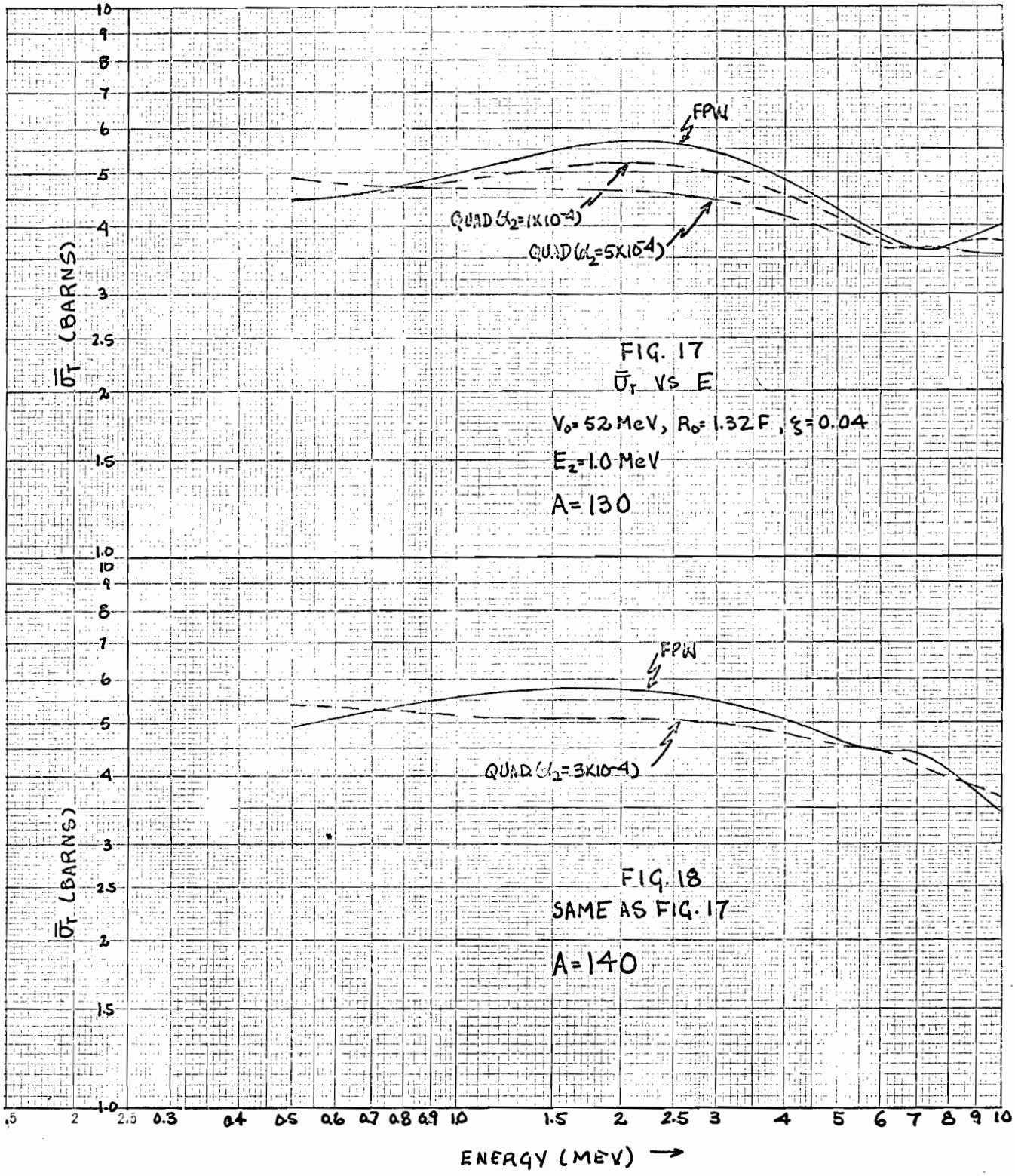

FIG. 17
$\bar{\sigma}_T$ VS E
V_0= 52 MeV, R_0= 1.32 F, ξ= 0.04
E_2=1.0 MeV
A=130

FIG. 18
SAME AS FIG. 17
A=140

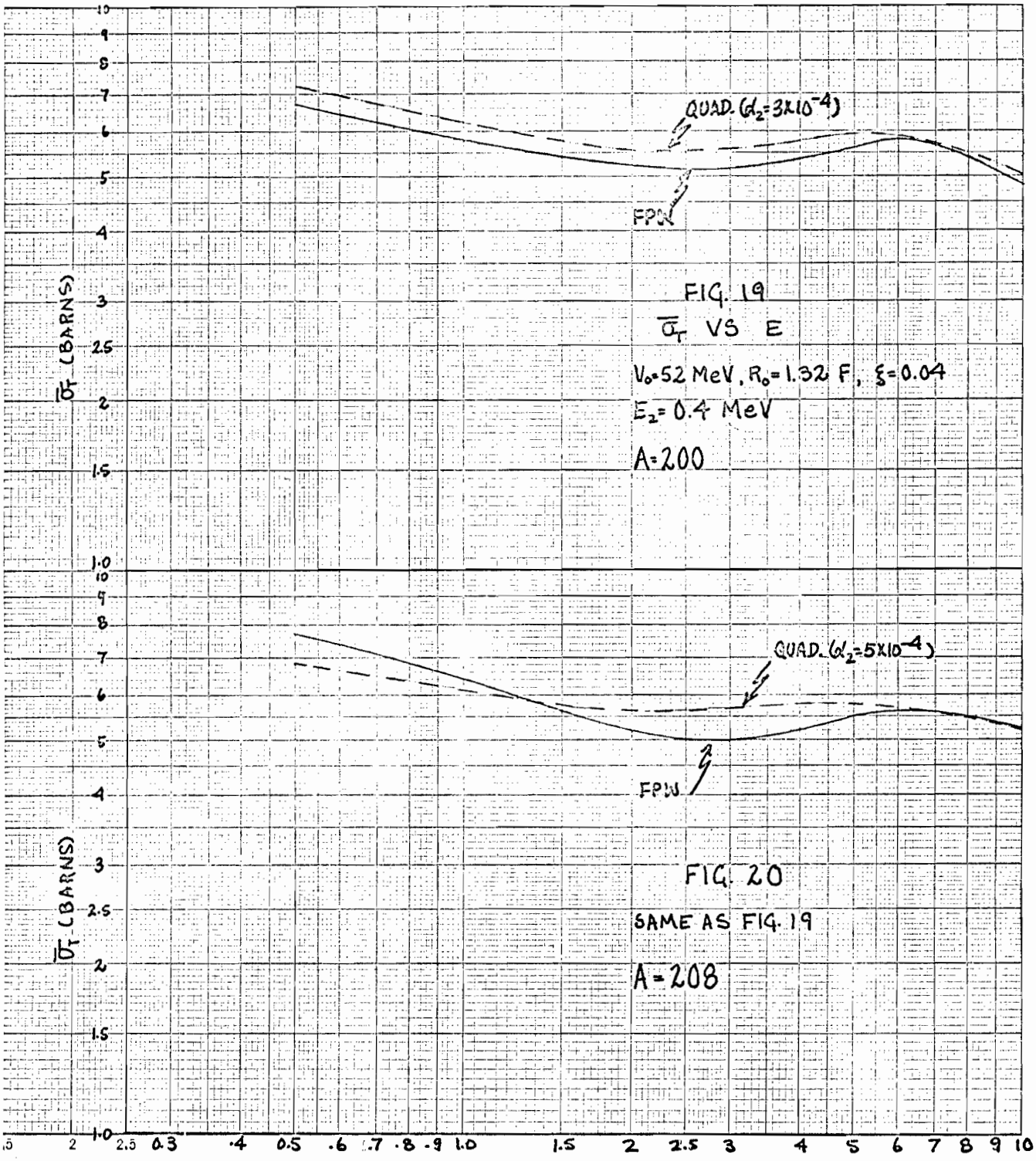

FIG. 19
$\overline{\sigma}_T$ VS E
V_0=52 MeV, R_0=1.32 F, ξ=0.04
E_2= 0.4 MeV
A=200

FIG. 20
SAME AS FIG. 19
A=208

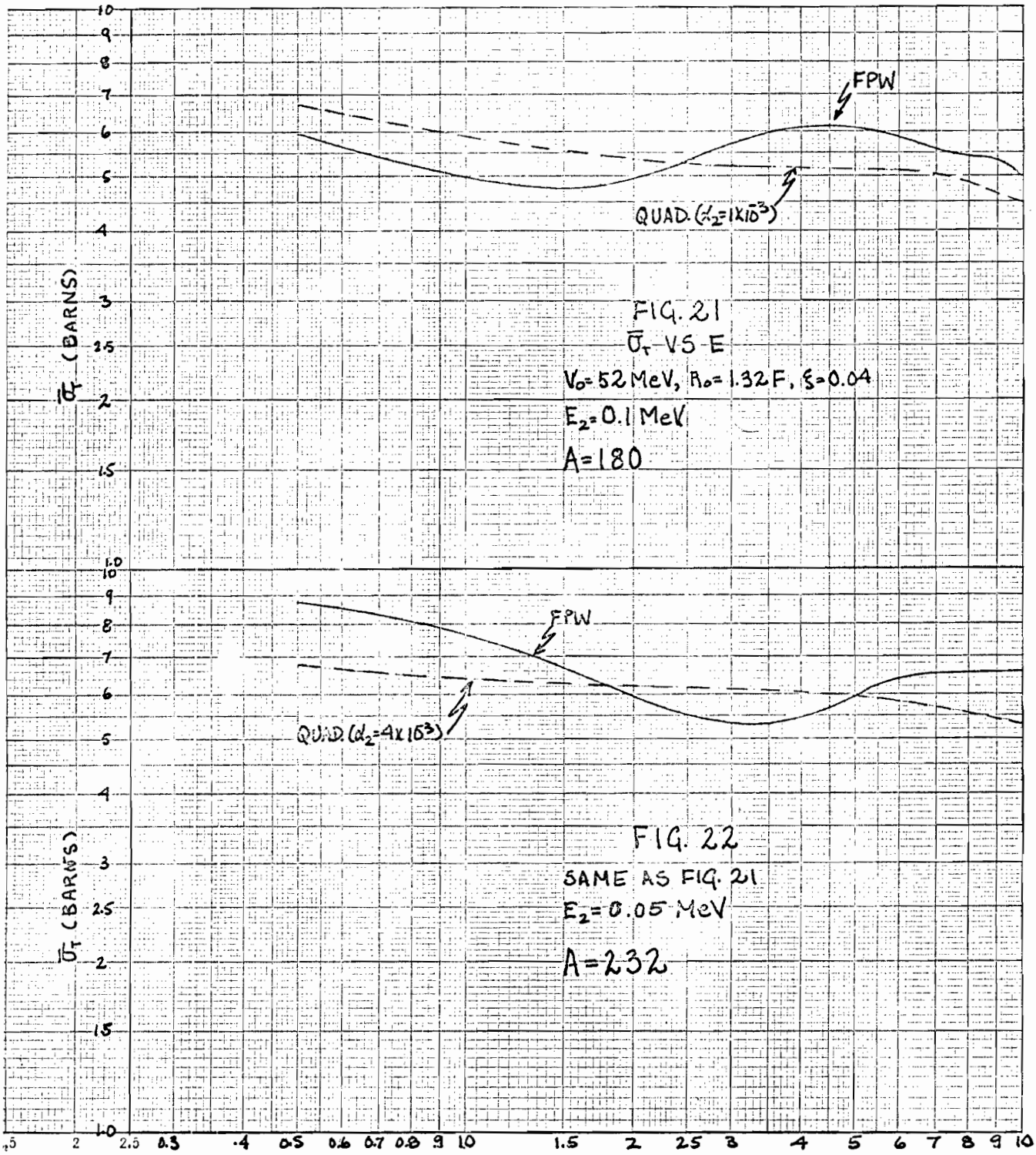
FPW
QUAD. ($\alpha_2 = 1 \times 10^{-3}$)
$\bar{\sigma}_T$ (BARNS)
FIG. 21
$\bar{\sigma}_T$ VS E
$V_0 = 52$ MeV, $R_0 = 1.32$ F, $\xi = 0.04$
$E_2 = 0.1$ MeV
A = 180
FPW
QUAD. ($\alpha_2 = 4 \times 10^{-3}$)
$\bar{\sigma}_T$ (BARNS)
FIG. 22
SAME AS FIG. 21
$E_2 = 0.05$ MeV
A = 232
ENERGY (MeV)

4.3 Shape Elastic, Total Reaction, and Differential Cross Sections

The FPW cross sections for shape elastic scattering, compound nucleus formation, and angular distribution are given in Equations (2.21) (2.22), and (2.24).

These cross sections can be expressed in terms of the model which was developed in Chapter 3 by replacing $f_\ell(X)$ of these equations by $f^J_{\ell' I'}(X, y, Y)$ in the prescribed manner. This substitution is easily accomplished, and we will not present the explicit results here. A portion of the results are plotted in Figures 23 through 31.

The total reaction cross section of our model is exactly analogous to the cross section for compound nucleus formation of the FPW optical model as has been discussed in Section 3.3. The distinction between these cross sections, which, incidently, accounts for the difference in name, is that the total reaction cross section includes the direct inelastic scattering of the 2^+ collective state.

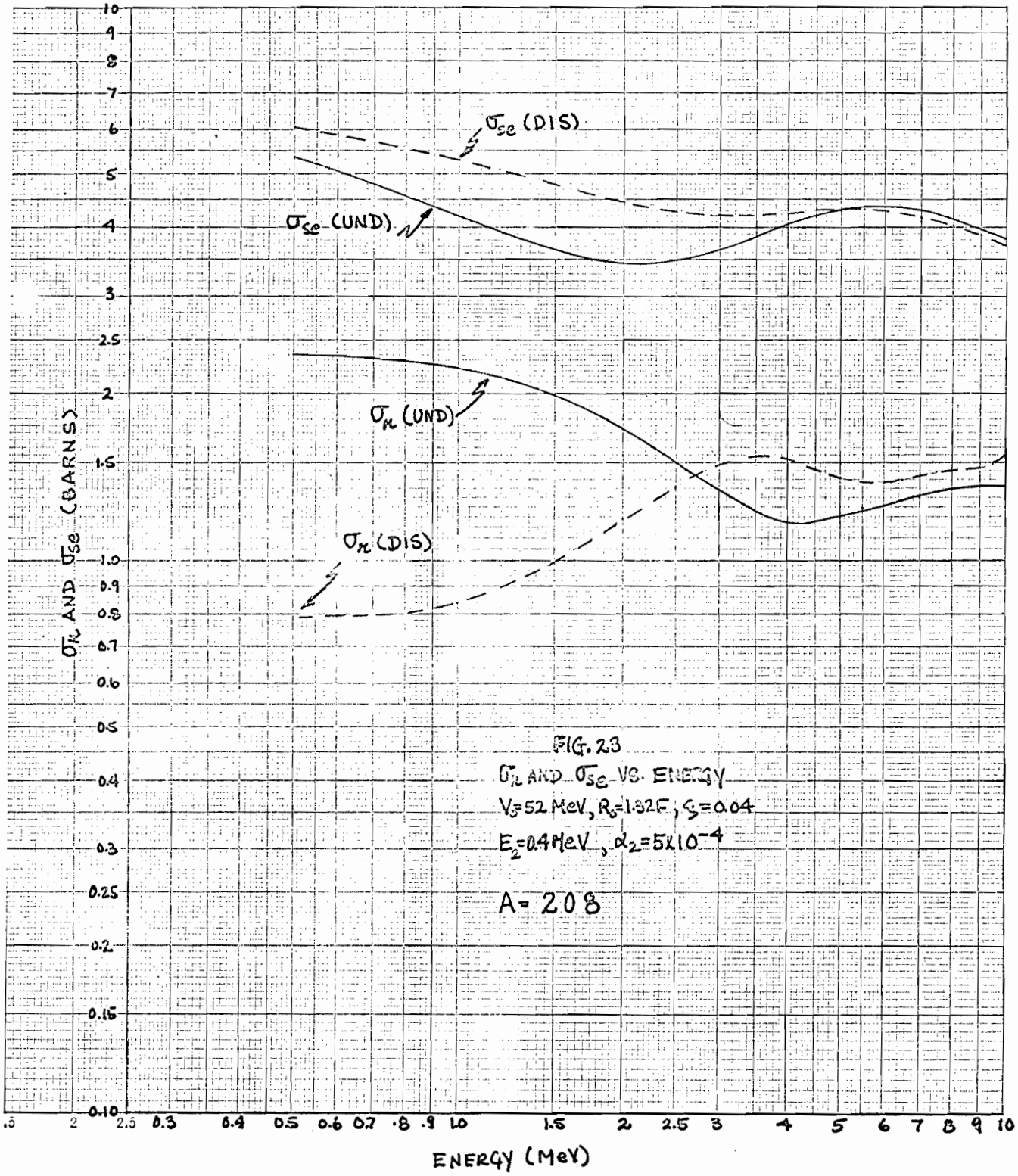

FIG. 23
σ_R AND σ_{se} VS. ENERGY
V_0=52 MeV, R_0=1.32F, ζ=0.04
E_2=0.4MeV, α_2=5x10^{-4}

A= 208

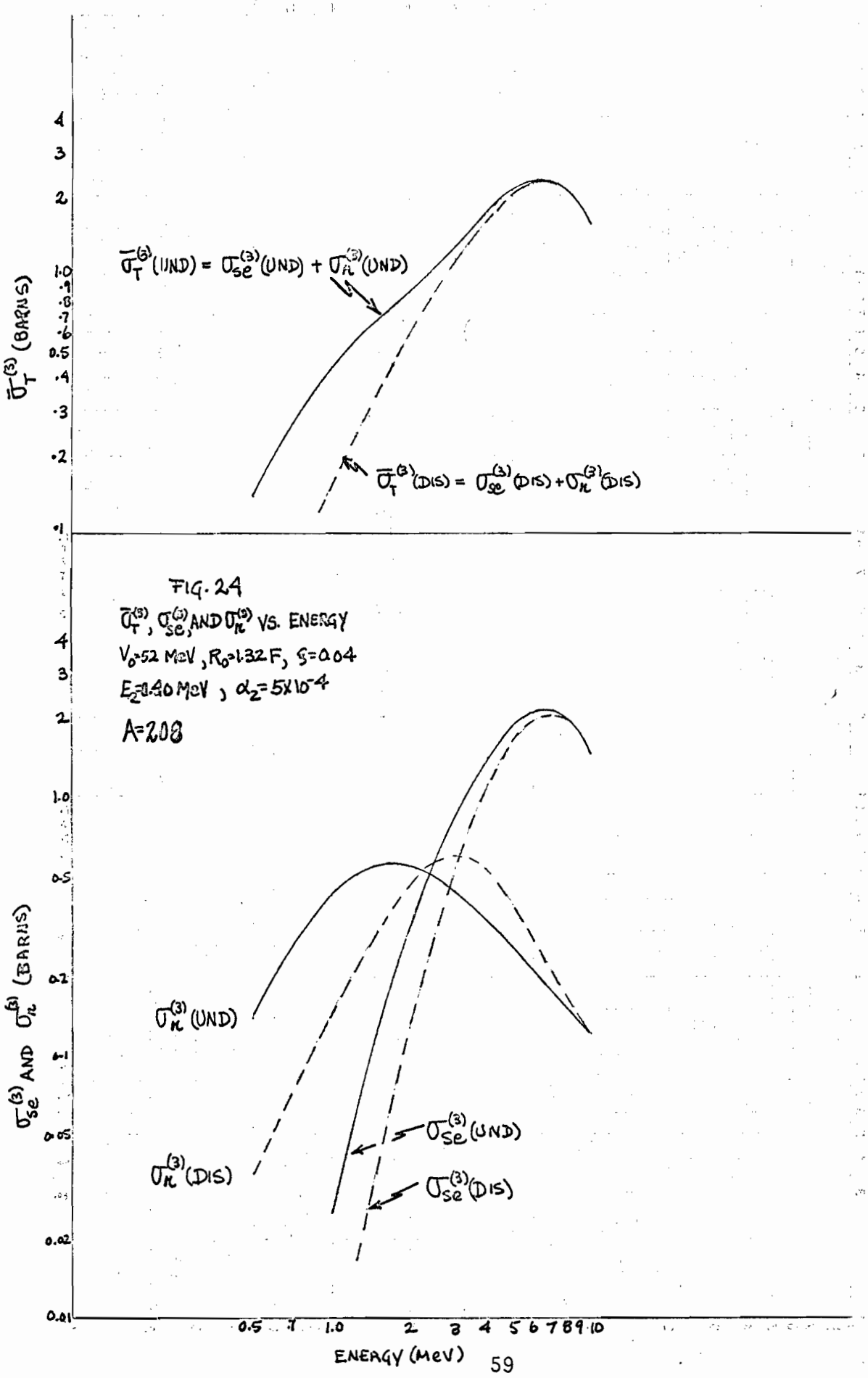

FIG. 24
$\bar{\sigma}_T^{(3)}$, $\sigma_{se}^{(3)}$, AND $\sigma_R^{(3)}$ VS. ENERGY
V_0=52 MeV, R_0=1.32 F, ζ=0.04
E_2=1.40 MeV, $\alpha_2 = 5 \times 10^{-4}$
A=208

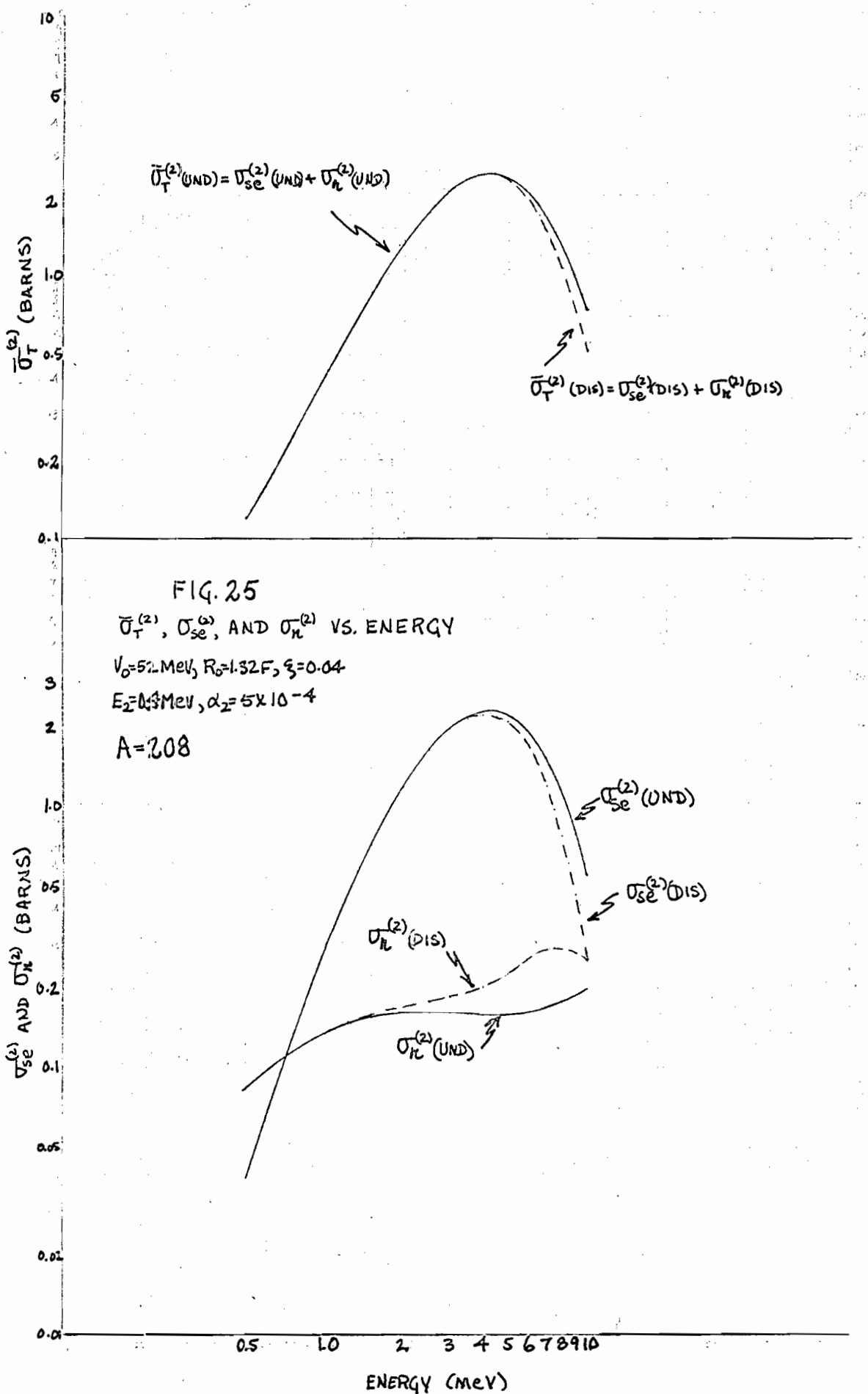

FIG. 25

$\bar{\sigma}_T^{(2)}$, $\sigma_{se}^{(2)}$, AND $\sigma_R^{(2)}$ VS. ENERGY

V_0=52 MeV, R_0=1.32F, ξ=0.04

E_2=0.3MeV, α_2= 5X10^{-4}

A=208

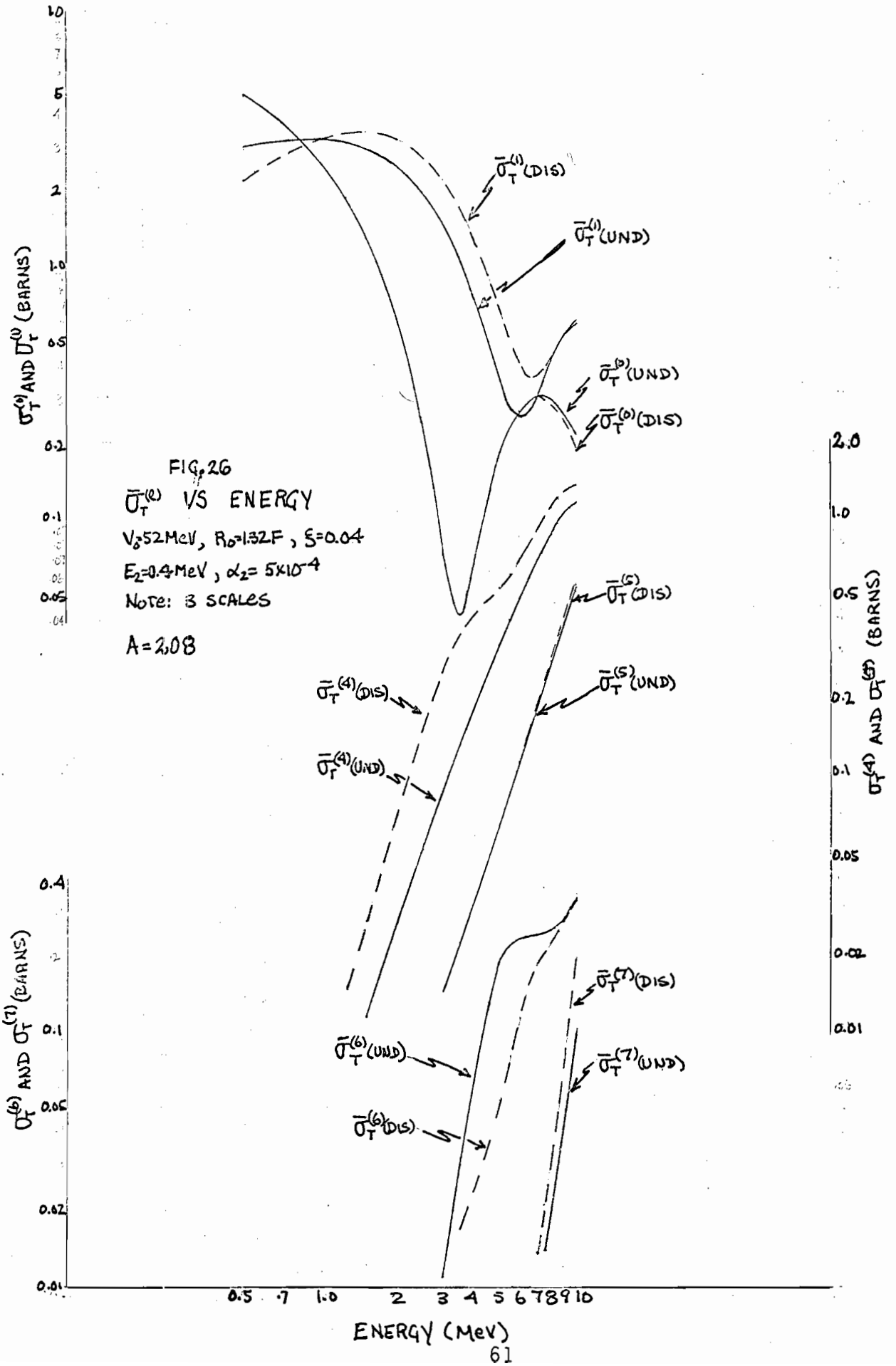

FIG. 26

$\bar{\sigma}_T^{(\ell)}$ VS ENERGY

V_0 52 MeV, R_0 = 1.32 F, ξ = 0.04

E_2 = 0.4 MeV, $\alpha_2 = 5 \times 10^{-4}$

NOTE: 3 SCALES

A = 208

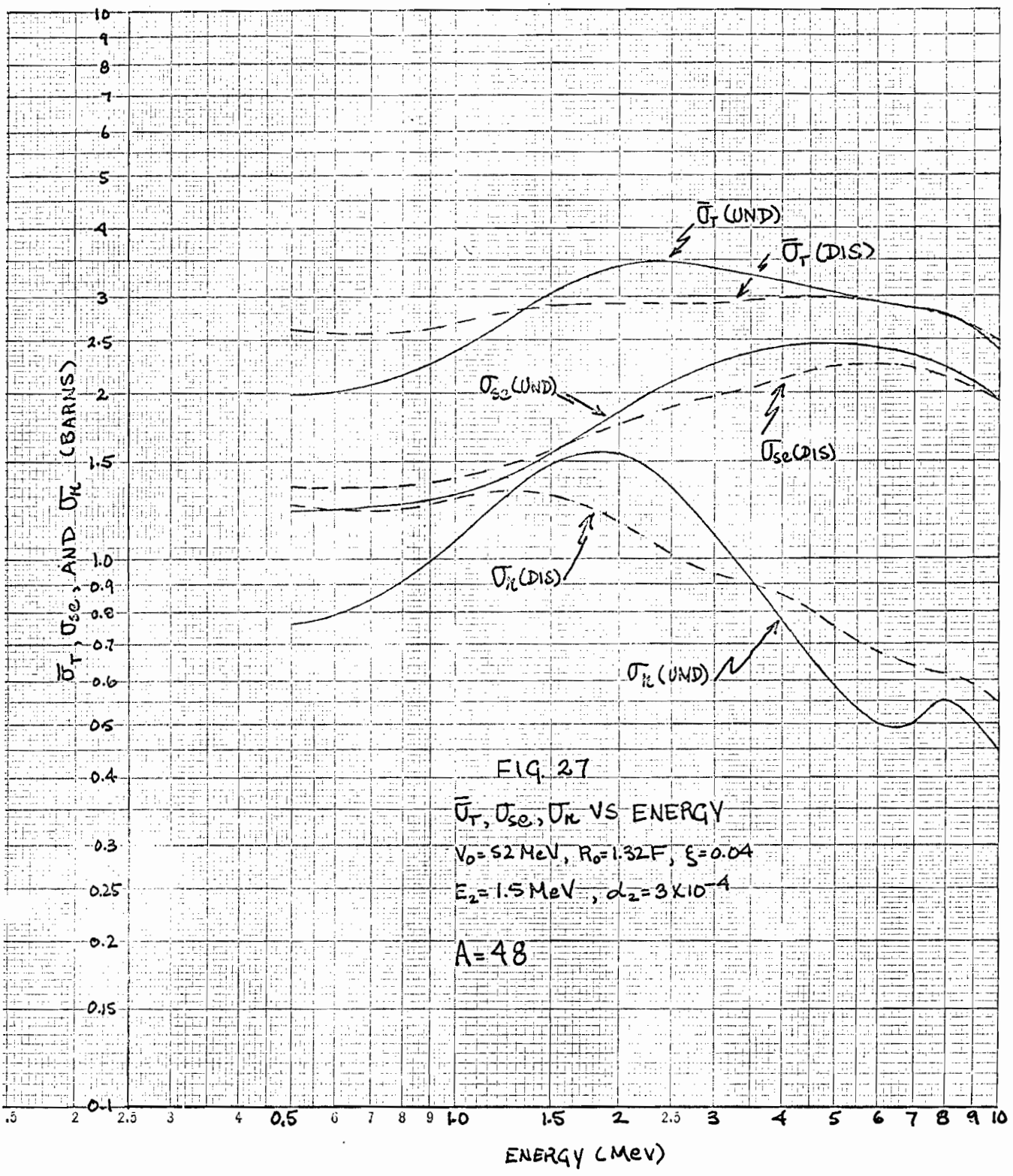

FIG. 27

$\bar{\sigma}_T$, σ_{se}, σ_R VS ENERGY

$V_0 = 52$ MeV, $R_0 = 1.32$F, $\xi = 0.04$

$E_2 = 1.5$ MeV, $\alpha_2 = 3 \times 10^{-4}$

A = 48

FIG. 28

$\bar{\sigma}_T$, $\bar{\sigma}_T^{(0)}$, $\bar{\sigma}_T^{(1)}$, AND $\bar{\sigma}_T^{(2)}$ VS ENERGY

$V_0 = 52$ MeV, $R_0 = 1.32$F, $\xi = 0.04$

$E_2 = 1.5$MeV, $\alpha_2 = 3 \times 10^{-4}$

A=48

Note: 4 Scales

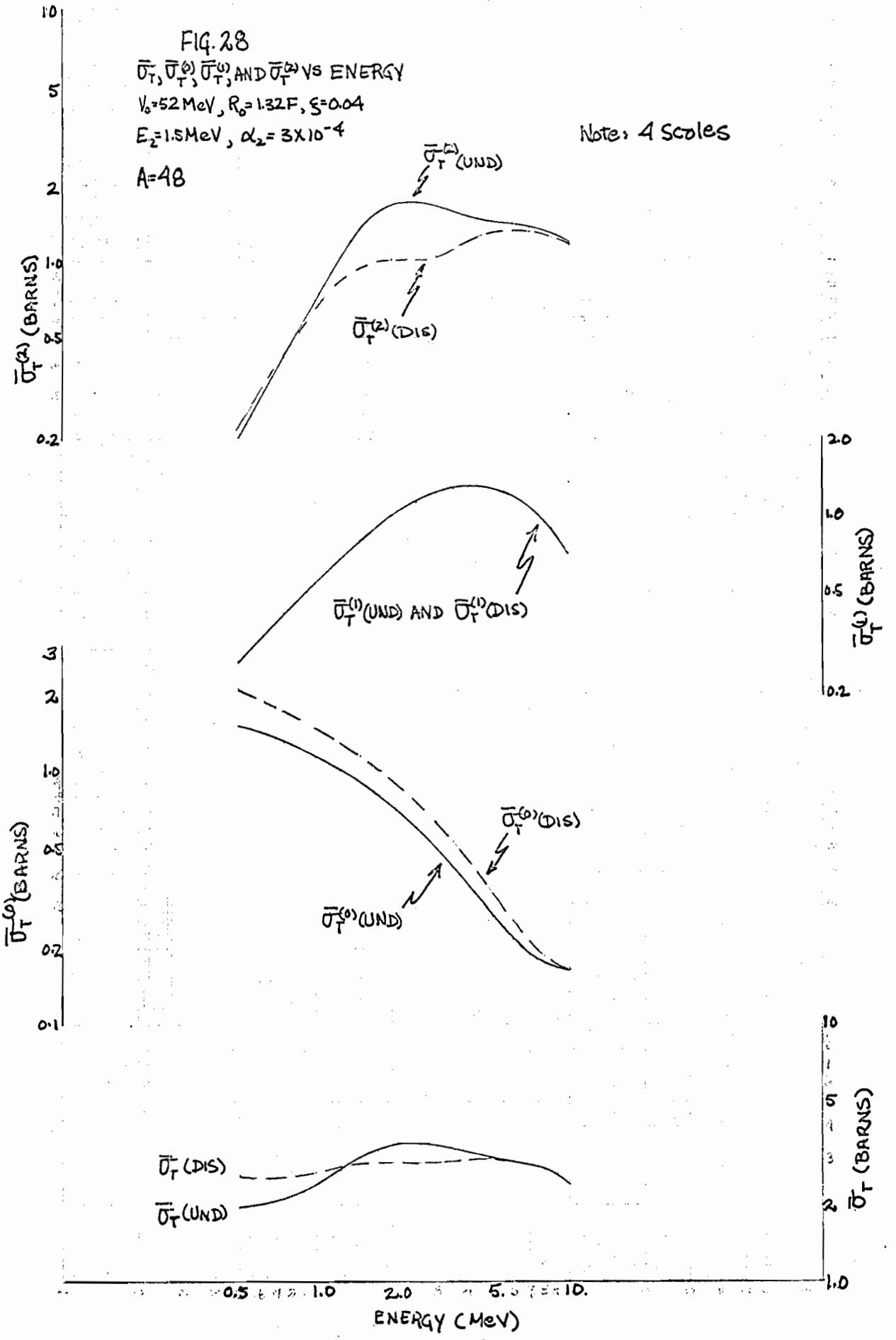

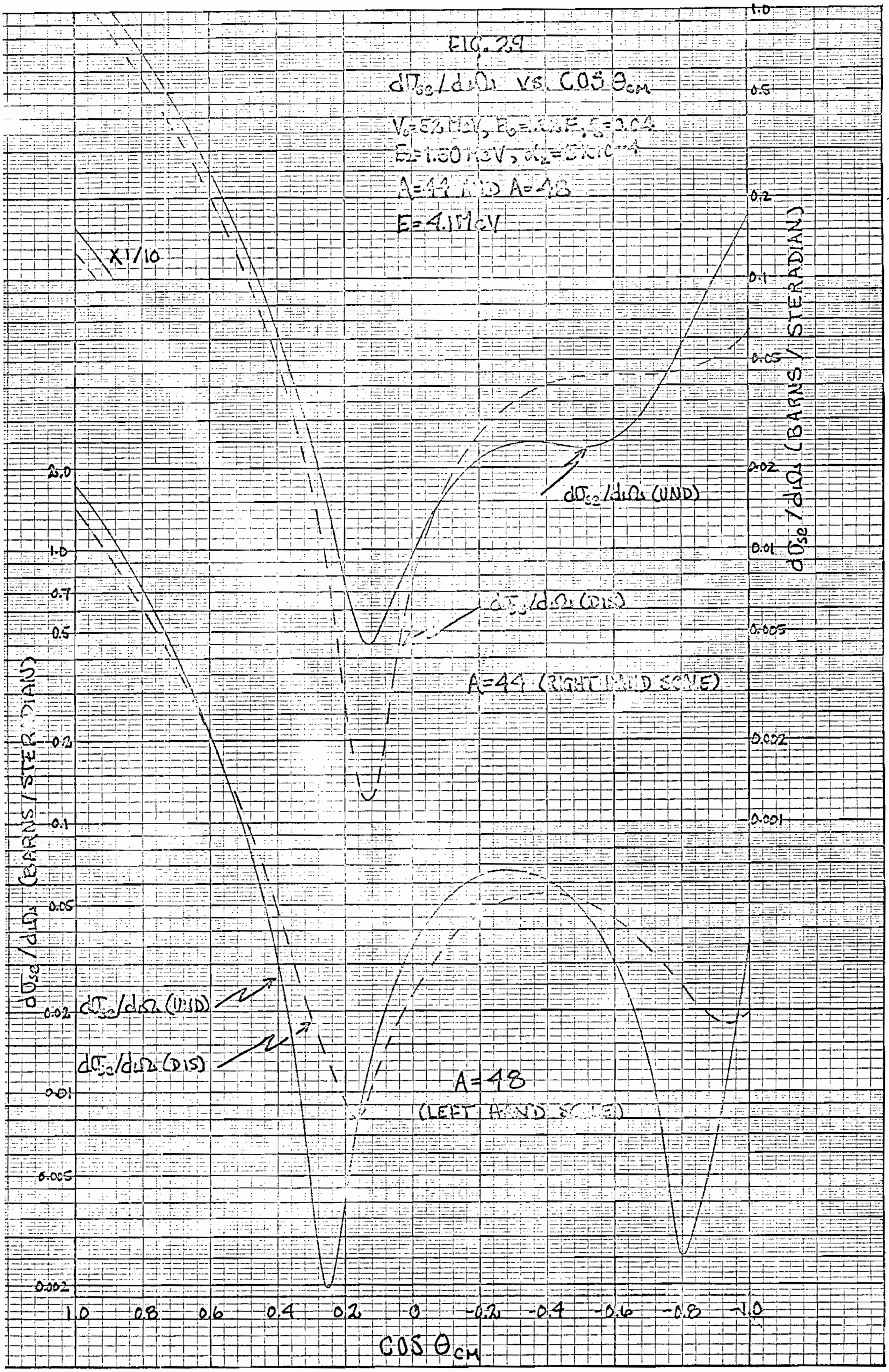

FIG. 29
dσse/dΩ vs. COS θcm
E=4.1MeV
X1/10
dσse/dΩ (UND)
dσse/dΩ (DIS)
A=44
A=48
dσse/dΩ (BARNS/STERADIAN)
COS θCM
1.0
0.8
0.6
0.4
0.2
0
-0.2
-0.4
-0.6
-0.8
-1.0

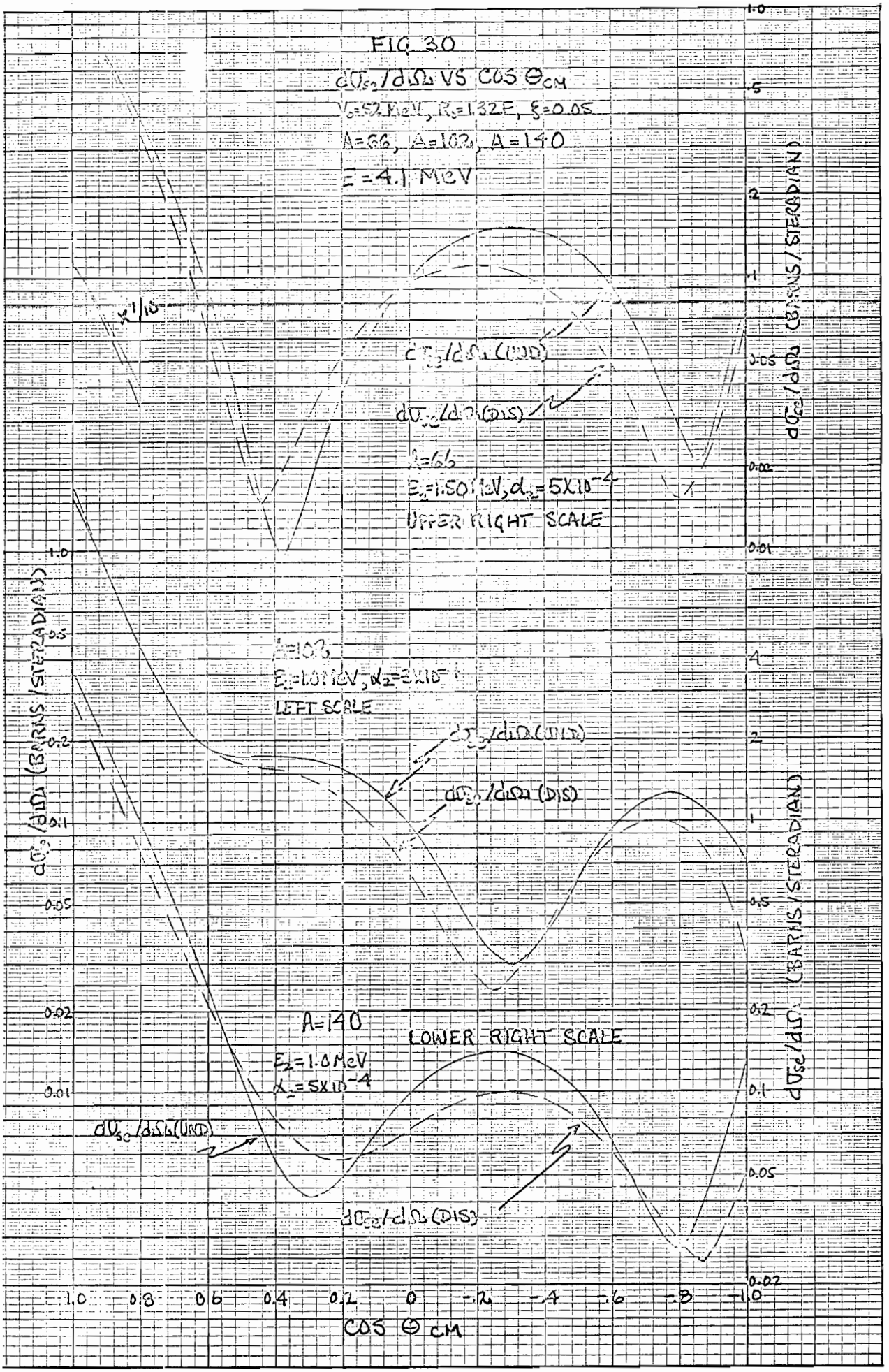
FIG 30
dσ_sc/dΩ VS COS Θ_CM
V_0=52 MeV, R=1.32E, ξ=0.05
A=66, A=103, A=140
E=4.1 MeV
dσ_sc/dΩ (UND)
dσ_sc/dΩ (DIS)
A=66
E_2=1.50 MeV, α_2=5X10^-4
UPPER RIGHT SCALE
A=103,
E_2=1.01 MeV, α_2=5X10^-4
LEFT SCALE
dσ_sc/dΩ (UND)
dσ_sc/dΩ (DIS)
A=140
E_2=1.0 MeV
α_2=5X10^-4
LOWER RIGHT SCALE
dσ_sc/dΩ (UND)
dσ_sc/dΩ (DIS)
dσ_sc/dΩ (BARNS/STERADIAN)
dσ_sc/dΩ (BARNS/STERADIAN)
COS Θ CM
1.0
0.8
0.6
0.4
0.2
0
-.2
-.4
-.6
-.8
-1.0

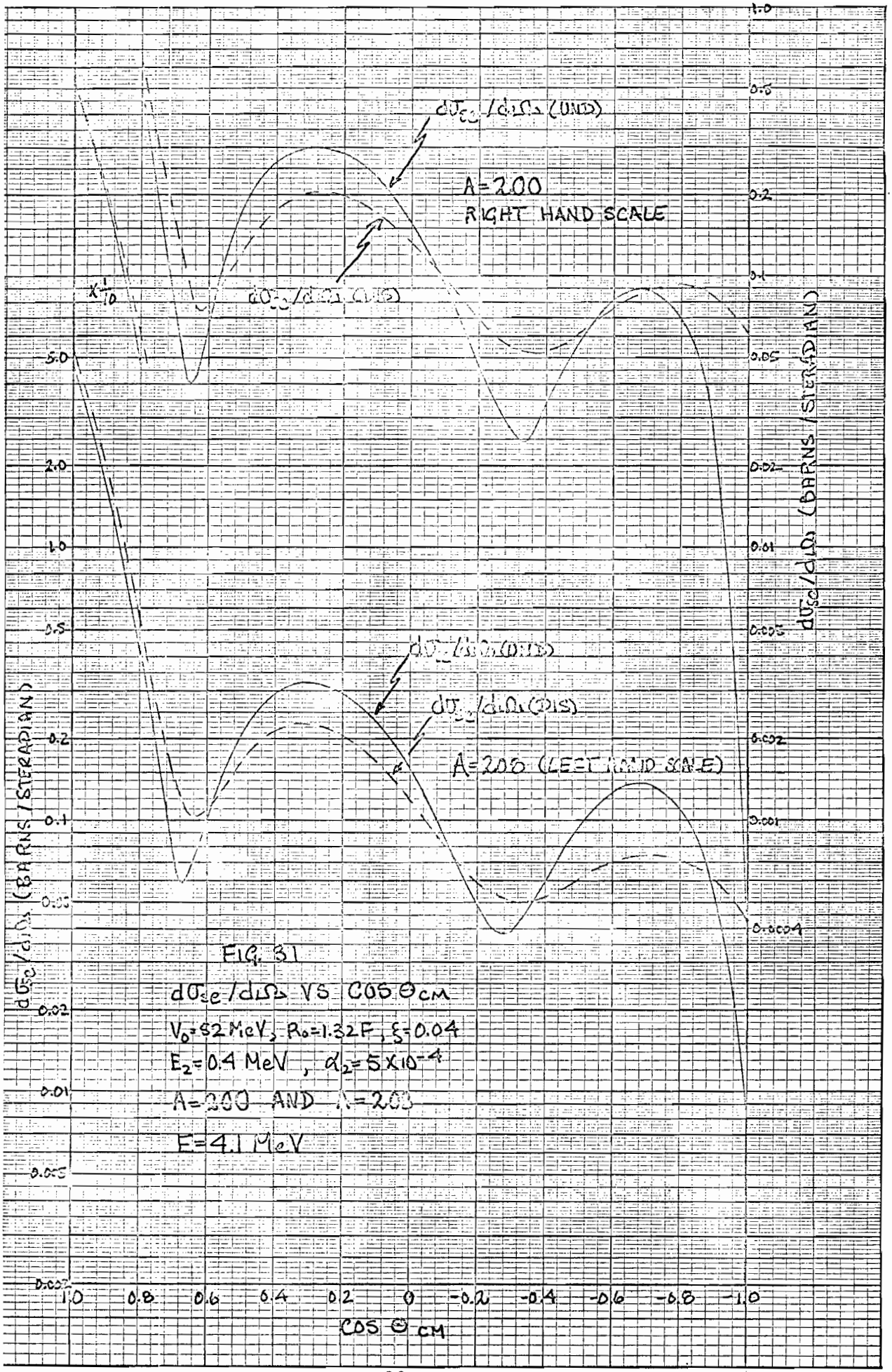

FIG. 31

$d\sigma_{se}/d\Omega_2$ VS COS Θ_{CM}

V_0=52 MeV, R_0=1.32F, ξ=0.04

E_2=0.4 MeV, $\alpha_2 = 5 \times 10^{-4}$

A=200 AND A=208

E=4.1 MeV

CHAPTER 5

DISCUSSION OF RESULTS

5.1 Collective and Optical Model Parameters

All the curves of Figures 1 through 31 are plotted for both the FPW square well optical model and the spheroidal well surface interaction of our model. The optical model parameters which were used throughout are $V_o = 52$ Mev, $R_o = 1.32$ F, and $\zeta = 0.04$. The new parameters introduced by taking the effect of collective excitation into account are the energy of the excited state and the amount of deformation associated with the particular nucleus in question.

We have called the quantity, $\hbar\omega_n / 8\pi C_n$, the polarizability of the n^{th} multipole vibration. This is a convenient and meaningful term to define, and aside from a factor of 4π it is just the square of the off-diagonal matrix element of the target wave functions. The polarizability, so defined, is essentially a measure of the amount of deformation in the nuclear surface. The vibrational correction term to the logarithmic derivative is simply proportional to this polarizability. The strength of the polarizability can be determined from Coulomb excitation measurements.[9] The energies, $\hbar\omega_n$, can also be determined experimentally, and as a result no free parameters have been introduced. This fact is particularly important in the view of extending this work to a quantitative rather than a qualitative study.

Experimentally determined values of the vibrational parameters, α_m and E_n, for even-even nuclei are listed in Table 1 where we have introduced the notation $\alpha_m = \hbar\omega_m / 8\pi C_m$ and $E_m = \hbar\omega_m$. The quadrupole parameters are fairly representative of the nuclear regions in which we are interested. The octupole parameters are less informative since they are few in number and only located near closed shells. On theoretical grounds, however, one would expect C_3 to remain fairly constant[14] in contrast to the quadrupole peaking near closed shells.

TABLE I

VIBRATION PARAMETERS FOR EVEN-EVEN NUCLEI[9] (QUADRUPOLE)

Nucleus	E_2(Mev)	C_2(Mev)	$E_2/8\pi C_2$
$_{22}Ti^{46}$	.890	14	2.529×10^{-3}
Ti^{48}	.990	29	1.358×10^{-3}
$_{26}Fe^{56}$	.854	36	9.44×10^{-4}
$_{28}Ni^{58}$	1.45	77	7.49×10^{-4}
Ni^{60}	1.33	59	8.97×10^{-4}
$_{30}Zn^{64}$	1.000	61	6.52×10^{-4}
Zn^{66}	1.040	86	4.81×10^{-4}
$_{32}Ge^{70}$	1.020	120	3.38×10^{-4}
Ge^{74}	0.593	19	1.242×10^{-3}
$_{34}Se^{74}$	0.635	32	7.895×10^{-4}
Se^{78}	0.615	20	1.223×10^{-3}
Se^{82}	0.880	190	1.843×10^{-4}
$_{42}Mo^{94}$	0.871	67	5.17×10^{-4}
Mo^{100}	0.528	20	1.050×10^{-3}
$_{44}Ru^{100}$	0.540	48	4.48×10^{-4}
Ru^{104}	0.362	10	1.44×10^{-3}
Pd^{108}	.430	15	1.14×10^{-3}
$_{48}Cd^{110}$	.654	58	4.49×10^{-4}
Cd^{116}	.508	32	6.32×10^{-4}
$_{52}Te^{120}$	.560	48	4.64×10^{-4}

Table I (continued)

Nucleus	E_2(Mev)	C_2(Mev)	$E_2/8\pi C_2$
$_{52}Te^{130}$	.850	170	1.989×10^{-4}
$_{60}Nd^{146}$	.455	150	1.207×10^{-4}
$_{62}Sm^{148}$	.562	100	2.24×10^{-4}
$_{78}Pt^{194}$	.330	39	3.37×10^{-4}
$_{78}Pt^{198}$	.403	60	2.67×10^{-4}
$_{80}Hg^{198}$	.411	88	1.858×10^{-4}
$_{80}Hg^{200}$	.370	120	1.227×10^{-4}
$_{80}Hg^{202}$	.439	170	1.027×10^{-4}
$_{82}Pb^{206}$	.803	1400	2.28×10^{-5}
$_{84}Po^{212}$	.719	640	4.47×10^{-5}
$_{84}Po^{214}$	.606	270	8.93×10^{-5}

(OCTUPOLE)[14]

Nucleus	E_3(Mev)	C_3(Mev)	$E_3/8\pi C_3$
$_{20}Ca^{40}$	3.73	370	4.01×10^{-4}
$_{38}Sr^{88}$	2.76	367	2.99×10^{-4}
$_{82}Pb^{208}$	2.61	1500 ± 750	6.93×10^{-5}

5.2 Strength Function

In Figure 1 we have plotted Re f_0 and Re $\Delta f^0_{00}(\alpha_2)$ as a function of mass number A. $Re f_0$ is the FPW result, and $Re \Delta f^0_{00}(\alpha_2)$ is the correction term written as a function of α_2. Figures 1 through 4 demonstrate the effect of varying E_2 in the vicinity of 1 Mev. $Re f^0_{00}(\alpha_2)$ is plotted for values of E_2 = .8 Mev and 1.5 Mev with $\alpha_2 = 3 \times 10^{-4}$. The curve for E_2 = 0.8 Mev intercepts $Re f_0$ above the A axis, and the curve for E_2 = 1.5 Mev intercepts $Re f_0$ below the A axis. The effect of this can be seen in Figure 2 where $Re f_0$ is added to $Re \Delta f^0_{00}(\alpha_2)$ to obtain $Re f^0_{00}$. In Figure 2, the curve for E_2 = 1.5 Mev has a slight asymmetry in which the positive peak to the right is diminished relative to the negative peak to the left while the opposite effect is observed for E_2 = 0.8 Mev. For E_2 = 1.0 Mev the two peaks are symmetric since for this energy, $Re f_0$ intercepts $Re \Delta f^0_{00}$ on the A axis.

Figures 3 and 4 illustrate the effect of this E_2 variation on the strength function. The strength function has been normalized to 1 ev and plotted vs A. The curves calculated from the square well optical model are labelled FPW and those for nuclei with consideration of collective quadrupole coordinates are labelled quadrupole effect. For nuclei in the vicinity of this 3s resonance, Table 1 suggests values of E_2 of about 0.8 to 1.5 Mev. However, in the vicinity of the right peak most of the E_2 values are greater than 1 Mev.

In Figures 5 and 6 the effect of increasing E_2 is observed. For these curves $\alpha_2 = 2 \times 10^{-4}$, and E_2 is, respectively, 2.0 Mev and

3.0 Mev. The effect is as expected, and the right peak becomes much like a shoulder to the left peak which is what we observe experimentally. The effect is presented more from the point of view of variation in parameters than quantitative experimental fit, however.

In Figure 7, the octupole correction, $Re\,\Delta f^{\circ}_{00}(\alpha_3)$, has been represented along with $Re\,f_0$ and $Re\,\Delta f^{\circ}_{00}(\alpha_2)$. The corresponding functions $Im f_0$, $Im\,\Delta f^{\circ}_{00}(\alpha_2)$, and $Im\,\Delta f^{\circ}_{00}(\alpha_3)$ are plotted in Figure 8. The collective parameters for these curves are $E_2 = 1.5$ Mev, $\alpha_2 = 7 \times 10^{-4}$, $E_3 = 3.0$ Mev and $\alpha_3 = 4 \times 10^{-4}$. Figures 7 through 11 are all plotted for the same parameters. From Figures 7 and 8 we see that whereas the quadrupole correction has its major contribution in the vicinity of the resonance, the octupole becomes increasingly important as we go to higher values of A.

Figures 9 and 10 are the corresponding sums of the curves in Figures 7 and 9, respectively, and are, in fact, the real and imaginary parts of the logarithimic derivative, f°_{00}, of our problem. Figure 11 is the strength function calculated from f°_{00} of Figures 9 and 10 and has been plotted so as to see the effect of the quadrupole correction alone as well as the combined effect of the quadrupole and octupole correction. With the inclusion of the octupole the left peak is relatively unaffected while the right peak is lowered increasingly from A = 60 to A = 110. This is what is desired experimentally both in decreasing the size of the right peak and in lowering the valley in the vicinity of A = 90. The experimental values of octupole polarizabilities given in Table 1 indicate that the octupole correction is effective in improving the desired qualitative behavior for the strength function.

Figure 12 demonstrates the effect of smaller polarizabilities, where here we have used $E_2 = 1.5$ Mev, $\alpha_2 = 9 \times 10^{-5}$, $E_3 = 3.0$ Mev and $\alpha_3 = 4 \times 10^{-5}$. The peaks are conspicuously closer together.

The real part of the logarithmic derivative of the square well optical model goes through zero at a value of A which is effectively the position of the strength function resonance. The width of the resonance is strongly dependent upon the imaginary part of the logarithmic derivative. For the spheroidal optical model, $Re\, f^0_{00}$ has three intercepts with the A axis. These positions correspond to the A values of the two peaks and the minimum between them. Increasing the polarizability as seen by comparing Figures 11 and 12 has the effect of splitting the peaks. The width of the peaks depends largely on $Im\, f^0_{00}$, and the relative sizes of the two peaks is adjusted by E_n as has been demonstrated in Figures 3 and 4.

The effect of the inclusion of quadrupole vibrations is to split the single 3s resonance of the FPW optical model into two peaks. This splitting develops because of the coupling of the incoming orbital angular momentum to the target spin 2. The principal peak of these two is the left peak, and so, in effect, the strength function has been shifted to lower A by the quadrupole correction. This type of behavior seems to be an improvement on the experimental agreement. The actual splitting, however, is much more of a shoulder effect than our calculations have indicated.

We expect that the qualitative results obtained with the present model justify the calculation of this collective effect with the more

realistic diffuse surface potential. E. Vogt[15] has shown that the effect of diffusing the well is mainly to multiply the strength function by a constant factor. This argument is based upon volume absorption, and one expects surface peaking of the imaginary potential. In spite of this, it is expected that the qualitative behavior arising from the inclusion of the quadrupole and octupole vibrations will maintain itself for the diffuse well. This expectation has been born out in the work of B Buck and F. Perey[7] where they have used a diffuse surface optical model with surface peaking of the imaginary part and spin-orbit coupling.

I. Furuoya and A. Sugie[15] have recently published a method of calculating the strength function with collective effects which is similar to the one we have employed. They obtained a triple peak in the strength function as a result of including the effect of the second 2^+ collective level which is a 2 phonon state. They did not consider the effect of the octupole excitation, however.

5.3 Total Cross Section

The total cross section as a function of energy is plotted in Figures 13 through 22 for selected values of A. The FPW total cross sections plotted with solid lines are compared to the total cross sections with the inclusion of the collective quadrupole effect, and the latter are plotted with broken lines. The collective parameters E_2 and α_2 are indicated on the various curves.

Most of the values of A for which we have represented the total cross section were chosen because they are in the regions of magic nuclei where either the proton number or the neutron number or both

are magic. This endeavor was limited somewhat because of the difficulties in matching the most well formed peaks with the appropriate nuclei. Again we emphasize that there is no quantitative attempt to coincide with experimental curves since we are not using a diffuse surface interaction or spin-orbit coupling. Values of A in the regions of permanently deformed nuclei are also included, and they will be discussed in context.

The results for A = 44 are plotted in Figure 13. A = 44 is representative of the region in which the proton number is near 20 and the neutron number is near 28. The quadrupole effect has been plotted for two values of α_2 for comparison. In this case an increase in the polarizability corresponds to a flattening of the peak and a shift in the peak towards a lower value of energy. The FPW peak is considered a d wave peak; what this actually means is that the partial wave which gives the largest contribution at the peak of the giant resonance is a d wave. This does not mean that the other partial waves contribute a minimum nor does it mean that the d wave is at its maximum.. In fact, other partial waves are usually quite significant in their contribution to the giant resonance in and around the peak itself. For the case in question the p wave gives a significant contribution. We shall call the giant resonance obtained with the inclusion of the collective effect, the distorted giant resonance. In Figure 13, the distorted giant resonance is a p wave resonance rather than a d wave.

Figure 14 illustrates the effect on the giant resonance in the vicinity of A = 66, or, alternatively, where the proton number is 28. Again,

the effect of including the quadrupole excitation is to flatten the giant resonance somewhat. However, the energy at which the maximum in the distorted resonance now occurs has shifted towards higher energy. The undistorted resonance is an f wave at 7.5 Mev. At 10 Mev the distorted resonance is predominantly a d wave and is still rising. The maximum value of the distorted resonance will occur at an energy in excess of 10 Mev and will most likely be a d wave.

When the neutron number is 50, the mass number is in the low 90's. Figure 15 illustrates the effect of the quadrupole excitation for A = 94. The FPW total cross section does not have a clear resonance in our energy region of 0.5 to 10 Mev. The effect of including quadrupole excitations is qualitatively the same, that is to flatten the total cross section and shift the position of the peak. At 0.5 Mev the principal partial wave constituent to the FPW curve is the p wave, and the s wave contributes only slightly less. In the distorted case the s wave is unaffected, but the p wave is diminished by about a factor of 3. At 10 Mev the g wave (ℓ = 4) gives the major contribution to the FPW curve. The distorted curve is an f wave, and the distorted maximum for this region will be shifted towards higher energy. The exact position of the resonance is beyond 10 Mev and, thereby, was not included in this analysis.

Figure 16 illustrates the quadrupole effect on the total cross section for A = 120, where the proton number is near 50. The slight FPW resonance at 1.8 Mev is due to the p wave. The distorted quadrupole resonance at 1.0 Mev is an s wave peak. The calculated quadrupole effect

in this region is observed to be different from that for the case of A = 94. At 0.5 Mev the s wave is the major consituent of the FPW, as well as the distorted, total cross section. The increase in the distorted cross section compared to the FPW cross section at this energy is due to the additional p and d wave contributions, but the s wave, although somewhat diminished, still contributes the major portion.

The quadrupole effect for A = 130 is presented in Figure 17. This region of A corresponds to a proton number near 50 and a neutron number near 82. The giant resonance for this vicinity of nuclei is well formed in the 0.5 to 10 Mev energy region. Two values of α_2 are used for comparison. The FPW peak at 2.0 Mev is designated as a p wave resonance. Both the s wave and the d wave give significant contributions; however, the distorted peak is also a p wave, and the position of the maximum has made no noticeable shift. The quadrupole effect of $\alpha_2 = 5 \times 10^{-4}$ has flattened the resonance so that a maximum value no longer occurs.

The fact that the position of the maximum of the distorted giant resonance does not shift for A = 130 can be understood in terms of the principal partial waves involved. As we have stated, both the distorted and undistorted giant resonance peak at 2.0 Mev. For this case it is also true that the p wave itself peaks at 2.0 Mev for both the distorted and undistorted giant resonance. The undistorted s wave peaks below 0.5 Mev and the distorted s wave shifts towards lower energy. The undistorted d wave peaks at 3.5 Mev, and the distorted d wave peaks at 4.5 Mev. Since the s and d wave contribute comparable amounts and since they shift in opposite directions, whereas the p wave remains stationary, the

position of the distorted giant resonance peak is unaffected.

Figure 18 illustrates the quadrupole effect for A = 140 which corresponds to a neutron number of 82. The FPW peak at E = 1.75 Mev is a p wave resonance. The quadrupole effect ($\alpha_2 = 3 \times 10^{-4}$) that is presented in Figure 18 is such as to eliminate the resonance character of the total cross section, but if the distorted curve were plotted for a smaller value of α_2 for which a resonance did occur, it would be a p wave resonance also.

In Figures 19 and 20 we plot the giant resonances for A = 200 and A = 208. These correspond to a proton number near 82 and a neutron number near 126. In Figure 19 the FPW peak for A = 200 at 6.0 Mev is an f wave. The distorted peak ($\alpha_2 = 3 \times 10^{-4}$) occurs at 5.5 Mev and is a d wave resonance. In Figure 20 the FPW peak is at 6.0 Mev and is also an f wave. The corresponding distorted peak ($\alpha_2 = 5 \times 10^{-4}$) for A = 208 is at 4.0 Mev and is a d wave resonance.

Figures 21 and 22 are plotted for A = 180 and A = 232. These mass numbers occur in the regions of rotational nuclei or permanently deformed nuclei as discussed in the Introduction. The model used in Chapter 3 for the inclusion of the effect of collective vibrational excitations does not apply to these nuclei. For application of the present theory to the rotational regions of nuclei the theory must be modified to allow for rotational excitations. Nevertheless, we have calculated the effect in these rotational regions with the expectation that, with the appropriate choice of parameters, one can obtain the qualitative behavior

in these regions. The energy of the excited state will, of course, be much smaller according to the experimental values of the rotational levels involved. The polarizability is related to the distortion parameter, β. This correspondence was obtained by comparing the calculations of CWE and those of the present model in the limit of low energy (s wave) incident neutrons, where the δ function surface interaction was used in both cases. The results of this calculation yield the identification of β with $\sqrt{5\hbar\omega_2/2C_2}$.

It is interesting to compare the dynamical distortions in the vibrational nuclei to the permanent distortions observed in rotational nuclei. Table 1 gives information regarding the experimentally determined values of the polarizability. These values were determined by the Coulomb excitation experiments of Reference 9. This same reference also provides us with experimentally determined values of the distortion parameter β. Values of β range from 0.2 to 0.5, but for the most part they are near 0.3. Table 2 lists some values of β and the corresponding values of the polarizability.

TABLE 2

COMPARISON OF ROTATIONAL AND VIBRATIONAL DISTORTION PARAMETERS

β	$\hbar\omega_2/8\pi C_2$
0.51	4×10^{-3}
0.25	1×10^{-3}
0.177	5×10^{-4}
0.137	3×10^{-4}
0.056	5×10^{-5}

The total cross section for A = 180, which is in the rotational region ($150 < A < 190$), is presented in Figure 21. The FPW peak is completely flattened with the inclusion of the quadrupole effect ($\alpha_2 = 1 \times 10^{-3}$). This value of α_2 is characteristic of this region of nuclei as is the energy, $E_2 = 0.1$ Mev. For the rotational region ($A > 220$)we have plotted the giant resonance for A = 232 in Figure 22. The polarizability used here ($\alpha_2 = 4 \times 10^{-3}$) is larger than experimentally observed in this region, but it is useful in demonstrating the effect of such a large polarizability, namely, that the distorted resonance remains flat. The energy $E_2 = 0.05$ Mev, is characteristic of this region of nuclei.

5.4 Total Reaction, Shape Elastic, and Differential Shape Elastic Cross Sections

The total reaction cross section and the shape elastic cross section for A = 208 is plotted in Figure 23. The FPW curves are designated as undistorted and the spheroidal well surface interaction curves are labelled distorted. The distortion parameters for the quadrupole collective effect are $E_2 = 0.4$ Mev and $\alpha_2 = 5 \times 10^{-4}$. The sum of the total reaction cross section and the shape elastic cross section is the total cross section for A = 208 illustrated in Figure 20. Comparison of σ_R and σ_{se} to experiment is not too meaningful because the experimental elastic scattering cross section includes the compound elastic scattering whereas in the optical model, compound elastic scattering is included in the total reaction cross section or the cross section for compound nucleus formation. In spite of this, the effect of quadrupole excitation on the

total reaction cross section for A = 208 is a clear improvement on the shape of the curve. This may be a coincidence, however.

We had pointed out in the discussion of Figure 20 that the FPW giant resonance at 6.0 Mev is an f wave peak and that the distorted resonance at 4.0 Mev is due to a d wave. In Figures 24, 25, and 26 we have plotted all the partial waves which contribute to the total cross section for both the undistorted and the distorted case. A study of the various contributions to the giant resonances will clarify how the distorted peak becomes a d wave resonance. The major partial wave contributions for both the distorted and undistorted case are the f wave and the d wave. Figures 24 and 25 illustrate the total contributions from the f and the d wave to the total cross section. The separation of the total cross section into the contributions from the total reaction and shape elastic cross sections for these partial waves is also illustrated. The separate contributions are indicated clearly on the appropriate curves. The other partial wave contributions to the respective total cross sections are presented in Figure 26. The partial wave contribution for l = 8 was calculated but was not plotted as it did not have a significant effect in this case. Figure 26 has three ordinate scales which are labelled according to which curves they represent.

The total cross section as well as the shape elastic and total reaction contributions for A = 48 are plotted in Figure 27. The total cross section for A = 48 was not plotted in the earlier section on total cross sections. A = 48 is representative of the doubly magic region with the proton number near 20 and the neutron number near 28. The FPW giant resonance at 2.5 Mev is considered a d wave but the p wave contributed almost as much as

the d wave. The distorted total cross section develops two peak values in the energy region from 0.5 to 10 Mev. There is a peak at 2.0 Mev which is a d wave resonance with a substantial amount of p wave present. The second resonance at 4.5 Mev is designated as p wave but contains considerable d wave as well.

Figure 28 illustrates the three main partial wave contributions to the total cross section as well as the total cross section itself. It is seen that the p wave contribution is insignificantly affected by the inclusion of collective effects. There are four ordinate scales for the four curves presented in this figure.

The differential shape elastic cross section as a function of $\cos \theta_{CM}$ and evaluated at 4.1 Mev is presented in Figures 29 through 31. The values of A and the corresponding collective parameters which are plotted, correspond for the most part ot the total cross sections presented earlier. The angular distribution for shape elastic scattering for A = 44 and A = 48 is shown in Figure 29. For A = 44 the inclusion of the effect of collective excitation deepens the minimum in the vicinity of 80°. Beyond 90° the effect of distortion is mainly one of flattening. The back scattering is diminished. For A = 48 the distorted shape elastic scattering is flattened and the positions of the two minima and the single maximum shown in the figure are all shifted slightly to the right. The forward and backward scattering are both slightly diminished.

In Figure 30 the differential shape elastic scattering is presented for A = 66, 102, and 140. In all three cases the back scattering is

lowered by taking collective effects into account. For A = 66 and 102 the peaks are shifted slightly to the left, and the curve is flattened throughout although the logarithmic scale is a bit misleading in determining this latter effect. For A = 140, the peaks are shifted slightly to the right and flattening is again observed for the distorted angular distribution.

Finally in Figure 31 the differential shape elastic scattering is presented for A = 200 and 208. In both cases the peaks are moved slightly to the right and considerable flattening is observed for the inclusion of collective vibrations.

5.5 Conclusions

The important effects of the present calculation for the inclusion of collective vibrations on the total cross section are the flattening of the giant resonances and the energy shifts in the positions of the peaks of these resonances.

Firstly, we shall discuss the flattening of the resonances. Evidence that the giant resonances flatten to some extent away from closed shells can be obtained by examining the peak to valley ratio of these resonances as a function of A. The total cross sections for neutron scattering, plotted as a function of energy for various nuclei, are complied in Neutron Cross Sections,[17] a Brookhaven National Laboratory report. The various isotopes are not plotted separately so that one must think in terms of the atomic number, Z, rather than the mass number, A. Here again we are making a qualitative study, and the fact that we do not have the total cross sections for the isotopes involved in our study is only of minor importance.

In order to see the evidence for flattening away from closed shells for these total neutron cross sections[17], we have prepared a plot of the peak to valley ratio as a function of Z as shown in Figure 32. The peak to valley ratio is rather a rough estimate due to the different depths of the valleys on either side of the resonances. Average values have been used, but the peculiar shapes of some of the resonances made it difficult at times to obtain good estimates of these average values. Nevertheless, the points give a fairly good description of the regions in which the giant resonances are most clearly defined or most well formed. The points are connected by broken lines for easy reading; there has been no attempt to plot a smooth curve.

There are certain regions in which we expect to find the giant resonance better formed than in neighboring nuclei. These regions are located near $_{20}Ca^{40}_{20}$, $_{20}Ca^{48}_{28}$, $_{28}Ni^{A}_{N,Z50}$, $_{50}Sn^{A}_{N,Z82}$, $_{82}Pb^{208}_{82,126}$, and also in regions where A is magic. X stands for any nuclei which can assume the associated neutron numbers. There is a peak at Z = 20 in the peak to valley ratio versus Z. After this first peak the P/V ratio drops and then rises again, and in the vicinity of Z = 28 there is a broader peak. This second peak corresponds to the overlap between Z = 28 and N = 28. The curve starts to rise again near Z = 40 and does not fall again until Z = 62. This region is an overlap of the effects of N = 50, Z = 50, and N = 82. Most of the isotopes of nuclei with Z = 62 through 74 are in the region of deformed nuclei defines by $150<A<190$. The peak to valley ratio of these nuclei is 1.0 corresponding to the flattening of the giant resonance for these nuclei. The curve starts to rise again after Z = 74 and peaks in the vicinity of Z = 82 and N = 126.

FIG. 32

PEAK TO VALLEY RATIO VS Z
PREPARED FROM REF. 17

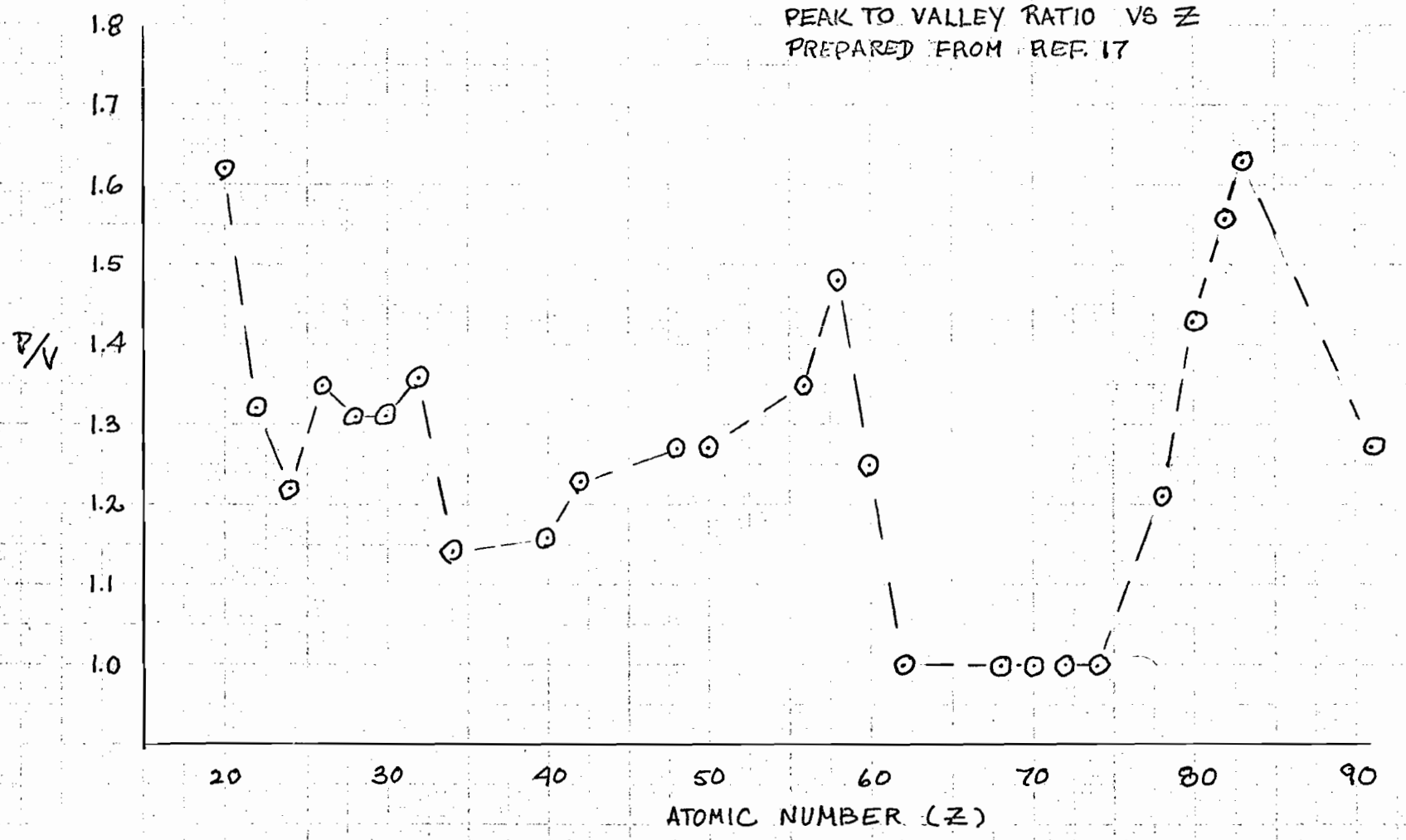

It should be borne in mind that this curve is plotted for nuclei as identified by atomic number and not for individual isotopes. As a result of this, for example, the P/V ratio for bismuth is larger than that for lead on the basis of atomic number, but if the giant resonances were plotted for the individual isotopes, one would expect $_{82}Pb^{208}_{126}$ to have a higher P/V ratio than $_{83}Bi^{207}_{124}$ because $_{82}Pb^{208}_{126}$ is a double magic closed shell nucleus. Nevertheless, the P/V ratio versus Z gives clear evidence of flattening of the giant resonances away from closed shells.

In Figures 13 through 22, we have presented the giant resonances for neutron scattering as predicted by the FPW square well optical model and as corrected by including the effect of collective vibrational excitations. We have seen that upon taking the vibrational excitation into account, the resonances are flattened according to how much distortion is assumed. The parameters of distortion are the polarizability and the energy of the excitation involved. The values of the distortion parameters that were used in calculating the total cross sections were representative of the particular region of nuclei involved. Of course, the experimental values α_2 and E_2 vary from nucleus to nccleus, and in many cases only one value for each of these parameters was plotted. Quite often the value used for α_2 was the largest available experimentally in order to see the full effect. The effects of smaller values of α_2, which were also calculated but not plotted, show the same behavior as the larger values except that the shifts and the flattening effects are less pronounced according to the values which are used.

As has been pointed out this is a qualitative study, and, therefore, it was deemed sufficient to apply the collective correction to closed shell

nuclei to obtain the qualitative behavior of the giant resonances of the neighboring nuclei. In particular for the cases of $_{20}Ca^{40}_{20}$, $_{20}Ca^{48}_{28}$, and $_{82}Pb^{208}_{126}$ which are doubly magic closed shell nuclei, one does not expect collective effects to contribute; however, collective effects were applied to these nuclei for the purpose of determining the effects away from closed shell regions. To apply the collective effect properly, the total cross section for each value of A should be determined with the appropriate collective parameters. It is clear, however, from our qualitative analysis that the inclusion of collective vibrational excitations has the flattening effect on the giant resonances that is desired from experimental observations.

The other important aspect of the total cross section results is the shifting of the energy position of the maximum value with increasing mass number. One of the main objectives to the FPW optical model as pointed out by J. M. Peterson[18] is that the FPW total cross sections plotted versus energy and mass number show a characteristic shift of the maxima towards lower energy with increasing mass number. Experimentally, however as first noted by Barschall[3], the maxima seem to shift to higher energy with increasing mass number. The reason that the FPW maxima shift to lower energy with increasing A has been explained, by Peterson, as a result of the fact that the FPW resonances all occur at energies which are below the height of the centrifugal barrier at the nuclear radius for the partial waves involved. The condition for a partial wave resonance is that a characteristic number of wavelengths fit in the radial wave function inside the well to obtain the internal reflection necessary for the resonance. As the radius, and thereby, the mass number is increased the energy must decrease to maintain kR for the resonance.

The present study has shown that the giant resonance maxima shift with the inclusion of the effect of collective excitations. The question is, then, whether these shifts are in the right direction. As has been pointed out, we have presented the results by applying the collective effect to the closed shell nuclei to obtain the qualitative effect of distortion. This is satisfactory for demonstrating the flattening effect, but is not reliable for understanding the characteristic shift in the maxima as a function of increasing mass number. For this purpose it is necessary to study the distorted total cross sections as a function of increasing A in the vicinity of a family of broad maxima or giant resonances. Such a study was made in the vicinity of A = 200 where the undistorted maxima are f waves. Due to lack of experimental values of the polarizability we have used a fixed value of $\alpha_2 = 1 \times 10^{-4}$. Table 3 indicates the results.

TABLE 3

THE EFFECT OF COLLECTIVE EXCITATIONS ON THE MAXIMA OF THE f WAVE GIANT RESONANCE

A	E_{max}(Mev)
200	5.75
208	6.0
212	6.5
214	7.25
220	7.75

For this case, then, the energy at which the maximum in the distorted giant resonance occurs increases with increasing A. It should be pointed out that this study may not be realistic since we have used the same polarizability for all A values. It does insure, however, that the characteristic decrease in the energy of the resonance with an increase in A of the FPW model is not a strict rule for the giant resonances that occur at energies below the centrifugal barrier as described above.

If one examines the distorted peaks for A = 44, 46, and 48, it is seen that the peaks shift in and out depending upon the amount of polarizability that is assumed. The evaluation of the effect of the shift in maxima in this region is not straight forward. Firstly, the experimental evidence does not really indicate that one should expect a smooth increase in the energy of the maxima with increasing A, although the overall trend does seem to be one of increase.

Other considerations arise from the model itself. For one thing the resonance for this region is very sensitive to distortion. This sensitivity is attributable to the character of the partial waves involved. Although the FPW resonance is designated as a d wave, the p wave contributes appreciably. This is an illustration of the fact that a particular family of giant resonances is not attributable to a single partial wave. For this region of A near 44, a transition of a p wave resonance into a d wave has taken place. Since the p wave is effectively unaltered by distortion in this region, the effect of the distortion on the d wave is all important. As a result of this sensitivity, the distorted giant resonance can be either a p wave or a d wave depending upon the amount of polarizability that is assumed.

Because of this sensitivity, the experimentally determined polarizability should be used for the appropriate isotopes involved when an examination of the effect of distortion on the shift in maxima is made. These experimental values were not available for this study, however.

Another point that applies here is that the effect of collective excitations has been taken into account in the spherical optical model by the optimal choice of the parameters available to that model. The parameters previously used may not be the best parameters for the present study. A change in the values of V_o and R_o could result in an alteration in the giant resonance character for this doubly magic region.

The main point here is that this qualitative study indicates that when collective effects are taken into account, there is a possibility of predicting the correct energy shift of the maxima as a function of increasing A. A more careful study with the appropriate parameters would have to be undertaken to determine this.

The strength function has been presented and discussed in Section 5.2. The main conclusions are that the quadrupole excitation produces a splitting of the 3s giant resonance in the strength function and shifts the main peak towards lower A. The octupole contribution is effective in decreasing the right hand peak and in lowering the strength function in the valley between the 3s and 4s giant resonances. Of course, this latter effect is not sufficient in magnitude to account for the large discrepancy between theory and experiment in this region.

We have said relatively little about the differential shape elastic cross section. The spherical optical model as applied by M. Walt, J. R. Beyster and E. W. Salmi[19] produced fairly good agreement between experimental and calculated differential cross sections. The inclusion of spin-orbit coupling by F. Bjorklund and S. Fernbach[20] improved these results still further. There still existed some discrepancies, however. A significant discrepancy in the case of tantalum was noticed by H. M. Schey[21]. Schey attributed this lack of agreement to the permanent quadrupole deformation in tantalum, and he obtained adequate improvement with experiment by including the effect of this collective deformation in the calculation of the differential cross section.

It has been demonstrated in Figures 29 through 31 that the inclusion of the effect of collective vibrations has considerable effect on the differential shape elastic cross section according to the present model. It should be pointed out that the energy for which these cross sections were determined is 4.1 Mev. At this energy some correction for compound elastic scattering is still necessary for certain mass numbers. There has been no attempt to make this correction. The kinds of discrepancies that existed for the cross sections of Reference 20 are qualitatively of the same nature as those in Figures 29 through 31, namely, a flattening and shifting of peaks. This evidence for the possibility of improvement in these cross sections by the correction for collective effects might suggest that a program be set up for including the effect of vibrational excitations on the Bjorklund-Fernbach model, which because of the spin dependent optical potential, is known to be applicable to many elements over a wide range of energies.

The present work has been devoted to the qualitative determination of the effect of collective excitations on the optical model. The work was facilitated by the choice of a delta function surface interaction for coupling between collective and individual particle coordinates. We were able to obtain an exact solution within the framework of the model, and, in addition, we were able to express this exact solution in a particularly convenient form for the purpose of comparison to the FPW spherical optical model.

The use of the delta function surface interaction is an approximation that should be justified if one is to believe the results which have been presented. It was expected that the delta function would be a good approximation if the distortion produced by the polarizability amounted to less than a quarter wavelength of the neutron near the surface. This condition can be written as $\sqrt{\frac{5\hbar\omega_2}{2C_2}}R \leq \frac{\pi}{2}\lambda\!\!\!^{-}$ where we have identified the polarizability with the permanent distortion parameter, β.

For the strength function, a low energy phenomenon, for which we have taken $V_0/2$ as the local kinetic energy at the surface, the condition for validity reduces to $\sqrt{5\hbar\omega_2/2C_2} \leq \frac{\pi}{KR}$. For the 3s resonance of the strength function KR is approximately 5/2 , and, therefore, in terms of the polarizability we obtain $\alpha_2 < 2.6 \times 10^{-3}$. This inequality is clearly satisfied, and our approximation is justified. To determine the validity of using the delta function for the total cross section, we examine one of the worst possible cases. We take A = 200 and an energy of 10 Mev. The condition for validity for this case reduces to $\alpha_2 \leq 5 \times 10^{-4}$. As we have seen, application of a polarizability of

this order flattens the curve more than is usually desirable. This consideration indicates that our approximation is valid although in some cases rather close to the borderline.

The results of the calculations with the present model represent qualitatively those results that would be obtained upon application of a more realistic diffuse surface optical model with spin-orbit coupling. The present calculations have been most rewarding in the magnitude and direction of the corrections that have been attained. The dependence of the giant resonance peak position on increasing mass number in the energy region of 0.1 to 10 Mev has never been properly reproduced, and the failure of the FPW optical model to predict this dependence is rather a serious drawback. Peterson[18] developed a nuclear Ramsauer effect to interpret these maxima, but his theory fails at zero energy, and there is some discrepancy in parameters that is not understood. The extension of the present model to a more realistic potential well seems in order, especially, in the view of obtaining the correct dependence of the giant resonance peak position as a function of increasing mass number in this 0.1 to 10 Mev energy region. The flattening effect of quadrupole excitation on the giant resonances as a function of experimentally determined collective quadrupole parameters is another important effect which should be incorporated into a more realistic potential model. An important point in this regard is that no free parameters have been introduced with the inclusion of collective effects. This connection between the quadrupole effect and the total neutron cross sections may have future applications upon improvement of the model.

APPENDIX I

I. 1 Radial Equations for J = 0

For J = 0, (3.12) and (3.14) can be reduced to

$$\left(-\frac{\hbar^2}{2m}\nabla^2+\bar{V}(r)-E\right)\frac{1}{r}u^0_{00}C_{00}(00|00)Y_{00} =$$

$$\sum_m \frac{1}{r}u^0_{22}RV_0(1+i\xi)\,\delta(r-R)\,Y_{2,m}C_{22}(m,-m|00)\langle 00|d_{2-m}|2,m\rangle\,Y_{2m}\,, \tag{I. 1}$$

and

$$\left(-\frac{\hbar^2}{2m}\nabla^2+\bar{V}(r)-E+\hbar\omega_2\right)\frac{1}{r}u^0_{22}C_{22}(m',-m'|00)Y_{2m'} =$$

$$\frac{1}{r}u^0_{00}RV_0(1+i\xi)\delta(r-R)Y_{2m'}Y_{00}C_{00}(00|00)\langle 2,-m'|d_{2m'}|00\rangle\,. \tag{I. 2}$$

Multiplying (I. 1) by Y^*_{00} and (I. 2) by $Y^*_{2m'}$ and integrating over the angular dependence yields

$$\left(-\frac{\hbar^2}{2m}\nabla^2+\bar{V}(r)-E\right)\frac{1}{r}u^0_{00} =$$

$$\frac{1}{r}u^0_{22}RV_0(1+i\xi)\delta(r-R)\sum_m\langle Y_{00}|Y_{2-m}Y_{2m}\rangle C_{22}(m,-m|00)\sqrt{\frac{\hbar\omega_2}{2C_2}}\,, \tag{I. 3}$$

and

$$\left(-\frac{\hbar^2}{2m}\nabla^2+\bar{V}(r)-E+\hbar\omega_2\right)\frac{1}{r}u^0_{22}C_{22}(m',-m'|00) =$$

$$\frac{1}{r}u^0_{00}RV_0(1+i\xi)\delta(r-R)\langle Y_{2m'}|Y_{2m'}Y_{00}\rangle(-1)^{m'}\sqrt{\frac{\hbar\omega_2}{2C_2}}\,. \tag{I. 4}$$

where we have introduced the notation

$$\langle Y_{00} | Y_{2-m} Y_{2m} \rangle = \int Y_{00}^{*} Y_{2-m} Y_{2m} \, d\Omega \tag{I. 5}$$

and where we have used (2.39) to evaluate the target matrix elements. Evaluation of the sum over m in (I. 3) involves the determination of the appropriate Clepsh-Gordon coefficients[12] as well as the use of the following relationship between the spherical harmonics[8]:

$$Y_{\ell m}(\theta,\phi) Y_{\ell' m'}(\theta,\phi) = \sum_{L} \sum_{M} \sqrt{\frac{(2\ell+1)(2\ell'+1)}{4\pi(2L+1)}} C_{\ell\ell'}(L0|00) C_{\ell\ell'}(LM|mm') Y_{LM}(\theta,\phi) \tag{I. 6}$$

with these simplifications imposed, (I. 3) and (I. 4) can be written

$$\left(-\frac{\hbar^2}{2m}\nabla^2 + \bar{V}(R) - E\right) \frac{1}{R} u_{00}^{0} = \frac{1}{R} u_{22}^{0} R V_0 (1+\xi) \delta(R-R) \sqrt{\frac{5}{4\pi}} \sqrt{\frac{\hbar\omega_2}{2C_2}} \tag{I. 7}$$

and

$$\left(-\frac{\hbar^2}{2m}\nabla^2 + \bar{V}(R) - E + \hbar\omega_2\right) \frac{1}{R} u_{22}^{0} = \frac{1}{R} u_{00}^{0} R V_0 (1+\xi) \delta(R-R) \sqrt{\frac{5}{4\pi}} \sqrt{\frac{\hbar\omega_2}{2C_2}} \tag{I. 8}$$

I. 2 Radial Equations for J = 1

Setting J = 1 in (3. 12) and multiplying by Y_{10}^{*} and integrating over $d\Omega$ yields

$$\left(-\frac{\hbar^2}{2m} + \bar{V}(R) - E\right) \frac{1}{R} u_{10}^{1} C_{10}(00|10) =$$

$$\frac{1}{R} u_{12}^{1} R V_0 (1+\xi) \delta(R-R) \sqrt{\frac{\hbar\omega_2}{2C_2}} \sum_{m=-1}^{1} \langle Y_{10} | Y_{2-m} | Y_{1m} \rangle C_{12}(m,-m|10) + \tag{I. 9}$$

$$\frac{1}{R} u_{32}^{1} R V_0 (1+\xi) \delta(R-R) \sqrt{\frac{\hbar\omega_2}{2C_2}} \sum_{m=-2}^{2} \langle Y_{10} | Y_{2-m} Y_{3m} \rangle C_{32}(m,m|30)$$

Setting J = 1 in (3.14), multiplying by $Y^*_{1m'}$ and $Y^*_{3m'}$, respectively and integrating over $d\Omega_1$ yields the following two equation:

$$\left(-\frac{\hbar^2}{2m}\nabla^2+\bar{V}(r)-E+\hbar\omega_2\right)\frac{1}{r}u^1_{12}C_{12}(m',-m'|10)=\frac{1}{r}u^1_{10}RV_0(1+\lambda\xi)\delta(r-R)\sqrt{\frac{\hbar\omega_2}{2C_2}}\left\langle Y_{1m'}\middle|Y_{2m'}Y_{10}\right\rangle, \quad \text{(I. 10)}$$

and

$$\left(-\frac{\hbar^2}{2m}\nabla^2+\bar{V}(r)-E+\hbar\omega_2\right)\frac{1}{r}u^1_{32}C_{32}(m',-m'|10)=\frac{1}{r}u^1_{10}RV_0(1+\lambda\xi)\delta(r-R)\sqrt{\frac{\hbar\omega_2}{2C_2}}\left\langle Y_{3m'}\middle|Y_{2m'}Y_{10}\right\rangle. \quad \text{(I. 11)}$$

In the same manner as for J = 0, (I. 9), (I. 10), and (I. 11) can be further reduced to

$$\left(-\frac{\hbar^2}{2m}\nabla^2+\bar{V}(r)-E\right)\frac{1}{r}u^1_{10}=\frac{1}{r}\left(-\sqrt{2}u^1_{12}+\sqrt{3}u^1_{32}\right)RV_0(1+\lambda\xi)\delta(r-R)\sqrt{\frac{\hbar\omega_2}{8\pi C_2}}, \quad \text{(I. 12)}$$

$$\left(-\frac{\hbar^2}{2m}\nabla^2+\bar{V}(r)-E+\hbar\omega_2\right)\frac{1}{r}u^1_{12}=-\frac{\sqrt{2}}{r}u^1_{10}RV_0(1+\lambda\xi)\delta(r-R)\sqrt{\frac{\hbar\omega_2}{8\pi C_2}}, \quad \text{(I. 13)}$$

and

$$\left(-\frac{\hbar^2}{2m}\nabla^2+\bar{V}(r)-E+\hbar\omega_2\right)\frac{1}{r}u^1_{32}=\frac{\sqrt{3}}{r}u^1_{10}RV_0(1+\lambda\xi)\delta(r-R)\sqrt{\frac{\hbar\omega_2}{8\pi C_2}} \quad \text{(I. 14)}$$

I. 3 Radial Equations for J = 2

Setting J = 2 in (3.12) and (3.14), multiplying by the appropriate complex

conjugate spherical harmonics, performing the integration over $d\Omega_R$ and completing the various sums over the azimuthal quantum number yields the following set of four coupled radial equations for J = 2.

$$\left(-\frac{\hbar^2}{2m}\nabla^2+\bar{V}(R)-E\right)\frac{1}{R}u^2_{20}=\frac{1}{R}\left(u^2_{02}-\sqrt{\frac{10}{7}}u^2_{22}+\sqrt{\frac{18}{7}}u^2_{42}\right)RV_0(1+\lambda\xi)\delta(R-R_e)\sqrt{\frac{\hbar\omega_2}{8\pi C_2}}\,, \tag{I.15}$$

$$\left(-\frac{\hbar^2}{2m}\nabla^2+\bar{V}(R)-E+\hbar\omega_2\right)\frac{1}{R}u^2_{02}=\frac{1}{R}\,u^2_{20}RV_0(1+\lambda\xi)\delta(R-R_e)\sqrt{\frac{\hbar\omega_2}{8\pi C_2}}\,, \tag{I.16}$$

$$\left(-\frac{\hbar^2}{2m}\nabla^2+\bar{V}(R)-E+\hbar\omega_2\right)\frac{1}{R}u^2_{22}=-\sqrt{\frac{10}{7}}\,\frac{1}{R}\,u^2_{20}RV_0(1+\lambda\xi)\delta(R-R_e)\sqrt{\frac{\hbar\omega_2}{8\pi C_2}}\,, \tag{I.17}$$

and

$$\left(-\frac{\hbar^2}{2m}\nabla^2+\bar{V}(R)-E+\hbar\omega_2\right)\frac{1}{R}u^2_{42}=\sqrt{\frac{18}{7}}\,\frac{1}{R}u^2_{20}RV_0(1+\lambda\xi)\delta(R-R_e)\sqrt{\frac{\hbar\omega_2}{8\pi C_2}}\,. \tag{I.18}$$

I.4 Radial Equations for J = 3

Setting J = 3 in (3.12) and (3.14) and integrating out the angular dependence as in the previous cases yields the following set of four coupled, radial equations for J = 3:

$$\left(-\frac{\hbar^2}{2m}\nabla^2+\bar{V}(R)-E\right)\frac{1}{R}u^3_{30}=\frac{1}{R}\left(\sqrt{\frac{9}{7}}u^3_{12}-\sqrt{\frac{4}{5}}u^3_{32}+\sqrt{\frac{50}{21}}u^3_{52}\right)RV_0(1+\lambda\xi)\delta(R-R_e)\sqrt{\frac{\hbar\omega_2}{8\pi C_2}}\,, \tag{I.19}$$

$$\left(-\frac{\hbar^2}{2m}\nabla^2+\bar{V}(r)-E+\hbar\omega_2\right)\frac{1}{r}u^3_{12}=\sqrt{\frac{9}{7}}RV_0(1+\lambda\xi)\sqrt{\frac{\hbar\omega_2}{8\pi C_2}}\delta(r-R)\frac{1}{r}u^3_{30}\,, \tag{I. 20}$$

$$\left(-\frac{\hbar^2}{2m}\nabla^2+\bar{V}(r)-E+\hbar\omega_2\right)\frac{1}{r}u^3_{32}=-\sqrt{\frac{9}{3}}RV_0(1+\lambda\xi)\sqrt{\frac{\hbar\omega_2}{8\pi C_2}}\delta(r-R)\frac{1}{r}u^3_{30}\,, \tag{I. 21}$$

and

$$\left(-\frac{\hbar^2}{2m}\nabla^2+\bar{V}(r)-E+\hbar\omega_2\right)\frac{1}{r}u^3_{52}=\sqrt{\frac{50}{21}}RV_0(1+\lambda\xi)\sqrt{\frac{\hbar\omega_2}{8\pi C_2}}\delta(r-R)\frac{1}{r}u^3_{30}\,. \tag{I. 22}$$

I. 5 Radial Equations for J = 4

Setting J = 4 in (3. 12) and (3. 14) and integrating out the angular dependence as in the previous cases yields the following set of four radial equations for J = 4.

$$\left(-\frac{\hbar^2}{2m}\nabla^2+\bar{V}(r)-E\right)\frac{1}{r}u^4_{40}=RV_0(1+\lambda\xi)\sqrt{\frac{\hbar\omega_2}{8\pi C_2}}\delta(r-R)\frac{1}{r}\left(\sqrt{\frac{18}{7}}u^4_{22}-\sqrt{\frac{100}{77}}u^4_{42}+\sqrt{\frac{25}{11}}u^4_{62}\right)\,, \tag{I. 23}$$

$$\left(-\frac{\hbar^2}{2m}\nabla^2+\bar{V}(r)-E+\hbar\omega_2\right)\frac{1}{r}u^4_{22}=\sqrt{\frac{10}{7}}RV_0(1+\lambda\xi)\sqrt{\frac{\hbar\omega_2}{8\pi C_2}}\delta(r-R)\frac{1}{r}u^4_{40}\,, \tag{I. 24}$$

$$\left(-\frac{\hbar^2}{2m}\nabla^2+\bar{V}(r)-E+\hbar\omega_2\right)\frac{1}{r}u^4_{42}=-\sqrt{\frac{100}{77}}RV_0(1+\lambda\xi)\sqrt{\frac{\hbar\omega_2}{8\pi C_2}}\delta(r-R)\frac{1}{r}u^4_{40}\,, \tag{I. 25}$$

and

$$\left(-\frac{\hbar^2}{2m}\nabla^2+\bar{V}(r)-E+\hbar\omega_2\right)\frac{1}{r}u^4_{62}=\sqrt{\frac{25}{11}}\,RV_0(1+\lambda\xi)\sqrt{\frac{\hbar\omega_2}{8\pi C_2}}\,\delta(r-R)\frac{1}{r}u^4_{40}\ . \qquad \text{(I. 26)}$$

I. 6 Radial Equations for J = 5

Setting J = 5 in (3. 12) and (3. 14) and integrating out the angular dependence as in the previous cases yields the following set of four radial equations for J = 5.

$$\left(-\frac{\hbar^2}{2m}\nabla^2+\bar{V}(r)-E\right)\frac{1}{r}u^5_{50}=RV_0(1+\lambda\xi)\sqrt{\frac{\hbar\omega_2}{8\pi C_2}}\,\delta(r-R)\frac{1}{r}\left(\sqrt{\frac{50}{33}}u^5_{32}-\sqrt{\frac{50}{39}}u^5_{52}+\sqrt{\frac{315}{143}}u^5_{72}\right), \qquad \text{(I. 27)}$$

$$\left(-\frac{\hbar^2}{2m}\nabla^2+\bar{V}(r)-E+\hbar\omega_2\right)\frac{1}{r}u^5_{32}=\sqrt{\frac{50}{33}}\,RV_0(1+\lambda\xi)\sqrt{\frac{\hbar\omega_2}{8\pi C_2}}\,\delta(r-R)\frac{1}{r}u^5_{50}\ , \qquad \text{(I. 28)}$$

$$\left(-\frac{\hbar^2}{2m}\nabla^2+\bar{V}(r)-E+\hbar\omega_2\right)\frac{1}{r}u^5_{52}=-\sqrt{\frac{50}{39}}\,RV_0(1+\lambda\xi)\,\frac{\hbar\omega_2}{8\pi C_2}\,\delta(r-R)\frac{1}{r}u^5_{50}\ , \qquad \text{(I. 29)}$$

and

$$\left(-\frac{\hbar^2}{2m}\nabla^2+\bar{V}(r)-E+\hbar\omega_2\right)\frac{1}{r}u^5_{72}=\sqrt{\frac{315}{143}}\,RV_0(1+\lambda\xi)\sqrt{\frac{\hbar\omega_2}{8\pi C_2}}\,\delta(r-R)\frac{1}{r}u^5_{50}\ . \qquad \text{(I. 30)}$$

I.7 Radial Equations for J = 6

Setting J = 6 in (3.12) and (3.14) and integrating out the angular dependence as in the previous cases yields the following set of four radial equations for J = 6.

$$\left(-\frac{\hbar^2}{2m}\nabla^2+\bar{V}(r)-E\right)\frac{1}{r}u^6_{60}=RV_0(1+\lambda\xi)\sqrt{\frac{\hbar\omega_2}{8\pi C_2}}\delta(r-R)\frac{1}{r}\left(\frac{15}{\sqrt{143}}u^6_{42}-\sqrt{\frac{14}{11}}u^6_{62}+\sqrt{\frac{28}{13}}u^6_{82}\right), \quad \text{(I.31)}$$

$$\left(-\frac{\hbar^2}{2m}\nabla^2+\bar{V}(r)-E+\hbar\omega_2\right)\frac{1}{r}u^6_{42}=\frac{15}{\sqrt{143}}RV_0(1+\lambda\xi)\sqrt{\frac{\hbar\omega_2}{8\pi C_2}}\delta(r-R)\frac{1}{r}u^6_{60}, \quad \text{(I.32)}$$

$$\left(-\frac{\hbar^2}{2m}\nabla^2+\bar{V}(r)-E+\hbar\omega_2\right)\frac{1}{r}u^6_{62}=-\sqrt{\frac{14}{11}}RV_0(1+\lambda\xi)\sqrt{\frac{\hbar\omega_2}{8\pi C_2}}\delta(r-R)\frac{1}{r}u^6_{60}, \quad \text{(I.33)}$$

and

$$\left(-\frac{\hbar^2}{2m}\nabla^2+\bar{V}(r)-E+\hbar\omega_2\right)\frac{1}{r}u^6_{82}=\sqrt{\frac{28}{13}}RV_0(1+\lambda\xi)\sqrt{\frac{\hbar\omega_2}{8\pi C_2}}\delta(r-R)\frac{1}{r}u^6_{60}. \quad \text{(I.34)}$$

I.8 Radial Equations for J = 7

Setting J = 7 in (3.12) and (3.14) and integrating out the angular dependence as in the previous cases yields the following set of four radial equations for J = 7.

$$\left(-\frac{\hbar^2}{2m}\nabla^2+\bar{V}(r)-E\right)\frac{1}{r}u^7_{70}=RV_0(1+\lambda\xi)\sqrt{\frac{\hbar\omega_2}{8\pi C_2}}\delta(r-R)\frac{1}{r}\left(\sqrt{\frac{21}{13}}u^7_{52}-\sqrt{\frac{280}{221}}u^7_{72}+\frac{6}{\sqrt{17}}u^7_{92}\right), \quad \text{(I.35)}$$

$$\left(-\frac{\hbar^2}{2m}\nabla^2+\bar{V}(r)-E+\hbar\omega_2\right)\frac{1}{r}u^7_{52}=\sqrt{\frac{21}{13}}RV_0(1+\lambda S)\sqrt{\frac{\hbar\omega_2}{8\pi C_2}}\delta(r-R)\frac{1}{r}u^7_{70}, \qquad (I.36)$$

$$\left(-\frac{\hbar^2}{2m}\nabla^2+\bar{V}(r)-E+\hbar\omega_2\right)\frac{1}{r}u^7_{72}=-\sqrt{\frac{280}{221}}RV_0(1+\lambda S)\sqrt{\frac{\hbar\omega_2}{8\pi C_2}}\delta(r-R)\frac{1}{r}u^7_{70}, \qquad (I.37)$$

and

$$\left(-\frac{\hbar^2}{2m}\nabla^2+\bar{V}(r)-E+\hbar\omega_2\right)\frac{1}{r}u^7_{92}=\frac{6}{\sqrt{17}}RV_0(1+\lambda S)\sqrt{\frac{\hbar\omega_2}{8\pi C_2}}\delta(r-R)\frac{1}{r}u^7_{70}. \qquad (I.38)$$

1.9 Radial Equations for J = 8

Setting in J = 8 in (3.12) and (3.14) and integrating out the angular dependence as in the previous cases yields the following set of four radial equations for J = 8.

$$\left(-\frac{\hbar^2}{2m}\nabla^2+\bar{V}(r)-E\right)\frac{1}{r}u^8_{80}=RV_0(1+\lambda S)\sqrt{\frac{\hbar\omega_2}{8\pi C_2}}\delta(r-R)\frac{1}{r}\left(\sqrt{\frac{28}{17}}u^8_{62}-\sqrt{\frac{24}{19}}u^8_{82}+\sqrt{\frac{675}{323}}u^8_{10,2}\right), \qquad (I.39)$$

$$\left(-\frac{\hbar^2}{2m}\nabla^2+\bar{V}(r)-E+\hbar\omega_2\right)\frac{1}{r}u^8_{62}=\sqrt{\frac{28}{17}}RV_0(1+\lambda S)\sqrt{\frac{\hbar\omega_2}{8\pi C_2}}\delta(r-R)\frac{1}{r}u^8_{80}, \qquad (I.40)$$

$$\left(-\frac{\hbar^2}{2m}\nabla^2+\bar{V}(r)-E+\hbar\omega_2\right)\frac{1}{r}u^8_{82}=-\sqrt{\frac{24}{19}}RV_0(1+\lambda S)\sqrt{\frac{\hbar\omega_2}{8\pi C_2}}\delta(r-R)\frac{1}{r}u^8_{80}, \qquad (I.41)$$

and

$$\left(-\frac{\hbar^2}{2m}\nabla^2+\bar{V}(r)-E+\hbar\omega_2\right)\frac{1}{r}u^8_{10,2}=\sqrt{\frac{675}{323}}RV_0(1+\lambda S)\sqrt{\frac{\hbar\omega_2}{8\pi C_2}}\delta(r-R)\frac{1}{r}u^8_{80}. \qquad (I.42)$$

APPENDIX II

The various cross sections and the strength function were evaluated with the aid of the IBM 1410. Programming involved separating these quantities into real and imaginary parts, and these parts are expressible in terms of the functions $Re f_\ell$, $Im f_\ell$, S_ℓ, Δ_ℓ, and δ_ℓ which all satisfy certain recursive relations because of their dependence on the spherical Bessel functions.

For the complex square well with $\ell = 0$ we get

$$f_0(X) = X \cot X \quad , \tag{II. 1}$$

$$\Delta_0(x) + i S_0(x) = iX \quad , \tag{II. 2}$$

and

$$\delta_0(x) = \arctan\left[j_0(x)/n_0(x)\right] . \tag{II. 3}$$

where the arguments have been defined in Section 2. 2. We can separate (II. 1) into real and imaginary parts obtaining

$$Re f_0 = \frac{X_R \sin 2X_R + X_I \sinh 2X_I}{\cosh 2X_I - \cos 2X_R} \quad , \tag{II. 4}$$

and

$$Im f_0 = \frac{X_I \sin 2X_R - X_R \sinh 2X_I}{\cosh 2X_I - \cos 2X_R} \quad . \tag{II. 5}$$

where

$$\mathbb{X} = \mathbb{X}_R + i\mathbb{X}_I \quad . \tag{II. 6}$$

Using the recurrence relations for the spherical Bessel function[13] we can write

$$f_\ell = \frac{\mathbb{X}^2}{\ell - f_{\ell-1}} - \ell \quad . \tag{II. 7}$$

It follows, therefore, that

$$\mathrm{Re} f_\ell = \frac{(\mathbb{X}_R^2 - \mathbb{X}_I^2)(\ell - \mathrm{Re} f_{\ell-1}) - 2\mathbb{X}_R \mathbb{X}_I \mathrm{Im} f_{\ell-1}}{(\ell - \mathrm{Re} f_{\ell-1})^2 + (\mathrm{Im} f_{\ell-1})^2} \quad , \tag{II. 8}$$

and

$$\mathrm{Im} f_\ell = \frac{(\mathbb{X}_R^2 - \mathbb{X}_I^2)\mathrm{Im} f_{\ell-1} + 2\mathbb{X}_R \mathbb{X}_I (\ell - \mathrm{Re} f_{\ell-1})}{(\ell - \mathrm{Re} f_{\ell-1})^2 + (\mathrm{Im} f_{\ell-1})^2} \quad . \tag{II. 9}$$

Similarly

$$\Delta_\ell + i S_\ell = \frac{x^2}{(\ell - \Delta_{\ell-1}) - i S_{\ell-1}} - \ell \quad , \tag{II. 10}$$

and therefore

$$\Delta_\ell = \frac{x^2(\ell - \Delta_{\ell-1})}{(\ell - \Delta_{\ell-1})^2 + (S_{\ell-1})^2} - \ell \quad , \tag{II. 11}$$

and

$$S_\ell = \frac{x^2 S_{\ell-1}}{(\ell - \Delta_{\ell-1})^2 + (S_{\ell-1})^2} \quad . \tag{II. 12}$$

The recurrence relations that are convenient for calculating $j_\ell(x)$ are just[13]

$$j_{\ell+1}(x) = \frac{2\ell+1}{x} j_\ell(x) - j_{\ell-1}(x) \quad , \tag{II. 13}$$

which is also satisfied by the spherical Neumann function.

For the calculation of the cross sections with the inclusion of collective vibrations we must evaluate $Re^{J}_{J0}(X,y,Y)$ and $Im\, f^{J}_{J0}(X,y,Y)$. For the case, J = 0, we can separate f^{0}_{00} into real and imaginary parts as follows:

$$Re f^{0}_{00}(X,y,Y) = Re f_0(X) + \left(\frac{2m}{\hbar^2}\right)^2 V_0^2 R^4 5 \frac{\hbar\omega_2}{8\pi C_2} \frac{a[\Delta_2(y) - Re f_2(Y)] + b[S_2(y) - Im f_2(Y)]}{[\Delta_2(y) - Re f_2(Y)]^2 + [S_2(y) - Im f_2(Y)]^2}, \quad \text{(II. 14)}$$

and

$$Im f^{0}_{00}(X,y,Y) = Im f_0(X) + \left(\frac{2m}{\hbar^2}\right)^2 V_0^2 R^4 5 \frac{\hbar\omega_2}{8\pi C_2} \frac{b[\Delta_2(y) - Re f_2(Y)] - a[S_2(y) - Im f_2(Y)]}{[\Delta_2(y) - Re f_2(Y)]^2 + [S_2(y) - Im f_2(Y)]^2}. \quad \text{(II. 15)}$$

where $a = 1 - \xi^2$ and $b = 2\xi$. The evaluation of (II. 14) and (II. 15) can be carried out by using the recurrence relations just developed for the complex square well except that the functions in the correction term contain different arguments. In the case that the incident energy, E, is less than then the following modification must be made

$$\Delta_\ell(y) + i S_\ell(y) = -y, \quad \text{(II. 16)}$$

and then from (II. 10)

$$\Delta_\ell(y) = \frac{-y^2}{\ell - \Delta_{\ell-1}} - \ell, \quad \text{(II. 17)}$$

and

$$S_\ell(y) = 0. \quad \text{(II. 18)}$$

For higher values of J, $\mathrm{Re}\, f^{J}_{J0}$ and $\mathrm{Im}\, f^{J}_{J0}$ are obtained in a similar fashion.. The results are too lengthy to present here, but the method is straight-forward, and the solution in terms of the recursion relations is analogous to the discussion above.

REFERENCES

1. N. Bohr, Nature 137, 344 (1936).

2. H. Feshbach and V. F. Weisskopf, Physical Review 76, 1550 (1949).

3. H. H. Barschall, Physical Review 86, 431 (1952).

4. H. Feshbach, C. Porter, and V. F. Weisskopf, Physical Review 96, 448 (1954).

5. B. Margolis and E. S. Troubetzkoy, Physical Review 106, 105 (1957).

6. D. M. Chase, L. Wilets, and A. R. Edmonds, Physical Review 110, 1080 (1958).

7. B. Buck and F. Perey, Physical Review Letters 8, 444 (1962).

8. J. M. Blatt and V. F. Weisskopf, Theoretical Nuclear Physics, John Wiley and Sons, Inc., New York, 1952.

9. K. Alder, A. Bohr, T. Huus, B. Mottleson, and A. Winther, Reviews of Modern Physics 28, 432 (1956).

10. A. Bohr, Kgl. Danske Videnskab. Selskab, Mat.-fys. Medd. 26, No. 14 (1952).

11. A. Bohr and B. Mottleson, Kgl. Danske Videnskab. Selskab, Mat.-fys. Medd. 27, No. 16 (1953).

12. E. U. Condon and G. H. Shortley, Theory of Atomic Spectra, Cambridge University Press, London, 1935.

13. L. I. Schiff, Quantum Mechanics, McGraw-Hill Book Company, Inc., New York, 1955.

14. A. M. Lane and E. D. Pendlebury, Nuclear Physics 15, 39 (1960).

15. E. Vogt, Physics Letters 1, 84 (1962).

16. I. Furuoya and A. Sugie, Nuclear Physics 44, 44 (1963).

17. Neutron Cross Sections compiled by D. J. Hughes and R. Schwartz, Brookhaven National Laboratory Report BNL-325 (Superintendent of Documents, U. S. Government Printing Office, Washington, D. C., 1958). and Supplement BNL-325, 1960.

18. J. M. Peterson, Physical Review 125, 955 (1961).

19. M. Walt, J. R. Beyster, and E. W. Salmi, Physical Review 104, 1319 (1956).

20. F. Bjorklund, and S. Fernbach, Physical Review 109, 1295 (1958).

21. H. M. Schey, Physical Review 113, 900 (1959).